

Carbon Dioxide Absorbers for Active Food Packaging: Heterogeneous Chemical Precipitation of  
Lime on TEMPO Oxidized Cellulose Nanofiber Template

by

Karthik Ramachandran Shivakumar

A thesis submitted in partial fulfillment of the requirements for the degree of

Master of Science

In  
Chemical Engineering

Department of Chemical and Materials Engineering  
University of Alberta

© Karthik Ramachandran Shivakumar, 2019

## **ABSTRACT**

Cellulose nanofibers are fibers of high aspect ratios with exceptional barrier properties and are manufactured from renewable source. In this study, cellulose from various sources such as Kraft pulp and bleached chemical thermomechanical pulp (BCTMP) with different dispersion methods was used to make cellulose nanofibers using 2,2,6,6-Tetramethylpiperidine-1-oxyl (TEMPO) mediated selective oxidation method [1]. The oxidation levels of the fibers from different cellulose sources were correlated with the amount of primary oxidizer used. The self-assembly of the nanofibers due to freeze-drying was analysed and the thermal degradation properties of these freeze-dried fibers were studied. The nanofibers produced from the TEMPO oxidation was used as a template for the growth of calcium hydroxide particles. A novel heterogeneous chemical precipitation method was used to deposit calcium hydroxide on the surface of the nanofibers. This research was aimed at developing a carbon dioxide absorber in active food packaging applications, as calcium hydroxide could absorb the carbon dioxide to form calcium carbonate to prevent the excess carbon dioxide damage in packaged food produces, especially climacteric fruits like apple, bananas etc. The metal-fibre composite was studied under thermal degradation at high temperature before and after carbonation of the calcium hydroxide particles. The crystal formation was analysed using x-ray diffraction (XRD), Fourier transform infrared spectroscopy (FTIR) and field emission scanning electron microscopy. The flow properties of cellulose nanofibers at different dilutions, cellulose nanofiber blends and hydroxyethyl cellulose blends with metal-fiber composite at different concentrations were measured and the respective films made from the blends were studied using dynamic mechanical analysis.

## **PREFACE**

The thesis is divided into 5 parts, Chapter 1 introduces the project concept and hypothesis and Chapter 5 summaries results and presents some conclusions. Chapter 2 gives a brief literature review of packaging material, a detailed review of cellulose nanofibers and a brief review of addition of properties to cellulose nanofibers by various methods and information of the ways biomaterials can be utilized in food packaging was also discussed. Chapter 3 discusses the manufacturing methods and the characterization scheme used for the specific purpose. Chapter 4 shows the results with discussion along with the shelf life study.

## **AWKNOWLEDGEMENTS**

I want to thank my supervisors Dr. Yaman Boluk and Dr. Phillip Choi for their timely comments, opinions, ideas and most importantly, inspiration. I want to also thank them for their enthusiasm, optimism and their belief in my work. I want to thank Dr. Yussef Esparza for performing TEM on my initial samples to prove the formation of cellulose nanofibers. I want to thank Dr. Yussef Esparza, Dr. Swayamdipta Bhaduri and Dr. Xiaoyu Gong for answering my questions anywhere, anytime and commenting on the ideas that I had.

I would like to thank our project funder ‘Alberta Innovates- BFR-16-015’.

# TABLE OF CONTENTS

<b>Chapter 1</b> .....	<b>1</b>
<b>INTRODUCTION</b> .....	<b>1</b>
1.1. Introduction .....	1
1.2. Hypothesis .....	3
1.3. Objectives .....	4
<b>Chapter 2</b> .....	<b>6</b>
<b>LITERATURE REVIEW</b> .....	<b>6</b>
2.1. Food Packaging .....	6
2.1.1. Introduction to Food Packaging .....	6
2.1.2. Types of Food Packaging .....	8
2.1.2.1. Passive Food Packaging .....	9
2.1.2.2. Modified Atmosphere Packaging .....	10
2.1.2.3. Active Packaging .....	11
2.1.2.3.1. Oxygen Scavengers .....	11
2.1.2.3.2. Moisture Control .....	12
2.1.2.3.3. Carbon Dioxide Emitters and Absorbers .....	12
2.2. Biomaterials .....	13
2.2.1. Cellulose .....	14
2.2.1.1. Cellulose Nanoparticles .....	16
2.2.1.1.1. Cellulose Nanocrystals .....	17
2.2.1.1.2. Cellulose Nanofibers .....	17
2.2.1.1.2.1. Mechanical Defibrillated Cellulose .....	17
2.2.1.1.2.2. TEMPO Oxidized Cellulose .....	18
2.2.2. TEMPO Oxidized Cellulose .....	18

2.2.2.1. Mechanism.....	21
2.2.2.2. Pre-processing of Cellulose .....	23
2.2.2.3. Properties of Cellulose Nanofibers.....	24
2.2.2.4. Problems with Biomaterials.....	25
2.2.5. Possible Ways of Using Biomaterials .....	25
2.2.5.1. Coating.....	25
2.2.5.2. Blends .....	26
2.2.5.3. Chemical Modification .....	26
2.2.6. Adding Properties to Biomaterials .....	27
<b>Chapter 3 .....</b>	<b>29</b>
<b>EXPERIMENTS AND CHARACTERIZATION.....</b>	<b>29</b>
3.1. Materials .....	29
3.2. Cellulose Nanofibers .....	29
3.2.1. Preparation of Cellulose Nanofibers.....	29
3.2.1.1. Wood Pulp Pre-Processing .....	29
3.2.1.2. TEMPO Oxidation.....	30
3.2.1.3. Mechanical Defibrillation.....	31
3.2.2. Characterization of Cellulose Nanofibers.....	31
3.2.2.1. Measurement of Carboxylate Content.....	31
3.2.2.2. Thermogravimetric Analysis .....	32
3.2.2.3. Electron Microscopy.....	32
3.3. CNF-Nanolime Processing.....	33
3.3.1. Chemical Precipitation of Nanolime on CNF.....	33
3.3.2. Characterization of CNF-Nanolime Composite .....	33
3.3.2.1. Infrared Spectroscopy.....	33

3.3.2.2. Thermal Decomposition .....	33
3.3.2.3. Morphology .....	34
3.3.2.4. X-Ray Diffraction.....	34
3.4. Carbonation of CNF-Nanolime Composite.....	34
3.4.1. Experimental Setup.....	34
3.4.2. Characterization of Carbonated CNF-Nanolime Composite.....	35
3.5. Coating and Film Processing.....	35
3.5.1. Blending.....	35
3.5.2. Film Processing .....	36
3.5.2.1. Flow Properties.....	36
3.5.2.2. Film Properties .....	36
3.5.3. Paperboard Coating .....	37
3.5.3.1. Shelf Life Test .....	37
<b>Chapter 4 .....</b>	<b>38</b>
<b>RESULTS AND DISCUSSION.....</b>	<b>38</b>
4.1. Cellulose Nanofibers .....	38
4.1.1. Carboxylation .....	38
4.1.2. Thermogravimetric Analysis .....	47
4.1.4. Reassembly of Cellulose Nanofibers as an Effect of Freeze-Drying	48
4.2. CNF-Nanolime Composite.....	53
4.2.1. Attachment of Nanoparticles .....	53
4.2.1.1. Spectroscopy.....	53
4.2.1.2. Self Assembly of Cellulose Nanofiber – Lime Composite .....	55
4.2.2. Thermal Decomposition .....	58
4.2.3. Analysis of Crystallography Using X-Ray Crystallography .....	60

4.3. Aging of CNF-Nanolime Composite.....	61
4.3.1. Conformation of Formation of Calcium Carbonate Particles.....	61
4.3.2. Thermal Degradation of Carbonated Particles .....	62
4.3.3. Analysis of Crystallography of Calcium Carbonate Particles .....	65
4.4. Flow and Film Properties of CNF-Lime Composite .....	67
4.4.1. Rheology.....	67
4.4.2. Mechanical Properties .....	73
4.5. Shelf Life Test .....	75
<b>Chapter 5 .....</b>	<b>79</b>
<b>SUMMARY AND CONCLUSION.....</b>	<b>79</b>
5.1. Summary.....	79
5.2. Conclusion.....	81
5.3. Future prospects.....	82
<b>Bibliography .....</b>	<b>83</b>

# List of Tables

Table 1: TEMPO oxidation of different cellulose sources .....	39
Table 2: Results of shelf life test.....	77

## List of Figures

Figure 1: Timeline of packaging materials .....	7
Figure 2: Concept of active food packaging .....	10
Figure 3: Molecular structure of cellulose I.....	16
Figure 4: Mechanism of TEMPO oxidation of cellulose molecule .....	22
Figure 5: Schematic diagram of the test bench used for carbonation .....	35
Figure 6: Correlation between carboxylate content and primary oxidant of different cellulose sources.....	40
Figure 7: (a) Mechanically dispersed Kraft pulp in the order of carboxylate content 1,1.2,1.35,1.6; (b) BCTMP of carboxylate content 1.2,1.35,1.7 (c) image indicating the gel nature of the CNF	40
Figure 8: Films made from mechanically dispersed Kraft pulp, (b) BCTMP, (c) Beaten Kraft pulp .....	41
Figure 9: TEM images of cellulose nanofibers produced from beaten cellulose Kraft pulp (a) CNF carboxylate content 1.7 mmol (b) CNF carboxylate content 1.3 mmol (c) CNF carboxylate content 1.1 mmol; of scale 1 $\mu\text{m}$ and the respective inset image is of the scale 400 nm .....	43
Figure 10: FTIR spectra of cellulose nanofibers made from mechanically dispersed Kraft pulp	44
Figure 11: FTIR spectra of cellulose nanofibers of different carboxylate content made from mechanically dispersed Kraft pulp.....	45
Figure 12: FTIR spectra of cellulose nanofibers of different carboxylate contents made from supermasscollider BCTMP .....	46
Figure 13: TG and DTG curves of cellulose nanofibers of different carboxylate content made from mechanically dispersed Kraft pulp.....	47
Figure 14: SEM images of freeze-dried BCTMP shown at different magnifications .....	49
Figure 15: Reassembled cellulose nanofibers made from supermass collider BCTMP as a result of freeze-drying .....	50
Figure 16: Reassembled cellulose nanofibers made from supermass collider BCTMP. Individual fibers are being shown (a) CNF 1.7 (b) CNF 1.35 (c) CNF 1.23 .....	51
Figure 17: Reassembled cellulose nanofibers made from beaten cellulose Kraft pulp cellulose as a result of freeze-drying, the images are 10 microns in scale and the inset images are 200 nm scale. ....	52

Figure 18: FTIR spectra of CNF-lime made from (a) mechanically dispersed Kraft pulp (b) supermasscollider BCTMP .....	54
Figure 19: SEM images of CNF-Lime (a) CNF 1.7-Lime (b) CNF1.35-Lime (c) CNF 1.23-Lime at a scale of 20 $\mu\text{m}$ and the inset images are of 1 $\mu\text{m}$ in scale.....	56
Figure 20: SEM images of CNF-Lime (a) CNF 1.6-Lime (b) CNF1.35-Lime (c) CNF 1.23-Lime and (d) CNF 1-Lime at a scale of 50 $\mu\text{m}$ and the inset images are of 10 $\mu\text{m}$ in scale.....	57
Figure 21: TG and DTG curves of (a) CNF-lime produced from mechanically dispersed Kraft pulp (b) CNF-lime from supermasscollider BCTMP, of different carboxylate content. ....	59
Figure 22: XRD pattern of fresh CNF 1.35-lime indicating the portlandite peaks .....	60
Figure 23: FTIR curves of carbonated CNF-lime of different carboxylate contents.....	61
Figure 24: Carbonated TG and DTG curves of different CNF-limes of different carboxylate content .....	62
Figure 25: Carbonated vs fresh TGA curves and DTG curves of (a) CNF 1.23-Lime and (b) CNF 1.35-lime .....	63
Figure 26: Carbonated vs fresh CNF 1.7-lime shows the TG curve and DTG curve, indicating the increase in calcium carbonate and reduction in calcium hydroxide .....	64
Figure 27: XRD patterns of fresh CNF 1.35-lime and carbonated CNF 1.35-lime.....	65
Figure 28: XRD patterns of fresh CNF-Lime and carbonated CNF-Lime, (a) shows appearance of Whewellite; (b) shows the carbonate and hydroxide peaks.....	66
Figure 29: XRD of fresh CNF-lime and carbonated CNF-lime, indicating the peak shift.....	67
Figure 30: (a) shows storage modulus, (b) loss modulus and (c) shows the complex viscosity of CNF 1.7 at different concentrations.....	69
Figure 31: (a)(b)(c) shows the storage modulus, loss modulus and complex viscosity of CNF 1.35 at different concentrations; (d)(e)(f) shows the storage modulus, loss modulus and complex viscosity of CNF 1.23 at different concentrations. ....	70
Figure 32: (a)(b)(c) shows the storage modulus, loss modulus and complex viscosity of CNF 1.7 blended with CNF 1.7-Lime; (d)(e)(f) shows the storage modulus, loss modulus and complex viscosity of HEC blended with CNF 1.7-lime. ....	71
Figure 33: Stress-Strain diagram of different films measured by dynamic mechanical analysis; (a) CNF 1.23; (b)CNF 1.35; (c) CNF 1.7; (d) CNF 1.7 blended with CNF 1.7-Lime; (e) HEC blended with CNF 1.7-Lime; at different concentrations.....	73

Figure 34: Ultimate tensile strength of different films measured by dynamic mechanical analysis ..... 74

Figure 35: Storage modulus of the films measured by dynamic mechanical analysis ..... 75

Figure 37: Apples stored in box 1, images taken before storing (day 0) (a), day 7 (b), day 14 (c), day 21 (d), day 28 (e)..... 76

Figure 36: Apples stored in box 2, images taken after day 0 (before storing in the box) (a), day 7 (b), day 14 (c), day 21 (d), day 28 (e)..... 76

Figure 38: apple stored in Box 1 (a); apple stored in Box 2 (b) after 40th day ..... 78

## **List of Symbols and abbreviations**

BC – Beaten or refined cellulose Kraft pulp

BCTMP – Bleached chemical thermomechanical pulp

CNF – Cellulose Nanofibers

CNF<sub>n</sub> - Cellulose nanofibers and the underscore indicating the amount of carboxylic groups

HEC – Hydroxyethyl cellulose

Lime – Calcium hydroxide

Metal-fiber composite – Calcium hydroxide – Cellulose nanofiber composite

MC – Mechanically dispersed cellulose Kraft pulp

Nanolime – Calcium Hydroxide

SC – Supermass collider or grinded BCTMP

Td – Decomposition temperature

TEMPO – 2,2,6,6-Tetramethylpiperidin-1-oxyl

WV – Water vapour

WRV – Water retention value

## Chapter 1

# INTRODUCTION

## 1.1. Introduction

Cellulose nanofiber is a term referring to the nano-structure of complex interconnected fiber network of cellulose. These fibres have very high aspect ratios (length to width ratio). The typical fiber widths are in between 5-20 nm, with a wide range of lengths from 600 nm to several microns [1]. They are made from renewable source including pulp fibres, vegetable waste, crop waste and other sources. They are made from different processing methods like mechanical defibrillating, ultrasonication, micro-fluidization and 2,2,6,6-Tetramethylpiperidin-1-oxyl (TEMPO) oxidation. The TEMPO oxidation is the simplest and the most energy efficient method. It reduces the energy consumption from 30 - 72 MJ/kg to 0.2 MJ/kg, because the energy spent is only for the blending and the ultra sonication processes [2].

The TEMPO oxidized cellulose Nanofibers are shown to have better permeability property and the mechanical property is nearly as good as mechanically defibrillated cellulose. TEMPO oxidized fibres show pseudoplastic behaviour and exhibit thixotropy. Slow agitation over a certain period of time changes the viscosity behaviour and the gel eventually will regain the original viscosity when the fibrous network relaxes to original state. These properties along with the transparency of the cast film makes cellulose nanofibers the go-to choice for the selection of packaging material.

Cellulose nanofibers can also be used in a wide range of applications like in electronic devices as they have low thermal expansion, automobile bumpers, automotive parts which are exposed to high temperature changes, medicine, cosmetics, and even more making it a billion-dollar industry.

Over the past five decades, synthetic polymers such as polystyrene, polyethylene and polypropylene are the industry standards for good packaging materials. It is simply because they possess excellent barrier properties. They are mostly produced from petroleum sources and are non biodegradable and are the source of land and water pollution. Although using cellulose nanofibers can decrease the environmental impact and still maintain the industry standards for barrier properties, it is still not different from the existing packaging materials as it is a passive packaging material. The passive packaging used today increases the chances of carbon dioxide damage more than that of unpacked fruits. This is the other reason that apples and bananas are not packaged in stores. Both these cases reduce the shelf life of fruits and other fresh produce.

The alternative way of packaging is to use carbon dioxide absorbing materials to absorb the excess carbon dioxide produced. This can be done by several ways, but the easiest way is to introduce advanced properties to the cellulose nanofibers. Adding calcium hydroxide to cellulose nanofibers gives the nanofibers the necessary property to absorb carbon dioxide and increases the versatility of application. This nano composite can be used as a blend or coating with/over polymers or other biomaterials like cellulose nanofibers, hydroxyethyl cellulose, carboxymethyl cellulose for barrier material applications or can be used as an aerogel and can simply be placed under the packaging material to absorb carbon dioxide.

## 1.2. Hypothesis

Cellulose nanofibers are promising templates to grow particles on it, as it provides the necessary stability because the fibrils are distributed to give more surface area to grow a lot of particles on very small mass of cellulose nanofibers [3]. Cellulose nanofibers can hold particles twice its own weight or even higher. In this way, the surface area of the metal particles grown on the cellulose nanofibers can be increased with a larger amount of particles fixed to a fibrous network helping in the better interaction of particles with the environment. When casted the cellulose nanofiber- metal network forms a porous non-uniform film, the cellulose nanofibers lose its original property, the renewable source of cellulose nanofibers makes it a comparable and sustainable source.

Calcium hydroxide grown on cellulose nanofibers is a proper candidate for the application of active food packaging. The larger surface area of the calcium hydroxide gives the necessary instantaneous capture of carbon dioxide in a packaging film. This is necessary for packaged fresh produce like climacteric fruits (e.g., banana and apple). The detrimental effect of carbon dioxide is a well studied effect [4]. The only preventive method used currently is modified atmosphere treatment. There had not been any alternative carbon dioxide monitoring or removal system, so calcium hydroxide coupled with cellulose nanofiber is a promising alternative.

The chemical precipitation method gives the processing method a stability advantage over blending. Blending calcium hydroxide with cellulose nanofibers will not attach any particle to the fibre or the attachment will not be as strong as the attachment from the heterogeneous nucleation of calcium hydroxide on the fibre nodes. The surface area of the particles can also be reduced by heterogeneously precipitating particles as homogeneous precipitation can only give particles of

about 200 – 1,000 nm in diameter [5]. Heterogeneous precipitation has shown that the free energy barrier can be reduced by introducing non interacting template of fibres into the supersaturated salt solution, yielding smaller particles sizes and the changes of particles forming on the fibres are higher.

TEMPO oxidized cellulose nanofiber has an advantage over mechanically defibrillated cellulose nanofibers, as the surface of the molecule is chemically oxidized to form sodium salt of carboxylic acid, giving the fibres a negative surface charge. It can be hypothesized that the crystalline calcium hydroxide particles formed on the fibres select the carboxylic acid sites and the effect of carboxylation affects the growth of calcium. Even if the particles did not form on the carboxylic sites, the probability of formation of the fibres is higher as the fibre itself has a negative charge in water, zeta potential measurements show that cellulose nanofibers have a potential of -50 mV and that of calcium hydroxide is 7 mV. This also confirms that the heterogeneous nucleation of on the fibres is more favourable. The nucleation process is para-kinetic, meaning that the movement of the fibres in the solution also affects the nucleation.

### 1.3. Objectives

The objective of this project is two-fold. First, the objective is to produce cellulose nanofibers from different sources and to find

- The effect of TEMPO oxidation on different types of cellulose and its pre-processing at constant reaction time.
- Effect of NaClO on carboxylation of different cellulose and its pre-processing at constant reaction time.

- To analyze the effect of cellulose source and preprocessing on the primary properties of cellulose nanofibers, namely gelation, water retention and transparency.
- To check the self assembly of cellulose nanofibers by freeze drying and the aerogel application process.
- To check the mechanical and rheological properties at different dilutions to check the stiffness of the materials.

Secondly, the objective is to chemically precipitate calcium hydroxide on the cellulose nanofiber template.

- To chemically precipitate calcium hydroxide on CNF of different cellulose sources and carboxylation.
- To analyze the effect of cellulose self assembly on reassembly of calcium hydroxide particles
- Effect of carboxylation on shape of the calcium particles
- Effect of blending of cellulose nanofiber - calcium network on rheology and mechanical properties of cellulose Nanofiber and hydroxyethyl cellulose
- Shelf life test to study the proof of concept.

## Chapter 2

# LITERATURE REVIEW

## 2.1. Food Packaging

### 2.1.1. Introduction to Food Packaging

Petroleum based packaging materials have generated increasing concern on the environmental issues. Petroleum based packaging materials are non-biodegradable, which could take thousands of years to decompose. The plastic industry is the largest producer of oceanic waste with 42% of the total waste coming from this industry followed by building and construction industries with 19%. These wastes get accumulated together in the ocean by the oceanic currents, the largest oceanic garbage patch is near the north central Pacific Ocean aptly named “Great pacific garbage patch”. The patch is estimated to grow exponentially in the many years to come. One way to stop this is to use biodegradable materials. In the following literature review, the importance of food packaging and the types of food packaging materials are discussed.

The role of the packaging materials is to maintain the safety and quality of the packed food products during transportation and storage. The secondary aspect of a food packaging material is to limit the environmental interactions with the food thus increasing the shelf life of the food

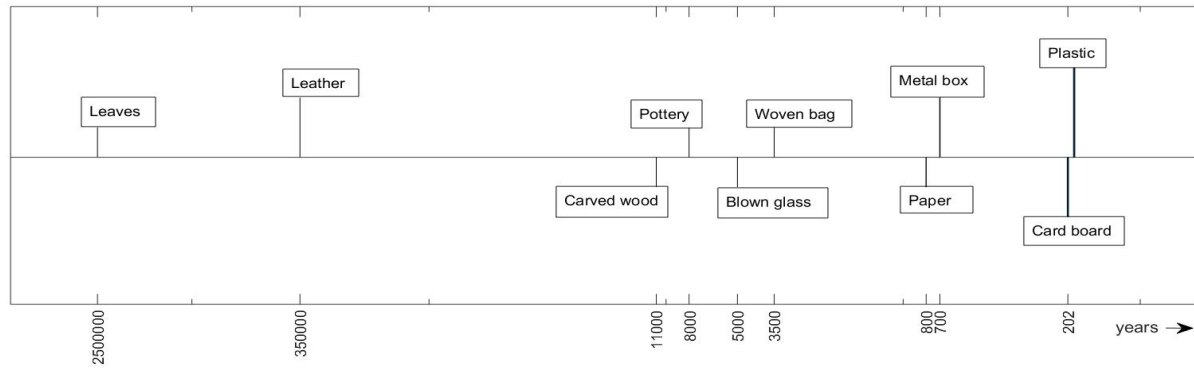


*Figure 1: Timeline of packaging materials*

product. In order for a package to protect the product and to ensure quality, the package should exhibit good mechanical strength and barrier properties. The mechanical properties include the ability to withstand impacts, carry the mass of the product stored and should have high elongation before break. The barrier properties include antimicrobial property, permeability to gases and other air borne pathogens. The first ever packaging material used was leaves, as the years progressed humans used leather. Later humans used woven sacks, carved wood, clay pots. The first ever package that was made for commercial use was blown glass. Only the past century or so the packing materials industry proliferated with innovation. Although plastics take the majority of the market, glass jars fitted with plastic or aluminium lids are still in use.

Packaging materials are usually made from multiple materials synergising the properties to make the packaging customizable per application. Only short-term storages use monolayered polymers. For any other purpose a combination of polymer, metal coating, antimicrobial coating is used. Sometimes, even additives are added in order to ease the processing of the films. Polymer coatings can be seen in paper cups, large paper board storage boxes and in other applications. Such versatility of polymers and waxes make them an everyday easy to fabricate material and it has become impossible to replace it.

Biopolymers are a viable plastic replaceable candidate. Some of the biodegradable polymers from natural sources that are in commercial use are starch, cellulose, polylactic acid and polyhydroxyalkanoates. Although biopolymers are degradable, they do not provide the necessary safe packaging environment for packaging. Biodegradable polymers, their properties and newer biodegradable materials will be discussed later in this chapter.

## 2.1.2. Types of Food Packaging

All packaging materials interact with the environment around it in different ways. Gases are the most common interaction for a packaging material as majority of the space around the packaging environment is air. The gases interact with the films with a phenomenon called permeability. Permeability is the product of solubility of gases on the film times the diffusion of gases through the film. Diffusion and solubility are in turn controlled by concentration difference between the gases inside and outside the package.

Nitrogen concentration is usually constant within the package, so the interaction of nitrogen with the film is almost unlikely, although nitrogen has no harmful effects on food. Oxygen and carbon dioxide are the most important gas interaction for a packaging film storing fresh produce, as the products respire aerobically changing the oxygen and carbon dioxide concentrations within the packaged volume. Permeation of gases through the film has some detrimental effects on the products. For example, the high permeation of oxygen could cause the product to respire at a faster rate, losing the carbon content, which causes shrinkage, water loss and browning. Browning can also be caused by excess carbon dioxide in the film. Although carbon dioxide can escape from the package to the atmosphere, it is not an instantaneous process, by the time carbon dioxide concentration reaches equilibrium, the damage would have been done. The most common example

of this type of carbon dioxide damage can be seen in apples. The exocarp of the apple shows no damage but the internal browning can be seen when dissected.

Based on the interaction of the gases with the product and the packaging film, food packaging can be classified into three types; passive package, modified atmosphere package and active package. A passive package is the most common type of packing found in a grocery store. It is usually a multi-layered polymer package (synthetic polymer). When the packaging film interacts with the gases inside the packing medium then it is classified into two, modified atmosphere packaging and active packaging. In such method of packaging the shelf life of the food can be increased. The only difference between the active and modified packaging is the method of execution. Modified atmosphere packaging does not control the atmosphere of the gases, but the gas atmosphere is completely changed/modified prior to the packing, and the gas atmosphere can be changed according to the application. In an active package, the atmosphere within the packaged volume is constantly changed as the food respire, to ensure controlled respiration rate, and no stress damage due to excess undesirable gases.

### **2.1.2.1. Passive Food Packaging**

Polyethylene (PE), oriented polypropylene (OPP) and cast polypropylene (CPP) are some of the commonly used packaging materials. These materials typically insulate the food from the environment to avoid damage from microbial activity and to reduce the premature bletting. Synthetic polymers are excellent barrier of oxygen, water vapour, microorganisms, and also has good mechanical properties. They are also a good barrier of Carbon dioxide, usually 1-1.5 times the oxygen permeability [6]. For some fresh produce like apple, strawberry, the increase in carbon dioxide over a critical value increases the solubility of ethylene, formaldehyde and other ripening

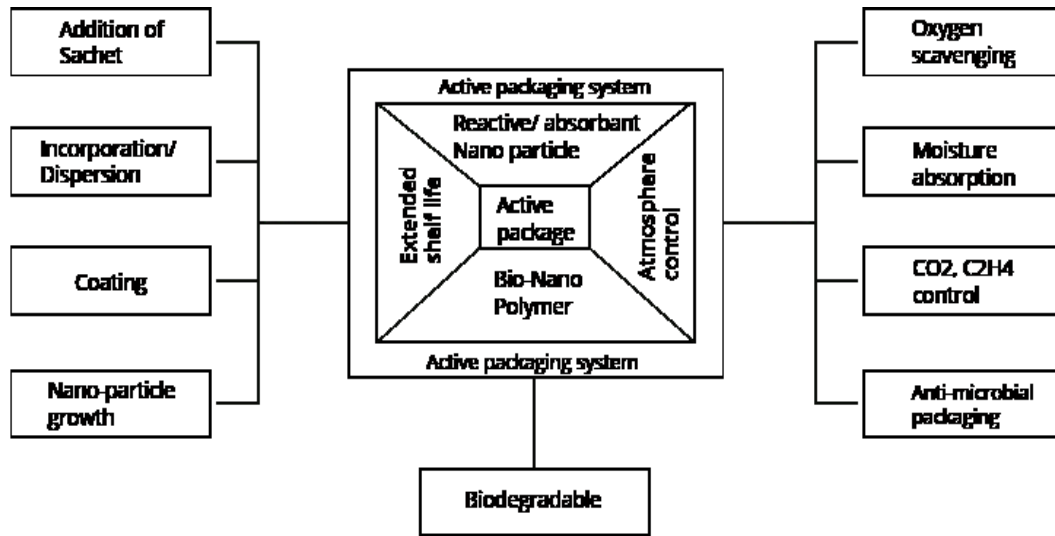


Figure 2: Concept of active food packaging

agents which are responsible for browning and rotting of foods, also known as carbon dioxide damage [4]. Passive packaging does not stop the carbon dioxide damage or internal breakdown of tissues, thus makes it a limiting factor for the shelf life of products.

### 2.1.2.2. Modified Atmosphere Packaging

Modified atmosphere packaging (MAP) is becoming the one the commonly used ways of packing fresh produce, especially chopped/cut fresh produce. MAP is defined as “enclosure of food products in gas-barrier materials in which the gaseous environment has been changed” in order to inhibit spoiling agents and therefore maintain quality, thus extend the shelf life. MAP is used to control the atmosphere surrounding the produce by continually monitoring and adjusting to maintain the optimal condition in mass storage [7]. This type of packaging technique uses the same materials as passive food packaging. The important controlling factor here is the diffusion of gases through the film, although polyethylene, poly(ethylene terephthalate) can give the best barrier properties, with time the modified atmosphere composition changes, shortening the theoretical shelf life [8]. Storing cooked meat in 100% CO<sub>2</sub> atmosphere is proven to be the safest way of

packing meat [9]. Fresh cut asparagus can be pre-treated with ozone to reduce the enzyme activity before packing [10] and this is an example of such packing method.

### **2.1.2.3. Active Packaging**

Active packaging, intelligent packaging, smart packaging refers to packaging systems used in food and pharmaceutical products to extend the shelf life, continually monitor freshness, improve safety and convenience. To avoid ambiguity, in this work we define the term “active” as having interactive functions beyond just being an inter barrier containment. “intelligent” and “smart” packaging means the ability of the package to measure an attribute of the food/package, progressive prediction of expiry date or expired product sensing, by monitoring the carbon dioxide percentage or ethylene percentage or some other techniques to help the end user.

Active packaging is defined as a system or package that involves in interactions between packaged components and food or internal gas atmosphere and complies with consumers’ demand for high quality [11]. Some of the important attributes of an active package are oxygen scavenging, carbon dioxide emitters or absorbers, ethylene emitters or absorbers, moisture control, removal of taints and food constituents. The most important concern about food packaging materials are its package related environmental pollution and disposal problems, so an active package should also be biodegradable.

#### **2.1.2.3.1. Oxygen Scavengers**

Elevated amounts of oxygen present in the package may facilitate microbial growth, off-flavours and off-odour developments, colour change, nutrition losses and higher respiration rate. These activities reduce the shelf life of the food significantly. Vacuum packaging and inert-gas flushing has provided solutions for some of the problems of oxygen sensitive foods, Meat packed with

vacuum and 100% CO<sub>2</sub> atmosphere has shown twice the shelf life when compared with air atmosphere packing, with 100% CO<sub>2</sub> giving the best result of the two methods studied [12]. Usually, oxygen scavenging chemicals are introduced into the package as sachets. Pyrogallol acid, sodium chloride, activated carbon, iron powder, iron oxide, sodium hydrogen carbonate and ascorbic acid are some of the oxygen scavenging chemicals or combination of chemicals filled in the sachet. Sachets can be efficient method of oxygen scavenging but it increases the exposure to the food products. Alternatively, these chemicals can be added to or dispersed in a packaging plastic. Photosensitisation can also be used to scavenge oxygen by exposing the packaged material to light.

#### **2.1.2.3.2. Moisture Control**

Relative humidity modifies the permeability of hydrophilic plastics. Products like cakes, can be packed in high water vapour permeable films to avoid the surface drying. In many cases, the problem is the fogging of water on the film because of the change in temperature. Microporous polymer such as polyethylene or polypropylene can work as water absorbers. Similar materials are used under whole chicken packages. Silica gel can act as water vapor buffer and humidifier type of setup can also be used.

#### **2.1.2.3.3. Carbon Dioxide Emitters and Absorbers**

Carbon dioxide can be beneficial for the storage of poultry products and meat as it inhibits microbial growth. Dry ice or a combination of chemicals can be used for such cases because the packaging materials usually have carbon dioxide permeability 2-4 times higher than oxygen permeability. Products like coffee, fresh fruits, the carbon dioxide emission due to respiration and other means is not beneficial, as it induces the production of ripening agents like ethylene,

formaldehyde, abscisic acid, anthocyanin and parascorbic acid or in the case of coffee beans ruptures the package due to increase in pressure. For such products, removal of carbon dioxide from the packaged area is necessary in order to control the ripening and bletting of climacteric fruits. Some of the carbon dioxide removers are calcium oxide, calcium hydroxide, sodium carbonate, magnesium oxide, magnesium hydroxide, activated carbon, zeolite [13]. These types of chemicals can also be used as dispersions in plastic packaging materials or used as a coating layer [14].

The increase in carbon dioxide inside the packaged area can slow down the rate of respiration of the fresh produce, as it reduces the evolution of carbon dioxide from the fresh produce and thus the ethylene solubilized in the carbon dioxide also gets trapped within the produce. This causes the so called “CO<sub>2</sub> damage” like browning of pericarp, especially visible on the exocarp region of climacteric fruits; drying of the area around the core and progressive deterioration of the fruit [15]. Using carbon dioxide absorbers can be helpful in controlling the carbon dioxide damage and extending the shelf life. The damage is not just because of the percentage of carbon dioxide in the package but also the amount of carbon dioxide. Evident from the data collected from ‘golden delicious apples’ show that with 50% carbon dioxide content at different volume, the storage at 10 l/m<sup>3</sup> and 30 l/m<sup>3</sup> produces relatively low volatiles when compared to storage at 20 l/m<sup>3</sup>. Whereas the change in CO<sub>2</sub> volume has very low effect on firmness [16].

## 2.2. Biomaterials

Biodegradable polymers or biomaterials are compounds that exist in nature or can be derived from natural sources. This is different from the biodegradable plastics like polycaprolactone (PCL) and poly (butylene succinate) (PBS) which are petroleum based. Biodegradable polymers can be

decomposed into small molecules like carbon dioxide, methane, water and inorganic compounds through enzymatic decomposition by microorganisms. To avoid ambiguity, it is important to distinguish between biopolymers and biodegradability. Biodegradability is a polymer that can be metabolized by microorganisms and fungi. Biopolymers are one type of polymer composed primarily of a few types of repeating units containing carbon which are used in or originate from biomass or polymerized from biobased monomers and those polymers produced by microorganisms [17]. Natural rubbers are probably the most commonly used natural polymer; some of the other commonly used biobased polymers are poly(lactic acid), starch, poly(hydroxyalkanoates), aliphatic-aromatic copolyesters and cellulose [18]. According to the origin and production method, biopolymers can be classified into four classes [19];

Class 1: biopolymers obtained from biomass like starch, cellulose, pectin, chitosan and proteins like collagen, casein and gluten etc.

Class 2: biopolymers obtained from usual chemical synthesis of biobased monomers like polylactic acid, bio-polyester.

Class 3: biopolymers produced by microorganism activity, some examples include bacterial cellulose, polyhydroxyalkanoates.

Class 4: biopolymers produced through chemical synthesis from both bio-derived monomers and petroleum derived monomers, for example polybutylene succinate, biobased terephthalic acid etc.

### **2.2.1. Cellulose**

Cellulose is a polysaccharide also known as polycarbohydrates as they are primarily made of carbon, hydrogen and oxygen; are polymeric fibres in biological systems. Cellulose is a linear 1,4-

$\beta$ -glucan, is the most abundant polymer as they are present in plants and trees along with lignin and hemicellulose. According to Leith and Whittaker's (1975) estimate, the amount of total standing crop is  $1.841 \times 10^{12}$  tons produced at the rate of  $1.7 \times 10^{11}$  tons/year. With a rough estimate of 50% of the crop weight is cellulose, the amount of existing cellulose is  $9.2 \times 10^{11}$  tons produced at a rate of  $0.85 \times 10^{11}$  tons/year [20]. Cellulose on an average is 70 – 75% crystalline, although cellulose behaves like an amorphous material in terms of the mechanical properties, permeability properties and film forming properties. This has limited the application of cellulose over the years.

Several types of interchangeable cellulose polymorphs have been identified depending on the inter and intramolecular interactions and molecular orientations. Native cellulose or cellulose I have the best mechanical property. Cellulose I has two forms  $I\alpha$  and  $I\beta$ , based on the linkage of the monomers, in 1 $\rightarrow$ 4 linkage  $\alpha$  glucose the monomers are in same orientation where as in 1 $\rightarrow$ 4  $\beta$  glucose every second monomer is upside down. Generally, 1 $\rightarrow$ 4  $\alpha$  glucose is called starch and 1 $\rightarrow$ 4  $\beta$  glucose is called native cellulose [21]. Thermodynamically, the  $I\beta$  can be hydrothermal annealed at about 200 °C in a number of different acidic or basic solvent media [22]. Lignin is plant structural material which supports the plant tissues. Lignin is the largest cellulose impurity, usually removed in the pulping process. Although the actual structure of lignin is unknown, various models have been proposed based on the source of the cellulose [23]. Hemicellulose is a complex carbohydrate molecule that is composed of linear as well as branched polymers of pentosans (e.g., xylose and arabinose) and hexosans (e.g., mannose, glucose and galactose), and sugar acids (e.g., galactouronic acid). The backbone of hemicellulose is either a homopolymer or a branched heteropolymer with short lateral chains linked by 1 $\rightarrow$ 4  $\beta$  glycosidic bonds and occasionally 1 $\rightarrow$ 3 glycosidic bonds. Because of the highly branched structure, hemicellulose lacks the crystalline structure. Hemicellulose and lignin can be removed from the cellulose by alkaline treatment. By

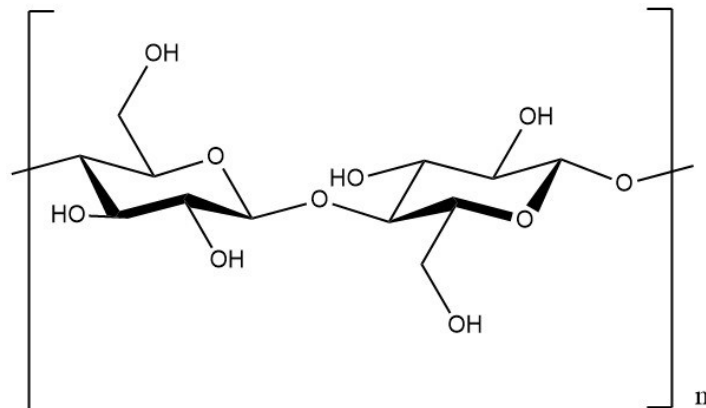


*Figure 3: Molecular structure of cellulose I*

this process, almost all hemicellulose can be removed but the lignin content of the final pulp depends on the pulping process. Bleached chemical or thermomechanical pulp have more lignin than the Kraft pulping process. Many cellulose derived water-soluble polymers of crystallinity 60 – 75 % are available, like carboxymethyl cellulose, hydroxyethyl cellulose, cellulose acetate, rayon, cellophane etc., However, the properties are not comparable to synthetic polymers. Cellulose has a primary alcohol on its structure, research efforts have been made since 1990's to use 2,2,6,6-tetramethylpiperidine-1-oxyl radical to oxidize primary alcohol to carboxylates to improve the hydrophobicity and helps to remove pectin and lignin [24]. Different forms of nanoparticles can be derived from cellulose; each has a distinctive property which are discussed below.

### 2.2.1.1. Cellulose Nanoparticles

Cellulose is a partially crystalline polymer with very high polydispersity index; thus, the randomness in the polymeric chain length and orientation makes the fibres more amorphous-like. Cellulose I is insoluble in almost all solvents, nor forms a gel with water; this affects the film formation properties of cellulose. Cellulose pulp suspensions can only yield porous white or pale-yellow sheets. The amorphous sites can be removed from the cellulose chain by acid treatment or

chemical oxidation, by doing so the characteristic dimensions of the cellulose fibres are reduced to an extent that it forms a nanomaterial. Based on the type of chemical treatment method chosen, the cellulose nanoparticles can be classified into the following types.

#### **2.2.1.1.1. Cellulose Nanocrystals**

Cellulose nanocrystals are formed by acid hydrolysis of cellulose fibres, this removes the amorphous sites in cellulose by primarily dissolving the amorphous regions, leaving a short, crystalline particles [25]. The crystallinity of cellulose nanocrystals is 80-81% depending on the cellulose source [26]. The particles have a diameter of 15 nm and length of 200-250 nm, the hydrodynamic diameter calculated from the Stokes-Einstein equation is about 95-100 nm [27]. CNC's have a higher thermal and mechanical properties when compared to cellulose, thus can be used as an additive to increase mechanical properties of cement and other materials [28].

#### **2.2.1.1.2. Cellulose Nanofibers**

Cellulose nanofibers are fibrillar network of cellulose resulting from either mechanical defibrillation of cellulose bundles or oxidation of cellulose. Although these processing of cellulose does not improve the crystallinity, it improves the formability and mechanical properties. Cellulose nanofibers form a gel in water, usually translucent, forms a transparent film when casted. There are two forms of cellulose nanofibers depending on the processing methods, one is mechanically defibrillated cellulose and the other type is TEMPO oxidized cellulose.

##### **2.2.1.1.2.1. Mechanical Defibrillated Cellulose**

When high shear is applied to cellulose bundles, the fibres bundles tend to defibrillate and form a network of entangled high aspect ratio fibrils, collectively known as cellulose nanofibers. This is usually achieved by using a machine called “super mass collider”, which is a high shear grinder

consisting of two nonporous ceramic plates operating at 1,500 rpm with a fibre concentration of 3-5 % w/w in water usually followed by sonication at 450 W and 20-25 kHz. Other methods have also been studied and they are the cryo-crushing, cryo-milling, microfluidizer. Cellulose processed through this machine form a thick gel of nanofibers in water [2].

#### 2.2.1.1.2.2. TEMPO Oxidized Cellulose

Cellulose nanofibers are formed by chemically oxidizing cellulose with the TEMPO radical. This oxidizes the primary alcohol to carboxylates and aldehydes, helping in the repulsion of the fibres from one another forming a network of fibres of high aspect ratios. Usually, TEMPO oxidized cellulose is defibrillated with a mechanical blender for a short time followed by ultrasonication [29]. Alternatively, TEMPO oxidized cellulose can also be defibrillated using super mass collider [30]. TEMPO oxidized cellulose has better properties when compared to mechanically defibrillated cellulose and consumes very less energy when compared with the latter. TEMPO oxidized CNF's are used in a variety of applications like food packaging with combination with polylactic acid, used as an additive in microneedle fabrication to increase the mechanical and thermal properties, and are also being used as 3D printing ink or bio ink for medical applications [31] [32] [33].

#### 2.2.2. TEMPO Oxidized Cellulose

Solvent interactions and chemical reactions of cellulose had been studied extensively over the years. Several modified forms of water-soluble cellulose are available commercially and are being used as functional films, membranes and in viscosity modifying applications. Primarily cellulose is used in the form of cellulose esters and ethers for such applications, cellulose acetate, cellulose nitrate are esters and carboxy methyl cellulose, hydroxyethyl cellulose are ethers. Cellulose is

hydrophobic in nature because of the presence of hydroxy groups, thus for etherification and esterification organic solvents are used and the reaction requires high temperature and long reaction time. Cellulose forms hydrogen bonds between the cellulose microfibrils, and also along the planes, it is impossible to obtain nanofibers without decreasing the microfibril length.

Prior to disintegration treatment of the cellulose, surface modification of the fibrils can substantially decrease the diameter of the fibrils leading to a higher extent of defibrillation. The chemical surface modification loosens the adhesion between cellulose fibrils, helping in the disintegration treatment. Nitrogen dioxide, sodium metaperiodate, sodium borohydride, dinitrogen tetroxide are some of the oxidizers used for cellulose oxidation, but recent interest in 2,2,6,6-Tetramethylpiperidin-1-yl)oxyl (TEMPO) radical has shown a variety of advantages, including reducing the diameter of the fibril without decreasing the microfibril length.

The TEMPO mediated oxidation is regioselective chemical oxidation of cellulose using TEMPO radical and sodium hypochlorite or sodium chlorite solution as primary oxidizer. This type of oxidation gives the advantage of oxidizing the fibres in water at room temperature. This type of catalytic oxidation gives the advantage of converting the alcoholic hydroxyl groups to aldehydes and carboxyl groups under mild conditions, without decreasing the crystallinity. Catalytic amounts of NaBr and TEMPO is required for TEMPO, although increase in TEMPO in the solution has shown to decrease the reaction time and yield in higher carboxylate content as shown in Chapter 3. Insufficient amounts of NaBr and TEMPO could increase the reaction time from hours to days and lower desired functionalities [34].

The negative charge introduced by the TEMPO oxidation by means of carboxyl units produces electrostatic repulsion in the microfibril, overcoming the interfibrillar hydrogen bonds present in native cellulose, creating a defibrillated nano-fibrillated structure.

When the fibres are chemically oxidized to form nanofibers, the semi-soluble slurry can be made into a transparent solution or suspension by applying shear force in means of either a laboratory blender or an ultrasonic homogenizer or both.

Although the carboxylation reduces the fibril length, the zeta potentials of the fibres are relatively constant ( $\sim 75$  mV) for fibres of different carboxylate contents [29]. The zeta potential measurements are constant because the Debye length of the particles are the same in water, the zeta potential calculation does not account for the surface conductivity of the fibres. There is no publication which discusses these measurements. Even if the analytical measurements accounted for the surface charge, the Dukhin number was not discussed, which gives a quantifiable measure of the surface charge.

The extent of defibrillation depends on different variables involved in the reaction. The amount of TEMPO used, amount of oxidizers used/spent, reaction temperature, external applied force (ultrasonication), oxidation time, defibrillation technique used are some of the important factors, usually the amount of oxidizer used is changed and the other factors are kept constant as the it is directly related to the amount of anionic carboxylic groups formed.

Cellulose nanofibers can be transparent, translucent or opaque depending on the processing methods and the starting cellulose fibres. When fibres of diameter 3-15 nm are densely packed the fibres does not scatter the light inside the sheet, and their appearance becomes clear transparent. Cellulose nanofibers have less than 1% haze when observed under incident light, thus forms a transparent film when casted. The light scattering of the fibres increase as the fibre diameter increases [35].

### 2.2.2.1. Mechanism

The mechanism shown in the Figure 4 indicates that the C6 primary hydroxyl groups of cellulose are converted into carboxyl groups by TEMPO/NaClO/NaBr oxidation in water at a pH of 10.5, NaOH is used as pH moderator. TEMPO is a nitrite radical which oxidises the primary alcohol from the cellulose molecule by removing the hydrogen atoms from the primary alcohol. TEMPO attracts an electron from the NaBrO which is formed from the reaction between NaClO and NaBr. The removal of hydrogen atoms from the cellulose converts the primary alcohol to aldehyde groups. The NaBrO and NaClO oxidizes the aldehydes to carboxylic acid. When the NaClO is being spent in the reaction the pH of the solution drops and initially during the reaction, the drop in pH is substantial, in order to maintain the reaction propagation, the pH is balanced to 10.5 with NaOH. NaOH reacts with the carboxylic acid to form COONa, thus producing sodium salt of polycellouronic acid.

The polyglucouronic acid formed from the oxidation in turn reacts with Na to form sodium salt of polyglucouronic acid, which can be monitored by the decrease in the pH during the reaction. Native cellulose, even in harsh conditions only produce very less amounts of water soluble uronic acid, cellouronic acid, glucuronic acid and hexeneuronic acid, whereas regenerated cellulose

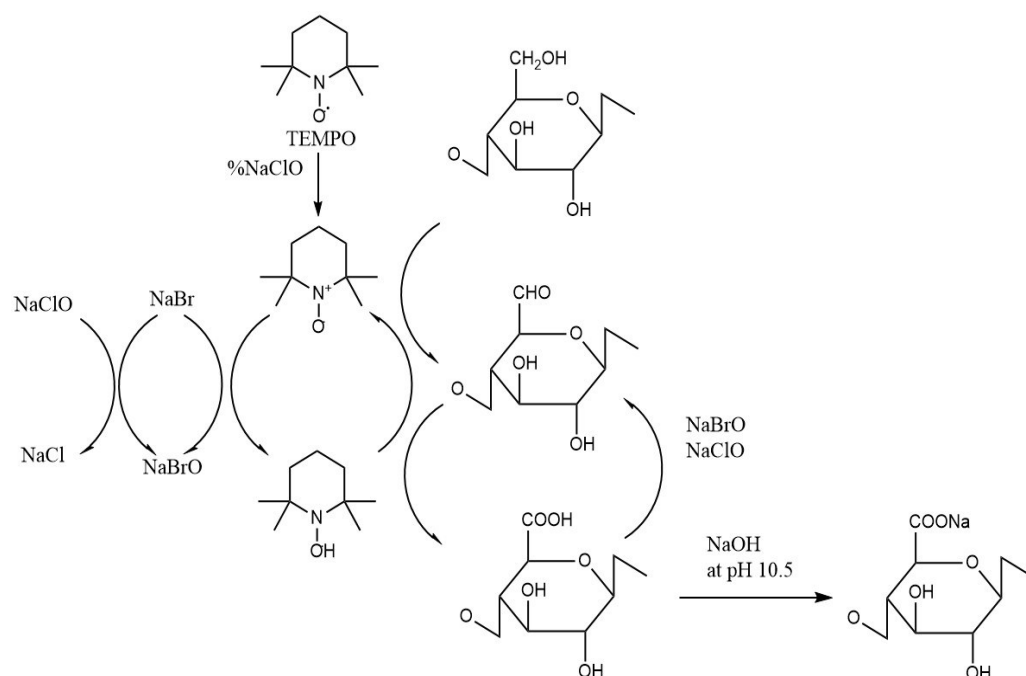


Figure 4: Mechanism of TEMPO oxidation of cellulose molecule

produces substantially high amounts of soluble under moderate conditions. This shows that the oxidation is more favourable in less crystalline cellulose. The crystallinity of the cellulosic materials can affect the oxidation reaction, as the radical has poor accessibility to the primary hydroxyl groups [36]. For high crystalline native cellulose, there is no change in crystallinity after oxidation and almost all the cellulose is insoluble after the reaction. Whereas when regenerated cellulose is used the reaction is much faster, less amount of insoluble is produced and the crystallinity of the cellulose is increased. This is also the reason for the low yield of regenerated cellulose, which is around 80% whereas for native cellulose it is higher than 90%. The soluble polysaccharides are produced because of the degradation of the oxidized polysaccharide. This reduces the degree of polymerization of the cellulose.

Solution state  $C^{13}$ -NMR containing oxidized product of  $\beta$ -(1 $\rightarrow$ 4)-anhydroglucouronic acid Na salt units, did not contain any residual C6 hydroxyl groups at 60 ppm, which was present before the TEMPO oxidation [37]. Solid state  $C^{13}$ -NMR showed a residual peak of C6 hydroxyl group present

in the oxidized product, it was quantified to be 20% from the peak calculation, which is directly dependent on the amount of carboxylation. A new peak appeared at 174 ppm shows the sodium carboxylate carbons [38].

The NMR results prove the regioselectivity of the TEMPO radical. Since the oxidation only happens on the C6 of the cellulose molecule, there seems to be no oxidation in other carbon atoms in cellulose, it is safe to assume that the oxidation only happens on the cellulose surface.

### 2.2.2.2. Pre-processing of Cellulose

Bleached wood pulps, Kraft pulps, bleached thermomechanical pulp, cotton linters, regenerated cellulose, jute fibres, etc. are some of the sources for producing cellulose nanofibers. Never dried fibres can be directly used for oxidation. When dried fibres, paperboards are used, the fibres are refined prior to oxidation. Dried films have lower water retention values which reduces the water accessibility to the cite, refining the fibres increase the water retention value. One of the widely used cellulose pre-processing technique is low consistency refining. Refining is a mechanical treatment process where the fibres are “beaten” with metallic bars. The machine applies both compression and shear to provide long straight and smooth form to fibres. This is generally used for paper making process as flattened fibres improve the bonding ability.

Alternatively, Masuko friction grinder popularly known as Supermasscollider can also be used. It uses friction generated by two non-porous grinding stones made of aluminium oxide, it enables contact grinding to produce ultrafine particle size. Two to three passes through this grinder produces particles of 100-200  $\mu\text{m}$  in size. Cellulose nanofibers can be directly produced in this machine by spending 10 kWh/Kg of energy [39].

Never dried wet pulps can be homogenized using a laboratory high speed dissolver. Such machines can also be used in post oxidation defibrillation step. One recent study shows that never dried bleached pulp can be TEMPO oxidized and then sent through the supermasscollider to produce cellulose nanofibers [30].

### 2.2.2.3. Properties of Cellulose Nanofibers

Cellulose nanofibers have higher water retention value when compared to its starting material. The retention values increase as the carboxylate content on the fibres increases. Sodium salts of carboxylic acid have shown higher degree of water retention than -COOH fibres. Water retention values signifies the swelling of the fibres in water, influenced by the distribution of the hydrophilic carboxylic groups introduced and degree of defibrillation [1]. Cellulose nanofibers have excellent permeability property. The oxygen permeability of the TEMPO oxidized standalone film is  $4.5 \text{ ml m}^{-2} \text{ day}^{-1} \text{ 0.1MPa}^{-1}$  or  $0.045 \text{ ml m}^{-2} \text{ day}^{-1} \text{ kPa}^{-1}$  [40]. Conventional synthetic polymers like PET have a permeability of about  $0.31 \text{ ml m}^{-2} \text{ day}^{-1} \text{ kPa}^{-1}$  [41], PLA has a permeability of about  $756 \text{ ml m}^{-2} \text{ day}^{-1} \text{ Pa}^{-1}$  [29]. Cellulose can be used as a coating over conventional polymers to improve the oxygen permeability of the substrate polymer; adding 0.4-micron coating over PLA decreased the permeability from 756 to  $1 \text{ ml m}^{-2} \text{ day}^{-1} \text{ Pa}^{-1}$ . In another study, the PET coated with 1.5-micron CNF had shown that the permeability of PET reduced from 0.3 to  $0.004 \text{ ml m}^{-2} \text{ day}^{-1} \text{ kPa}^{-1}$ , the study also shows that the permeability reduced even further when higher aspect ratio CNF were used. This trend of reduction in oxygen permeability also applies for PLA [42]. Adding CNF coating over PET and PLA did not have any significant reduction in water vapour permeability. The water vapor permeability of CNF is around  $23 \text{ g m}^{-2} \text{ day}^{-1} \text{ kPa}^{-1}$  at 50% RH, whereas PET has a WV permeability of  $20 \text{ g m}^{-2} \text{ day}^{-1} \text{ kPa}^{-1}$ . Permeability is also a factor of the film thickness as the diffusivity of the gas or vapor depends on the film thickness. There has been no comparison made

between PET and CNF by keeping the thickness of the film constant. Nevertheless, the permeability trend reduces as the film thickness increases, so it is well known that CNF performs better than conventional polymers in permeability property.

Cellulose nanofibers also have very compatible with conventional polymers. It has a tensile strength of about 256 MPa and an elastic modulus of 6.5 GPa.

#### **2.2.2.4. Problems with Biomaterials**

The interest for using biodegradable packaging materials from renewable sources has been increasing in the past decade or two. Although, the barrier properties, mechanical properties and poor processability properties have limited the scalable production and market use.

#### **2.2.5. Possible Ways of Using Biomaterials**

To use the biobased products as a commercial packaging material, the properties should at least match the properties of the Petro-based polymers if not make it better. There are certain ways to improve the properties of these materials some of those techniques are being Coating, Blends, Chemical modification etc.

##### **2.2.5.1. Coating**

Paper boards are widely used for mass storage and transportation of fresh produce. The permeability property of paperboards can be increased by coating it with PLA or HEC or Cellulose Acetate. Solvent casting lignin over paper board had decreased the oxygen permeability from 400,000 cc/m<sup>2</sup> day to 1,280 cc/m<sup>2</sup> day [43]. This is a simple fix to the problem, a much more sophisticated solution is coating poly(lactic acid) – paper board with aluminium oxide by either

atomic layer deposition, magnetron sputtering, or sol-gel process [44]. Atomic layer coating decreases the oxygen permeability from 400 to 2 cc/m<sup>2</sup> atm day [45].

### 2.2.5.2. Blends

Blending poly(hydroxybutyrate) can improve the crystallinity of poly(lactic acid), adding acetyl tributyl citrate can improve the mechanical properties, even the thermal stability can be improved by adding some compounds one of the material of increasing attention is being cellulose nanocrystals. Melt mixing and extrusion is one of the ways to process such transparent films. Addition of CNC-ATBC-PHB to PLA have shown 150% elongation at break, which is a significant improvement from the 41% elongation of PLA. This also improved the oxygen transmission rate of PLA by 24% [46]. Similar improvement in elongation at break can also be observed with just limonene blends but it increased the oxygen transmission rate by half [47], even in the CNC-ATBC and PLA-PHB blends, without addition of ATBC the OTR was 13 cc mm/ m<sup>2</sup> day, which is 80 % improvement from 30 cc mm/ m<sup>2</sup> day of PLA. It is a sweet spot between the mechanical property and permeability property.

### 2.2.5.3. Chemical Modification

Polymers like starch, cellulose can be surface modified to incorporate improved properties without the need for blends or coatings. Starch can be surface modified to form starch nanocrystals [48], which can be further used in ring opening polymerization of caprolactone to form starch nanocrystal-g-PCL copolymer, thus improving the properties of starch [49]. Cellulose can be surface modified into Nanocrystals and Nano-Fibres, each having its own unique properties. Cellulose Nanocrystals and nanofibers are made from acid hydrolysis and base oxidation of cellulose pulp [50], thus giving cellulose high strength and crystallinity.

## 2.2.6. Adding Properties to Biomaterials

Increased studies in the addition of properties have been carried out recently. Studies have shown that bioactive ingredients can be added to the packaging material to give it specific target properties to specific applications. These types of materials are called fillers, which gives improved optical and mechanical properties delivering unique functions by their use. Cellulose acts as a soft matrix to grow inorganic fillers to produce composites that bring together the special functionalities that was discussed before. Some of the nanoparticles that can be added to cellulose nanofibers include, Silver, Gold, Copper, Iron, calcium etc.

These nanoparticles can be added to cellulose in two different ways, 1. crystal growth or chemical precipitation, 2. blending. Blending can be done by adding direct colloidal suspension of the compounds to fibre. This does not yield a homogenous distribution of nanoparticles. In situ chemical precipitation deals with salt double decomposition on the cellulose fibres.

Chemical precipitation is driven by two main theories, coprecipitation theory and deposition theory. The coprecipitation depends on the heterogeneous nucleation of the supersaturated salts. The nucleation is propagated by the degree of supersaturation. When a tertiary inert system is introduced into the equilibrium, the rate of homogeneous nucleation is zero. The addition of an inert substrate reduces the height of the free energy barrier, thus only heterogeneous nucleation occurs. The formation of nucleus depends on the contact angle between the salt solution droplet and the horizontal surface, in this case the surface of cellulose nanofibers. When the droplet has less surface contact angle then faster nucleation on the surface of the substrate. TEMPO oxidized cellulose has an advantage in reducing the nucleus size as it has negatively charged carboxylate

groups on its surface, the chances of particle forming on the carboxylate groups is higher as all the metal ions are cationic.

In the deposition theory, the liquid phase nucleates to form crystals and forms a colloidal suspension; later, the colloidal suspension deposits on the cellulose and further grows in contact with the liquid phase.

## Chapter 3

# EXPERIMENTS AND CHARACTERIZATION

## 3.1. Materials

Bleached Chemi-Thermo Mechanical wet pulp (processed from Super Mass Collider) was supplied by Alberta Innovates, “beaten” hardwood Kraft pulp was also supplied by Alberta Innovates, Hardwood Kraft pulp paper board and sigma Aldrich microcrystalline cellulose, was used as cellulose sources. TEMPO (2,2,6,6-Tetramethylpiperidin-1-yl) oxyl, sodium bromide, sodium hypochlorite solution (10-15%), calcium hydroxide tetrahydrate, sodium hydroxide, hydrogen chloride, hydroxyethyl cellulose and other chemicals and solvents were purchased from Fischer Scientific. The chemicals were used without further purification.

## 3.2. Cellulose Nanofibers

### 3.2.1. Preparation of Cellulose Nanofibers

#### 3.2.1.1. Wood Pulp Pre-Processing

Cellulose fibres cannot be directly used for the TEMPO oxidation process. In the case of never dried wet pulp, no further processing is needed and it is the easiest cellulose source to oxidize [51]. The dried cellulose sheets can be dispersed in water using different methods, each of them having an advantage over the other, as the fibres lose the accessibility and reactivity during drying [52].

Paper boards are mostly made from hot press, making the fibres more grafted and non accessible for oxidation. This is the first time a raw paper board sample was used for the oxidation process.

All the cellulose sources were once dried when purchased. The hardwood Kraft pulp was mechanically dispersed in water with a concentration of 1% w/w using a laboratory mechanical stirrer. This sample is given a code name MC (mechanical dispersed cellulose). Hardwood Kraft pulp was sent through a refiner at a concentration of 2.5-3%, the beaten cellulose obtained was then diluted to 1% and dispersed using a mechanical stirrer, this sample is called BC (Beaten cellulose). The Bleached thermomechanical pulp was sent through a wet grinder at a concentration of 2.5-3% w/w using a “supermass collider” [53]. This cellulose is called SC (supermass collider cellulose).

### 3.2.1.2. TEMPO Oxidation

All the cellulose slurry from the preprocessing was 3% w/w solid samples. First, the suspension was diluted to 1% w/w, by adding calculated amounts of deionized (DI) water. 1-5 mmol of TEMPO was dissolved in this 1% cellulose suspension. Then, 0.5 g of sodium bromide was mixed to the solution. The reaction was started by adding desired amounts of NaClO, to the mixture. The solution turned yellow when NaClO was added, when the reaction proceeded, the solution turned pale yellow before turning pale brown. The pH of the solution was maintained at 10.5 for five hours with 0.5 M HCl and 0.5 M NaOH solutions [54] [55]. The drop in pH was rapid initially during the reaction and the pH drop reduced as the reaction proceeded. There was no pH change observed around about 2 hours from the start of the reaction. The mixture was stirred at 600 rpm with a magnetic stirrer.

The reaction was quenched with 5 ml ethanol, and the oxidized cellulose solution was filtered and washed with DI water for a few times. The washed insoluble fraction was re-dispersed in water, and the samples were centrifuged until the supernatant conductivity was constant or equal to the conductivity of DI water used. The centrifuged sample was collected and re-dispersed in water to make a 1% w/w suspension. The other cellulose sources were also oxidized in a similar fashion.

### **3.2.1.3. Mechanical Defibrillation**

The re-dispersed oxidized cellulose collected from the centrifugation step was then mixed well with water using a magnetic stirrer at 1% w/w solid concentration until the solution was uniform and the suspension was further defibrillated with a laboratory blender for about 5 min, this resulted in a gel. The gelation can be observed by the change in flow pattern of the fluid in the blender. Gelation can be tested by centrifuging the sample at 20,000 rpm. The nanofibre gel was then further ultrasonicated for 1 hour. About 5 ml was dried to measure the mass recovery ratio.

## **3.2.2. Characterization of Cellulose Nanofibers**

### **3.2.2.1. Measurement of Carboxylate Content**

The carboxylate content of the sample was measured using the strong acid – strong base potentiometric titration method. The measurements were made using SCAN-CM 65:02 total acid group content conductometric titration method. To a 10-15 g of cellulose suspension 90 ml of water was added and stirred at 500 rpm. The pH of the solution was brought down to 2-3 using 0.1 M HCl, to this solution 5 ml of 0.01 M NaCl was added and the solution was sufficiently stirred for 15 mins. A 0.05 M NaOH solution was added at a rate of 0.01-0.1 ml/min until the pH of the solution reaches 11 or when the change in conductivity rised back to its original value [56]. The

carboxylate content can be calculated using the conductivity vs volume plot, by drawing 3 tangents to the resultant curve. The carboxylate content can be calculated using the following equation.

$$\text{Carboxylate content (mmol/g of cellulose)} \\ = \frac{\text{Volume of NaOH (ml)} * \text{concentration of NaOH (M)}}{\text{amount of solids (g)}}$$

The presence of carboxylates was confirmed using Fourier transform Infrared Spectroscopy (FTIR). The measurement was made with FTIR-is50, in ATR mode. About 0.4 mm thick sample was made using film casting method to make the measurements. The measurements were made with transmittance mode with 64 scans.

### 3.2.2.2. Thermogravimetric Analysis

About 5 mg of the sample was placed in a high temperature platinum pan, and the thermal decomposition was measured using Discovery TGA analyser. The temperature sweep was set to 1,000 °C at a rate of 20 °C/min with a nitrogen flow of 20 ml/min, after the sample was kept in an isothermal condition for 3 min. The weight loss vs temperature was plotted.

### 3.2.2.3. Electron Microscopy

The morphologies, particle size and the extent of defibrillation were analysed with scanning electron microscopy using the Zeiss Sigma FESEM. The sample was prepared by freeze drying 10 µl of CNF in 1 ml of DI water. The freeze-dried sample was placed on a carbon tape and carbon coated with Leica ACE600 carbon coater. The coating thickness was 5 nm, at a pulse rate of 0.1 nm/min. The imaging was performed under field emission mode with an accelerating voltage of 10 to 15 kV. The images were analysed and processed using ImageJ.

### 3.3. CNF-Nanolime Processing

#### 3.3.1. Chemical Precipitation of Nanolime on CNF

100 ml of 0.2% w/w cellulose nanofibres were mixed with 250 ml of 0.4 M calcium hydroxide tetrahydrate solution and stirred for 10 min at 35 °C with a stirring speed of 600 rpm. To this mixture, under the conditions of stirring, 250 ml of alkaline 0.4 M NaOH solution was added drop wise for one hour [57]. A white precipitate of calcium hydroxide was produced. The precipitate was filtered with Whatman paper, the sodium nitrate by-product was removed by washing and centrifuging a few times with DI water. The centrifuged sample was then stored under excess water at 4 °C to avoid drying and carbonation.

#### 3.3.2. Characterization of CNF-Nanolime Composite

##### 3.3.2.1. Infrared Spectroscopy

The synthesised fibrous material was then characterized with Fourier transform infrared spectroscopy (FTIR), the spectrum was recorded in the range of 400-4000  $\text{cm}^{-1}$ . The FTIR was used for the measurements under attenuated total reflectance transmittance mode with 64 scans. Freeze dried samples were used for the measurements.

##### 3.3.2.2. Thermal Decomposition

About 5 mg of the freeze-dried sample were placed on high temperature platinum TGA pan. Discovery TGA analyser was used for the measurements, with a temperature ramp of 1,000 °C at a rate of 20 °C/ min with a nitrogen flow of 20 ml/min after the samples were soaked in isothermal

condition for 3 mins. The weight vs temperature curve was further analysed with TRIOS (TA instruments) software and MATLAB.

### 3.3.2.3. Morphology

The morphology, particle size of the calcium hydroxide particles, attachment of the calcium hydroxide particles to the fibers was observed using a Zeiss Sigma FESEM. The sample was prepared by freeze-drying 10  $\mu$ l of the sample dispersed in 1 ml of DI water. The freeze-dried sample was coated with carbon sputter. Although calcium is conductive, the cellulose is almost invisible. This was the reason carbon sputter was used. Because of the aforementioned method, the calcium particles might look brighter than the fibre, making the particle resemble a pearl. The image was further analysed with ImageJ.

### 3.3.2.4. X-Ray Diffraction

The crystallography of the sample was measured using Bruker XRD. Powdered samples were used for the measurements. The measurements were made for the  $2\theta$  value from 8 to  $110^\circ$  with an x-ray accelerating voltage of 40 kV and 30 mA of amperage. The divergence slit orifice was set at 0.3 with a scan speed of 5 degrees per min. The data was analysed with JADE software (Materials Data, Inc).

## 3.4. Carbonation of CNF-Nanolime Composite

### 3.4.1. Experimental Setup

To induce the carbon dioxide capture, the freeze-dried samples were kept in a reactor (Parr instrument company). All samples were kept inside vials protected with kimwipes. Along with the

samples, a vial of water was also kept inside the reactor to ensure that the humidity inside the reactor reaches 100%. The reactor was connected to a carbon dioxide cylinder, and the pressure inside the reactor was maintained at 100 kPa for 7 days. The process instrumentation diagram is shown in the figure below.

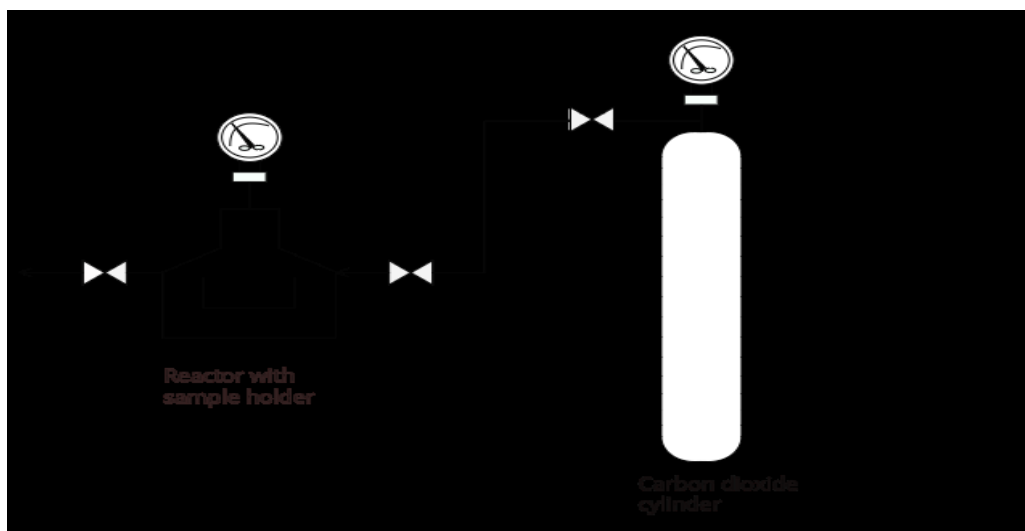


Figure 5: Schematic diagram of the test bench used for carbonation

### 3.4.2. Characterization of Carbonated CNF-Nanolime Composite

Fourier transform infrared spectroscopy, scanning electron microscopy, thermogravimetric analysis and X-ray diffraction analysis were done using the characterization method discussed in Section 3.3.2.

## 3.5. Coating and Film Processing

### 3.5.1. Blending

Cellulose nanofibre – lime metal composite suspension was blended with cellulose nanofibre of a carboxylate content of 1.7 made from BCTMP at 0.8% gel concentration and hydroxyethyl

cellulose (10%) at different suspension concentrations. The CNF 1.7-CNF-lime blend appeared to be like a slurry and lost its gel like appearance once CNF-lime was blended to it. HEC CNF-lime blend on the other hand maintained its gel appearance.

### **3.5.2. Film Processing**

Cellulose nanofibers and CNF-nanolime were made into standalone films using the film casting method. All the films were made by transferring 10 ml of the sample to a polystyrene petri dish and then allowed to air dry for 4 days. The CNF films were transparent in appearance, CNF – CNF/lime blends were translucent to opaque and the HEC CNF/lime blends had a yellowish tint. The CNF films were about 400-100 microns thick. The blend films were about 700-800 microns in thickness.

#### **3.5.2.1. Flow Properties**

The rheology of CNF, CNF-nanolime, CNF-nanolime-CNF and CNF-nanolime-HEC was measured using TA Instruments AR 2000. The CNF samples at different dilutions were prepared by adding water to the sample and stirring for 20 mins, followed by 10 mins to ultrasonication. The blend samples were also produced using the same condition. The samples were tested under frequency sweep tests to measure storage and loss modulus, to observe the viscoelastic properties of the suspensions.

#### **3.5.2.2. Film Properties**

The films made from the different blends at various concentrations and cellulose nanofibres at different dilutions were tested mechanical analysis to measure the stress – strain behaviour of the films. From this measurement, the ultimate stress or the failure of the material was measured.

Based on the behaviour of the material the tensile strength, stiffness of the material was also measured.

### **3.5.3. Paperboard Coating**

Paper board of size 20x20 cm was cut, 6 of the squares were coated with hydroxyethyl cellulose (10%). On each square, 20 ml of the sample was spread and air dried for 7 days. On the other squares, 20 ml of HEC(10%) blended with 10% CNF-Lime and air dried for 7 days. The boxes were sealed with cellophane tapes and paper tapes to make a box.

#### **3.5.3.1. Shelf Life Test**

The boxes prepared from paperboards coated with HEC and HEC-CNF-lime were sealed. Apples of similar appearance and hardness was randomly chosen. The HEC coated box was named Box 1, and the box coated with HEC-CNF-lime was named Box 2. The box was opened after every 7 days for 4 weeks to check the appearance and harness.

## RESULTS AND DISCUSSION

### 4.1. Cellulose Nanofibers

#### 4.1.1. Carboxylation

The carboxylate content measured from the potentiometric titration was analysed to find the amount of carboxylate content. Table 1 shows the carboxylate content of the native fibres and the corresponding TEMPO oxidized products were analysed in a similar fashion. Figure 6 shows the effect of the primary oxidant NaClO on oxidation of cellulose. Kraft pulp is the easiest to oxidize as it only requires a very small amount of NaClO to increase the carboxylate content of the cellulose above 1 mmol/g of cellulose. Almost twice as much of primary oxidizer is required for BCTMP to reach similar carboxylation values as Kraft pulp. This could be because of the higher lignin, as the residual hemicellulose and lignin content of the thermomechanical pulp can cause the resistance to oxidation by TEMPO radicals [58].

Table 1: TEMPO oxidation of different cellulose sources

Cellulose	Na ClO	Reaction time	Total reaction time	Carboxylate content	Gelation	water retention values	Appearance
MC	5	45	5	1	Yes	89	2
	6	60	5	1.2	Yes	113	2
	7	90	5	1.3	Yes	194	2
	9	105	5	1.6	Yes	216	1
BC	5	120	5	1.1	Yes	26	3
	7	150	5	1.3	Yes	38	3
	9	200	5	1.7	Yes	121	3
SC	12	60	5	1.23	Yes	64	4
	15	90	5	1.37	Yes	103	4
	20	120	5	1.7	Yes	119	2
Microcrystalline Cellulose	5	15	5	-	NO	-	-
	7	20	5	-	NO	-	-
	9	20	5	-	NO	-	-

1. Transparent 2. Translucent 3. White 4. Pale yellow

After the TEMPO oxidation process, the fibres form a gel with the help of blender. The fibres which are white in color turn to translucent or sometimes transparent depending on the starting fibre and the carboxylate content. As shown in Figure 7, the color of the suspension becomes more transparent as the carboxylate content reaches 1.7 mmol/g of cellulose in the case of hardwood.

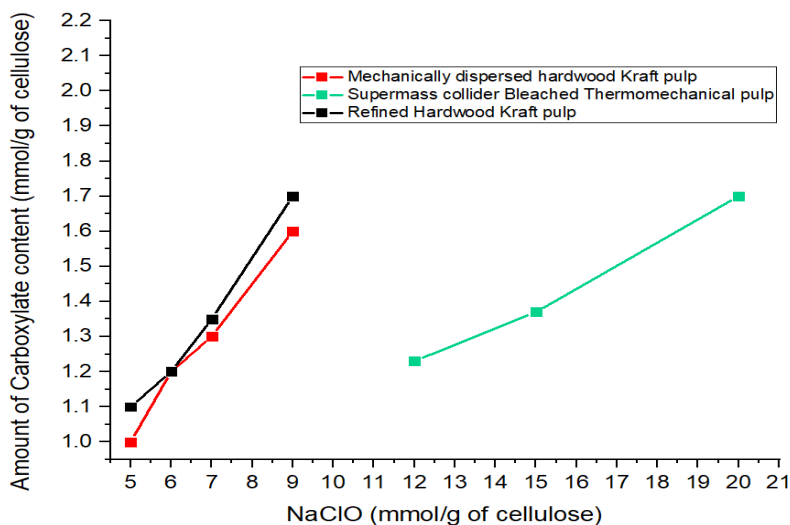


Figure 6: Correlation between carboxylate content and primary oxidant of different cellulose sources

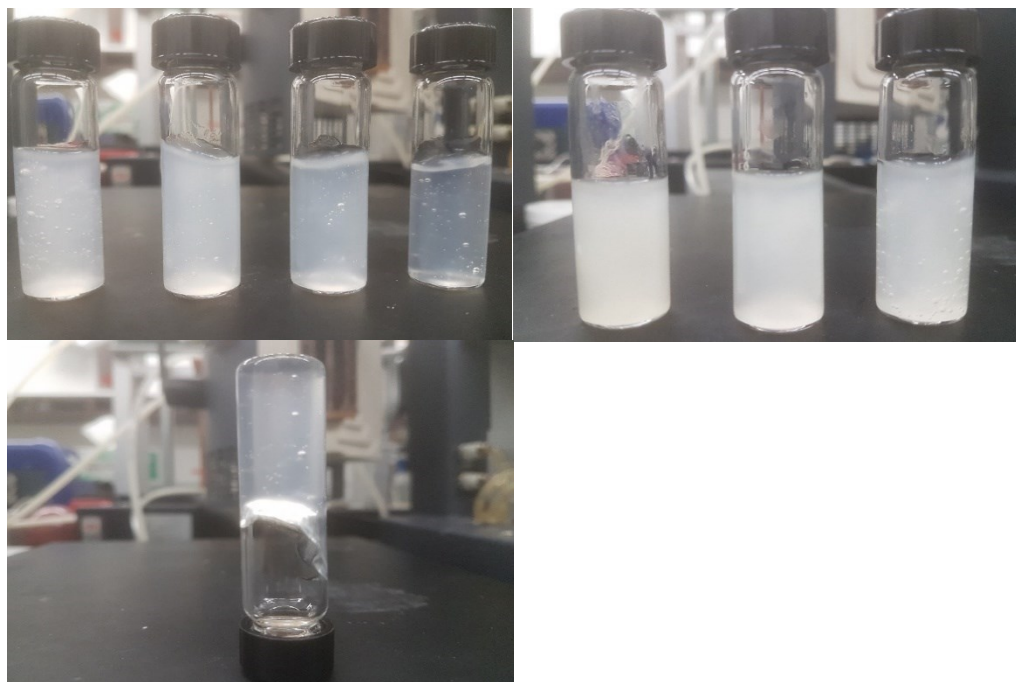


Figure 7: (a) Mechanically dispersed Kraft pulp in the order of carboxylate content 1, 1.2, 1.35, 1.6; (b) BCTMP of carboxylate content 1.2, 1.35, 1.7 (c) image indicating the gel nature of the CNF

The water retention values of the water insoluble fractions are obtained from TEMPO mediated oxidation at different oxidation levels. The WRV increased roughly linearly with increasing in the carboxylate content of the water insoluble fraction. The retention values are influenced by the fines fraction and the ability of the fibers to swell. The increase in WRV is because of the shorter fibers formed from the higher carboxylate content or in other words the higher oxidation. This shows that WRV can be controlled by the amount of oxidation and the oxidation time. The WRV of the beaten cellulose Kraft pulp is very low and remained almost constant relatively to the starting



*Figure 8: Films made from mechanically dispersed Kraft pulp, (b) BCTMP, (c) Beaten Kraft pulp fibers. In the case of mechanically dispersed cellulose the water retention increased substantially and formed the most stable suspensions.*

The defibrillation of the cellulose nanofibers can be visually confirmed by observing three distinctive features of the suspension. After washing the TEMPO oxidized fibres, the suspension was white in color. To avoid agglomeration or drying of fibers during the washing and centrifugation process the suspension was always maintained at about 1% solid concentration by

assuming the yield to be around 85% to 95% depending on the fiber (These are values extensively discussed in the literature), and reducing the centrifugation speed from wash to wash.

Cellulose nanofibres form a gel when blended using a laboratory blender or a probe homogenizer. Mechanically dispersed Kraft pulp, beaten Kraft pulp and supermass collider thermomechanical pulp became a gel after blending. Kraft pulp forms a gel much quicker than TMP, the gelation can be observed at about 20-30 seconds into blending where as in TMP it would take around 2-3 mins.

Microcrystalline cellulose did not oxidize. There was no change in pH during oxidation indicating no formation of carboxyl groups. The microcrystalline cellulose did not suspend in water. This indicated that the higher the crystallinity the harder the oxidation, in this case no oxidation. Although microcrystalline cellulose can be solubilized in water prior to oxidation with the help of sodium hydroxide and cooling the mixture to  $-20\text{ }^{\circ}\text{C}$  or using a supercooled sodium hydroxide solution, this would convert the microcrystalline cellulose to cellulose II. The gels are shown in Figure 7. The gels are transparent when formed into a gel. The final observational feature was the transparency when casted as a film. The films are shown in Figure 8. The Kraft pulp was transparent, whereas the bleached thermomechanical pulp had a yellowish tint.

The transmission electron microscopy images of cellulose nanofibers prepared from the beaten Kraft pulp is shown Figure 9. The fibres were about 4-8 nm in diameter and the average diameter of the fibers decreased slightly as the carboxylation increased. The average diameter of the sample with a carboxylate content 1.7 mmol/g of cellulose was 4.4 nm, that of carboxylate content 1.3 was 5 nm and that of carboxylate content 1.1 was 5.3 nm. The fibres were well dispersed and

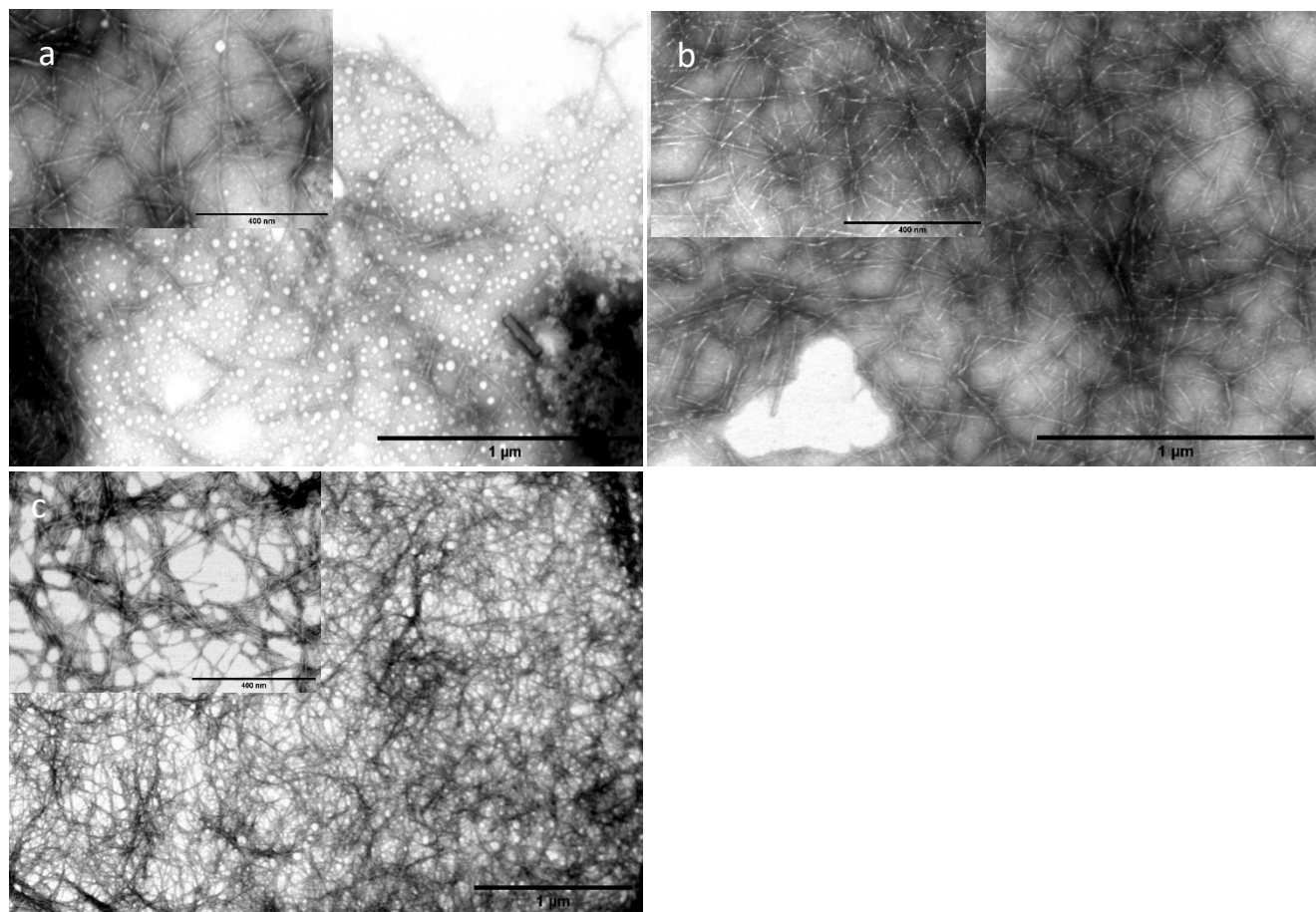


*Figure 9: TEM images of cellulose nanofibers produced from beaten cellulose Kraft pulp (a) CNF carboxylate content 1.7 mmol (b) CNF carboxylate content 1.3 mmol (c) CNF carboxylate content 1.1 mmol; of scale 1  $\mu\text{m}$  and the respective inset image is of the scale 400 nm*

individualized as the carboxylation increased. The images shown that the fibres are shorter as the carboxylate content increased. This also reduced the entanglement of the fibers. This observation also revealed that the fibres of tens of microns in diameter was reduced to just a few nanometers. The nanofibre widths are smaller than the wavelength of visible light. This is the reason that the

cellulose nanofiber suspensions in water and its cast films are transparent. These individualized fibres also prove that the presence of anionic charged sodium carboxylic groups cause the fibres to stay separated in a suspension giving it the characteristic gel appearance in water.

During the mechanical blending process, the increase in the viscosity also indicates the degree of defibrillation. The smaller the fiber diameter and longer the fibers were (i.e., fibres have higher aspect ratios), the water retention ratio was higher. This can be noticed in Figure 7 image (c), the gel has high enough viscosity that it flows very slowly under gravitational pull.

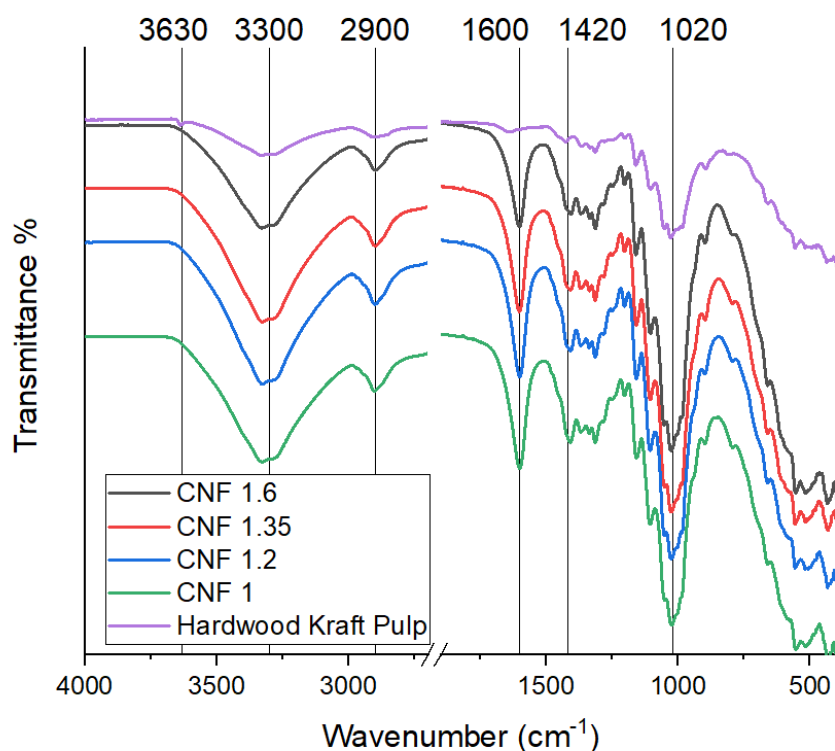


*Figure 10: FTIR spectra of cellulose nanofibers made from mechanically dispersed Kraft pulp*

The FTIR spectra of the cellulose and the cellulose nanofibers from the Kraft pulp is shown in Figure 10. The dominant peaks of OH stretching and C=O stretching are at approximately 3,300 and 2,900 cm<sup>-1</sup>. Alcohol OH stretching can be observed near 3,630 cm<sup>-1</sup> in the non-oxidized hardwood Kraft pulp. This disappears when the fibres are oxidized. Strong carboxylic salt

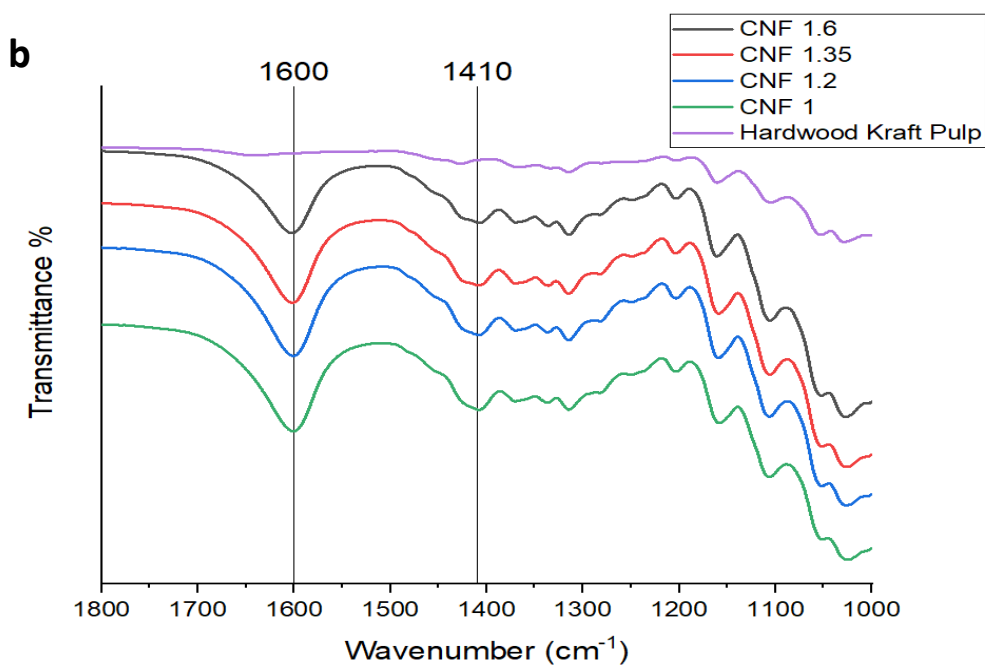
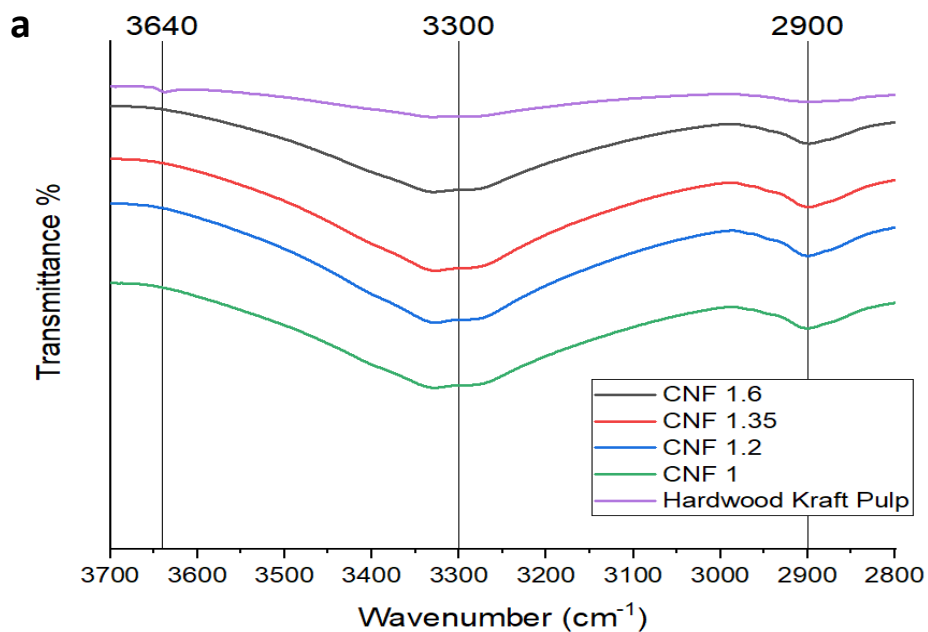


*Figure 11: FTIR spectra of cellulose nanofibers of different carboxylate content made from mechanically dispersed Kraft pulp*

stretching can be observed in all the oxidized fibres at  $1,600\text{ cm}^{-1}$ . Hardwood Kraft pulp has around  $0.1\text{ mmol}$  of carboxylic group (mostly  $\text{COOH}$ ) per gram of cellulose. This can be observed by a small peak around  $1640$ . This indicates that the addition of sodium hydroxide during the oxidation

process helped in the formation of COONa on the cellulose fibres. Strong C-O stretching can be observed at  $1,420\text{ cm}^{-1}$  and  $1,020\text{ cm}^{-1}$ . A very small peak around  $1,350\text{--}1,450\text{ cm}^{-1}$  shows -C-H bending. This could be because of the primary alcohols as the oxidized fibres do not have a distinctive peak.

Infrared spectra of bleached thermomechanical pulp from the supermass collider is shown in Figure 12 along with the oxidized cellulose fibers of different carboxylate content. Similar to the hardwood Kraft pulp, a strong broad peak at  $3,300\text{ cm}^{-1}$  and a weak broad peak  $2,900\text{ cm}^{-1}$  can be observed, indicating OH stretching and C=O stretching. Sharp peaks around  $1,600\text{ cm}^{-1}$  can be observed in all the samples, indicating the presence of COONa. Thermomechanical pulp could also have COONa on its surface because of the bleaching process. A C-C shoulder peak can be observed at  $1660\text{ cm}^{-1}$  in BCTMP, this peak would become hard to locate in the oxidized samples

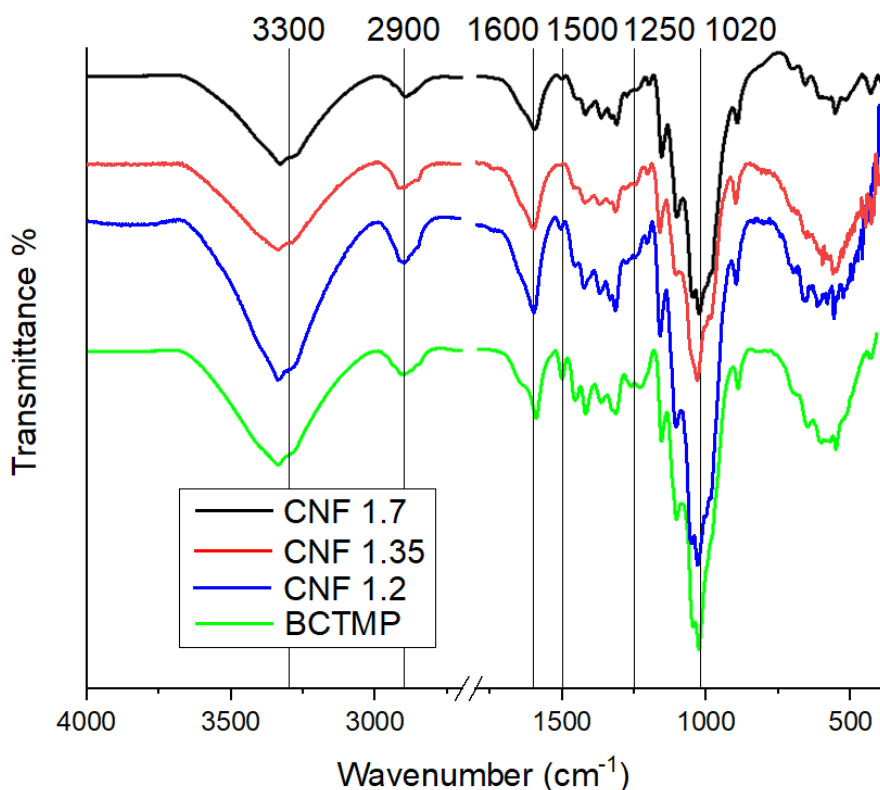


Figure 12: FTIR spectra of cellulose nanofibers of different carboxylate contents made from supermasscollider BCTMP

as the carboxylate peak has a symmetric sharper peak. A small sharp peak at  $1,500\text{ cm}^{-1}$  and weak broad peak at  $1,250\text{ cm}^{-1}$  shows CH bending, this could be because of the alcohols as this peak reduces as the oxidation increases. A typical CO stretching can be observed at  $1,020\text{ cm}^{-1}$ .

#### 4.1.2. Thermogravimetric Analysis

Thermogravimetric analysis and the corresponding derivative thermogravimetric (DTG) curves of the TEMPO oxidized cellulose with sodium carboxylate groups made from Hardwood Kraft pulp are shown in Figure 13. There are three decomposition points on the curve. The first decomposition occurs right after  $40\text{ }^{\circ}\text{C}$  and the decomposition reaches a plateau at around  $100\text{ }^{\circ}\text{C}$ . This decomposition is due to the water evaporation and yields the smallest derivative peak as the sample was a freeze-dried one. Unlike cellulose, the largest decomposition curve of TEMPO oxidized

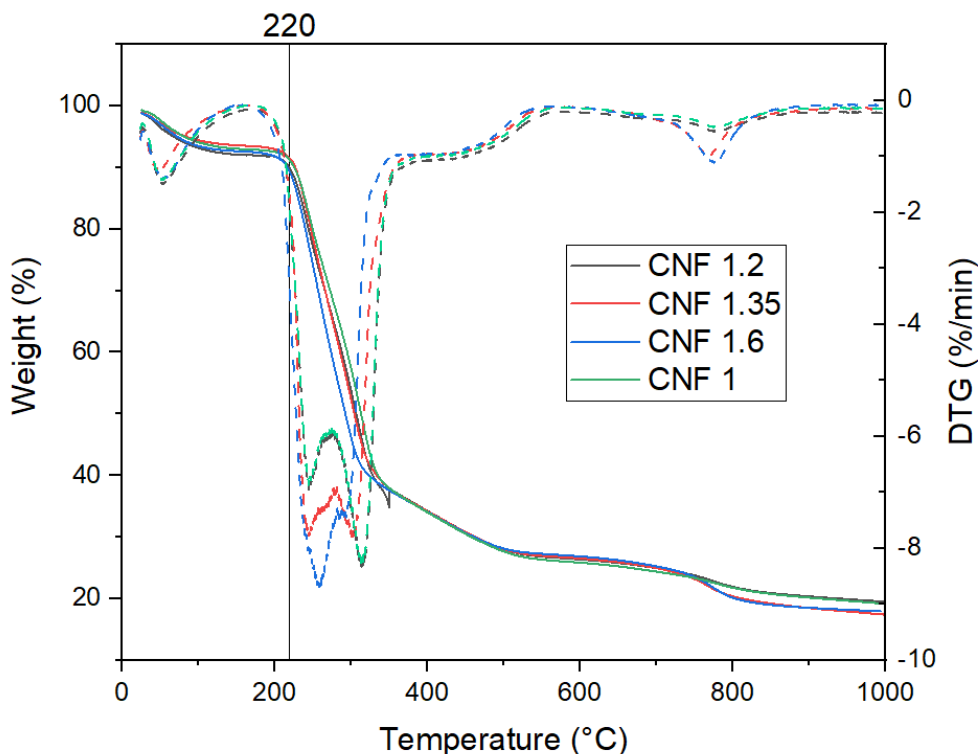


Figure 13: TG and DTG curves of cellulose nanofibers of different carboxylate content made from mechanically dispersed Kraft pulp

cellulose is bimodal. This decomposition occurs at approximately 220 °C, the decomposition of cellulose occurs at much higher temperature, usually over 300 °C [59]. As the oxidation only occurs on the surface of the cellulose molecule, the reduction in decomposition temperature should be because of the sodium carboxylate groups. The modes of the bimodal curves occurred around 256 and 314 °C, cellulose has Td around 320 °C as a result of the degradation of anhydroglucuronate units [60]. The third decomposition occurs at 750 °C, DTG shows that the decomposition is less than 5%. This is attributed to the cracking of functional groups in the cellulose residue [61]. The final residue at 1,000 °C was around 18%.

#### 4.1.4. Reassembly of Cellulose Nanofibers as an Effect of Freeze-Drying

Cellulose nanofibres can be reassembled by freeze drying at lower concentration. This phenomenon is observed at a weight percentage less than 1%. Cellulose nanofibre gel was diluted to about 0.1% w/w. The sample was frozen in two stages. In the first stage, the sample was frozen in a laboratory freezer and then was immersed in liquid nitrogen for 5 mins. The liquid nitrogen freezing generated small ice crystals to avoid any effect of water sublimation on the self-assembly. The freeze drying was carried on at -60 °C and 0.1 Torr. The frozen and lyophilized fibres were sponge-like and appeared white in color. All the samples visually looked the same. The fibres lose the nanostructure and form a substantially large macrostructure. Freeze dried 0.1% CNF suspensions of supermass collider thermomechanical pulp and beaten cellulose Kraft pulp were different in morphology. The thermomechanical pulp was more like a film whereas Kraft pulp was more fibrous. The nano structure of the fibre was compressed into a macroscopic film. This phenomenon does not seem to appear at concentrations higher than 2% [62]. Figure 14 shows

BCTMP, the fibres were about 20-30 microns in diameter. The higher magnification image shows the surface of the fibers, the fibres are smooth. Figure 15 shows fibres of diameter larger than 30 microns, as it is obvious from the SEM images. The high magnification inset images show the increase in surface roughness. The cellulose nanofibrils were tightly packed into sheets. Figure 16 shows individual fibres, fibres of carboxylate content 1.7 mmol/g of cellulose was tightly packed, as no individual fibres was found. Whereas in fibres with a carboxylate content 1.35 mmol/g of cellulose and 1.23 mmol/g of cellulose, the fibrils were present everywhere near the edges of the

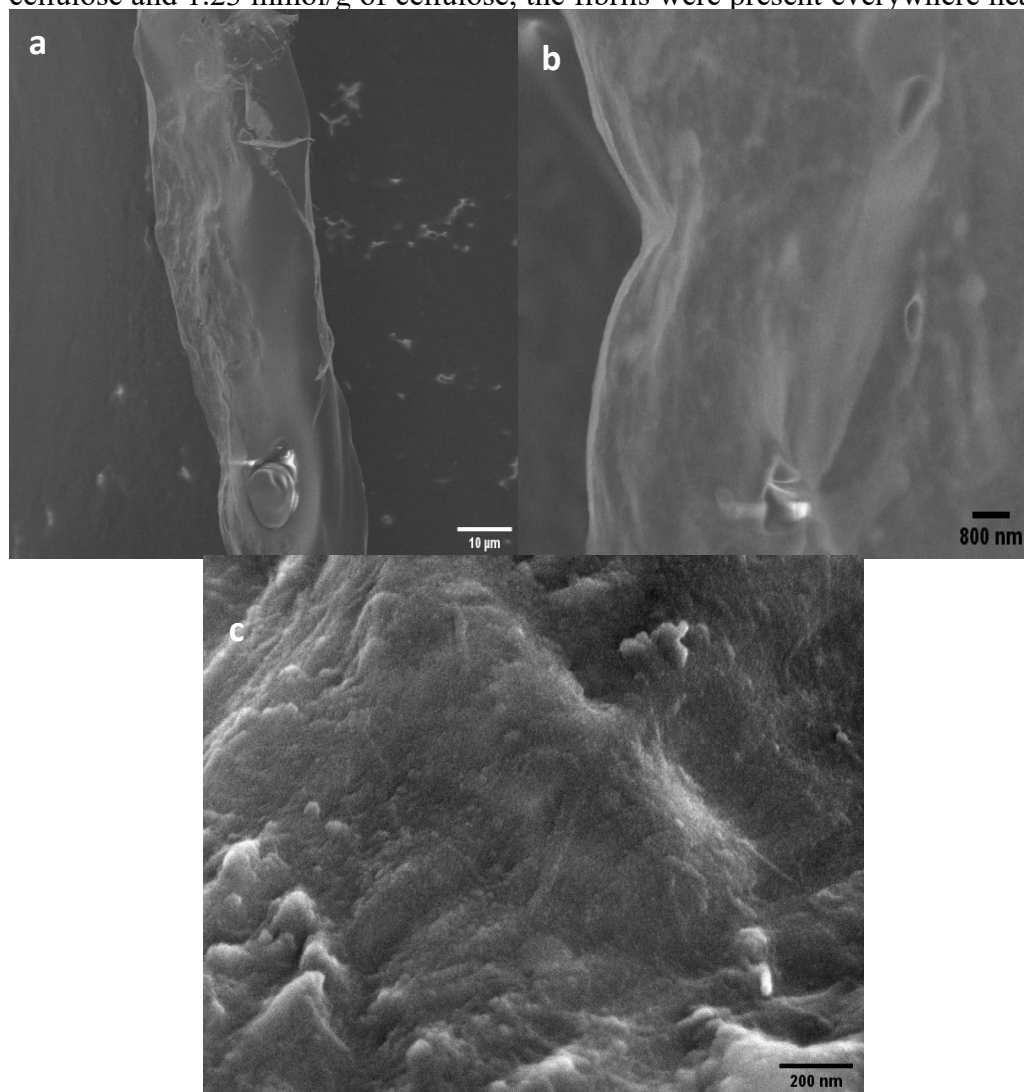


*Figure 14: SEM images of freeze-dried BCTMP shown at different magnifications*

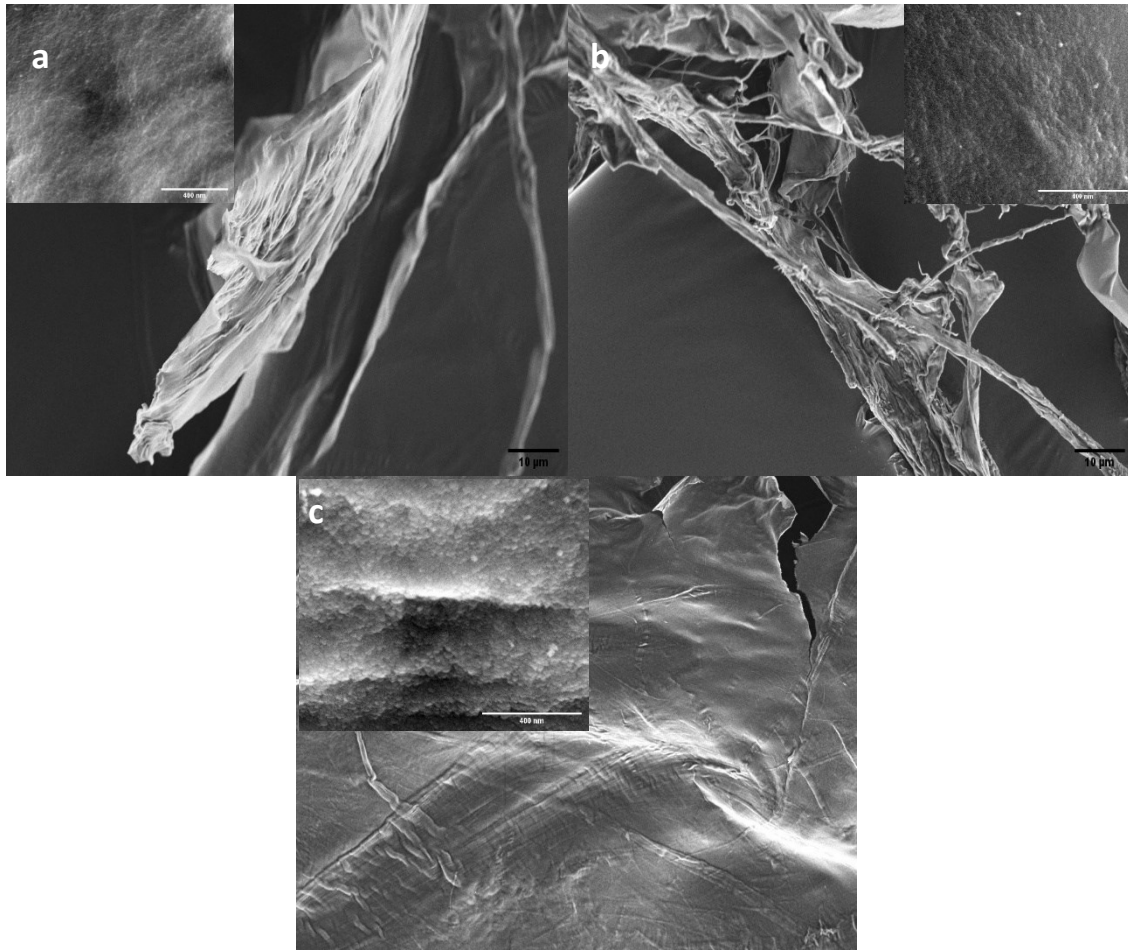


*Figure 15: Reassembled cellulose nanofibers made from supermass collider BCTMP as a result of freeze-drying*

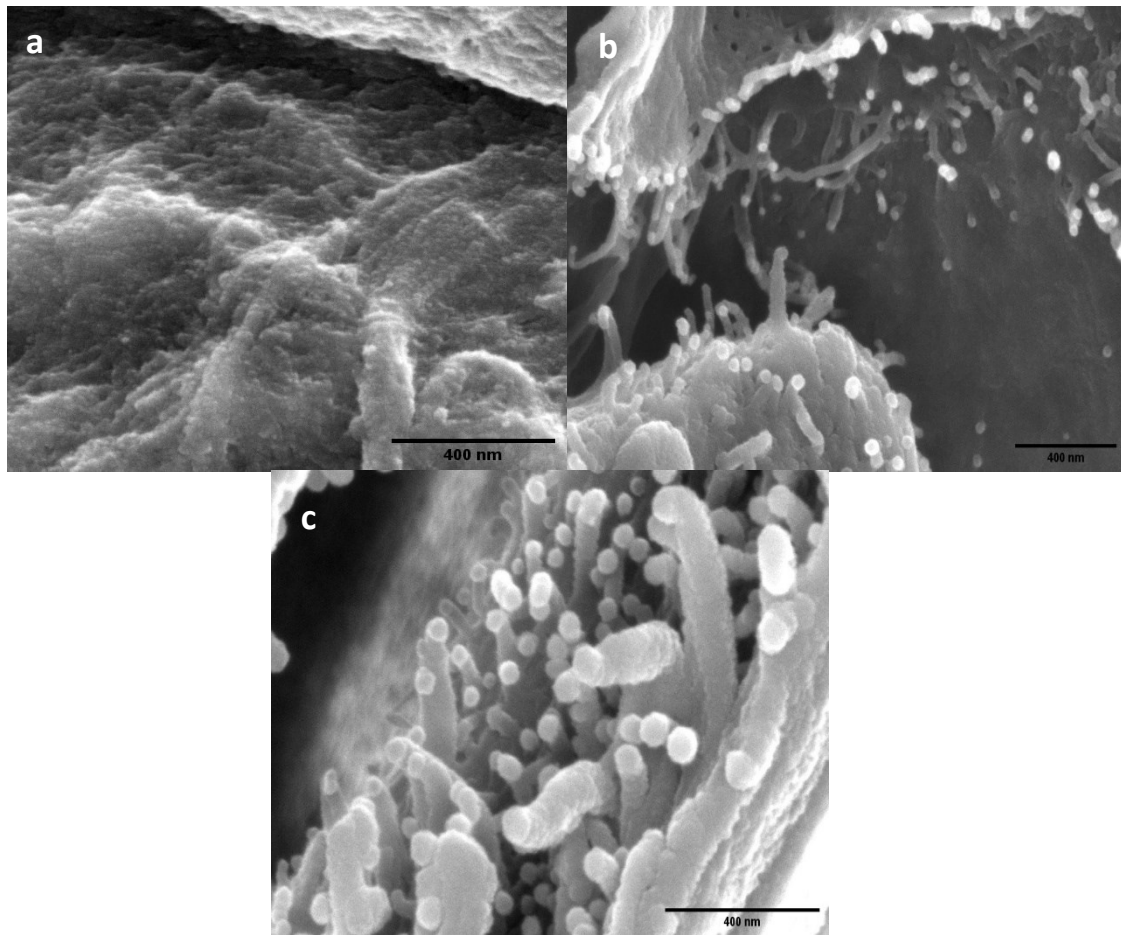


*Figure 16: Reassembled cellulose nanofibers made from supermass collider BCTMP. Individual fibers are being shown (a) CNF 1.7 (b) CNF 1.35 (c) CNF 1.23*

Freeze drying cellulose nanofibres produced from the beaten Kraft pulp produced fibres which appeared to look like a sheet with cracks all over it with fibres connects the ends of the crack. Increasing the magnification into the crack shows that the fibrils form like a scaffold which holds the fiber sheets together. Figure 17 shows the beaten cellulose nanofibres of different carboxylate contents. The images show the fibre with the crack structure on the surface of the sheet. The self assembly of the cellulose happened in the longitudinal direction along the direction of the vacuum opening or along the lower end of the temperature gradient. The self assembled long sized cellulose could be attributed to the strong hydrogen bonds and Van der Waals forces [63]. The critical concentration below which the self assembly can be avoided was about 0.05% [64].

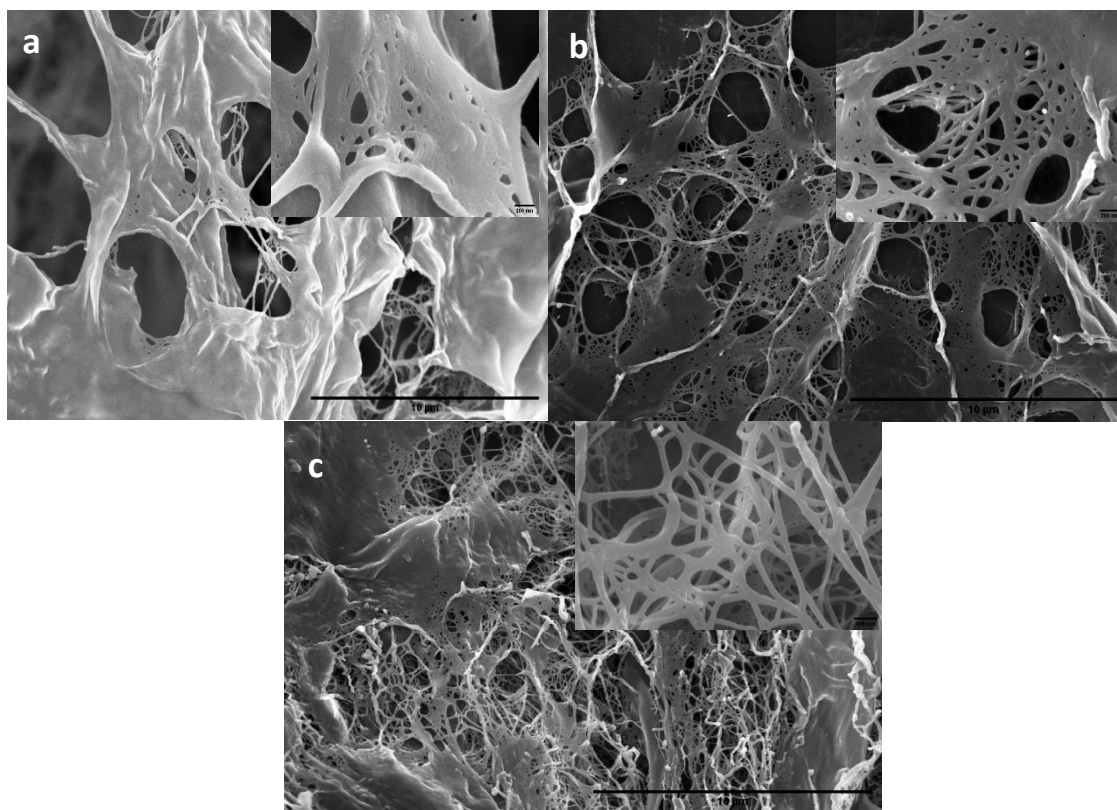


*Figure 17: Reassembled cellulose nanofibers made from beaten cellulose Kraft pulp cellulose as a result of freeze-drying, the images are 10 microns in scale and the inset images are 200 nm scale.*

## 4.2. CNF-Nanolime Composite

### 4.2.1. Attachment of Nanoparticles

#### 4.2.1.1. Spectroscopy

FTIR spectrum of the nanolime precipitated on cellulose nanofibre template is shown in Figure 18. The synthesised freeze-dried fibrous material showed the band characteristics of both cellulose nanofibers and calcium hydroxide. Strong band at  $3,630\text{ cm}^{-1}$  corresponds to the OH stretching [65]. High intensity of the peak indicates the formation of hexagonal calcium hydroxide. Higher concentrations of both Kraft pulp and BCTMP show lower intensity of this peak indicating the formation of a mixture of phases with very little hexagonal phase. A broad peak between  $3,250\text{ cm}^{-1}$  and  $3,500\text{ cm}^{-1}$  peaking at  $3,340\text{ cm}^{-1}$  also correspond to the OH stretching. Peaks at  $1,600\text{ cm}^{-1}$  indicate the carboxylic groups of cellulose. Broad band at  $1,420\text{ cm}^{-1}$  indicates the CH bending. This could be due to the cellulose template. This could also be the Ca-OH bonds present in calcium hydroxide. This peak shifts at high carboxylate content cellulose nanofibres. This peak is present at  $1,350\text{ cm}^{-1}$  and also indicates the presence of non hexagonal particles. SEM shows that most of the particles formed on cellulose nanofibres of a carboxylate content of  $1.6\text{ mmol}$  are ellipsoidal in shape and some hexagonal particles also present, shown in Figure 19 [5]. The peak at  $1,020\text{ cm}^{-1}$  could be because of the symmetric stretching mode of the  $\text{CO}_3$  group, present as a contamination of calcium hydroxide. It is possible that the contamination could happen during the

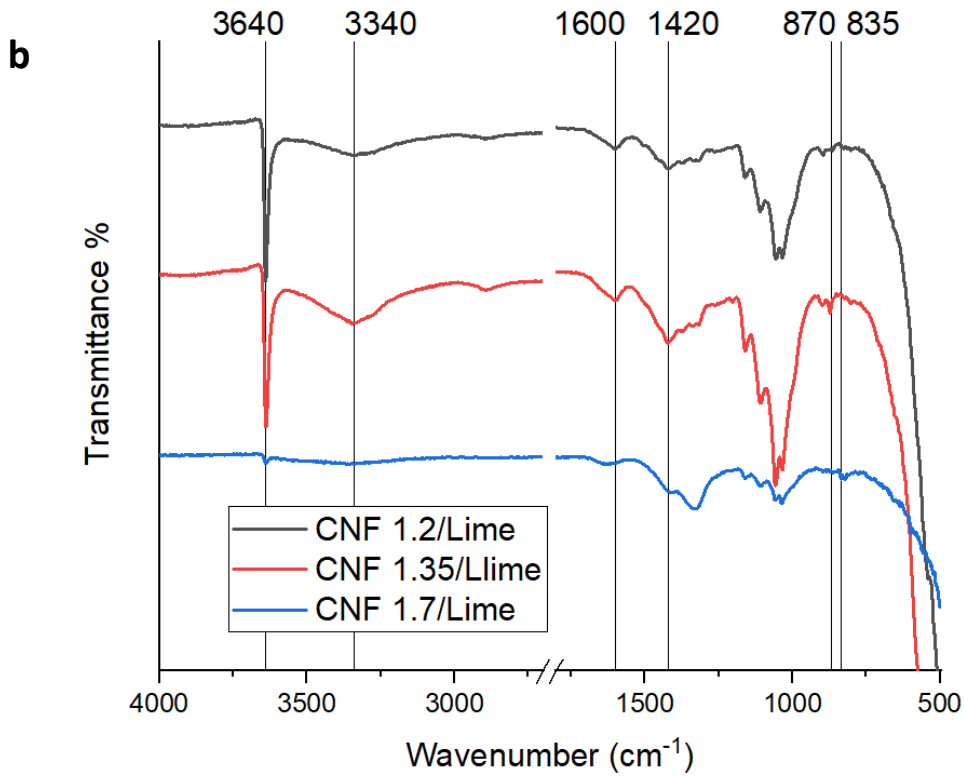
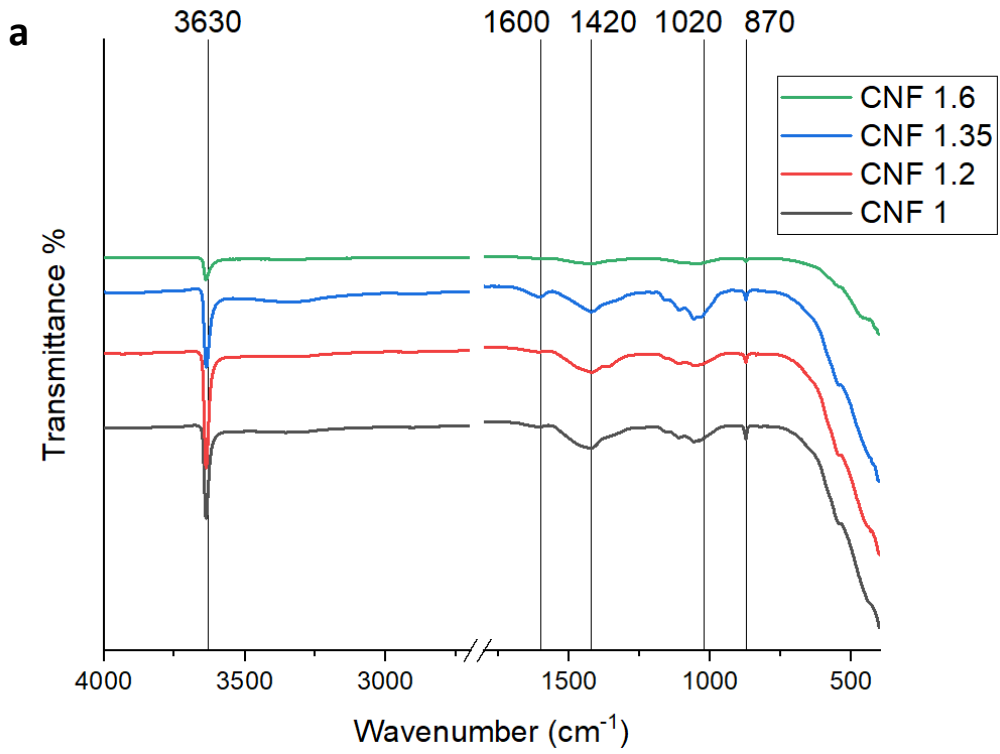


Figure 18: FTIR spectra of CNF-lime made from (a) mechanically dispersed Kraft pulp (b) supermasscollider BCTMP

washing cycle after chemical precipitation. A sharp peak around 870 cm<sup>-1</sup> is because the Ca-O

bonding this could be because of both Calcium hydroxide and calcium carbonate.

#### 4.2.1.2. Self Assembly of Cellulose Nanofiber – Lime Composite

Freeze drying CNF/lime at a concentration of 0.1% w/w also made the fibres self assemble into large macroscopic sheets as shown in the figures. In MC CNF/Lime both films and larger fibres can be found. In BCTMP, only sheets of CNF were present. The self assembly of the cellulose from freeze drying affected the lime. Densely packed lime can be found on the fibres and sheets of cellulose nanofibers. The lime particles appear to be hexagonal or cuboid in shape, the only exception is BCTMP CNF 1.7/lime which appears to be ellipsoidal in shape. The different shapes of particles are also confirmed with FTIR. The amount of lime on the film visually reduces as the carboxylate content reduces, shown in Figure 19.

The lime particles are of the same size in MC CNF/Lime whereas in BCTMP the lime particles are about 2 microns in length but appear to be in various shapes. CNF 1.7/lime self assembled into ellipsoid, CNF 1.35/lime self assembled into cubes and cuboids and CNF 1.23/Lime self assembled into polyhedron.

The possibility of the change in morphology of the lime due to freeze drying could be high as CNF's tend to become grafted onto the sheets. The lime particles could either pose resistance or fuse with other neighbouring particles forming larger particles [66].

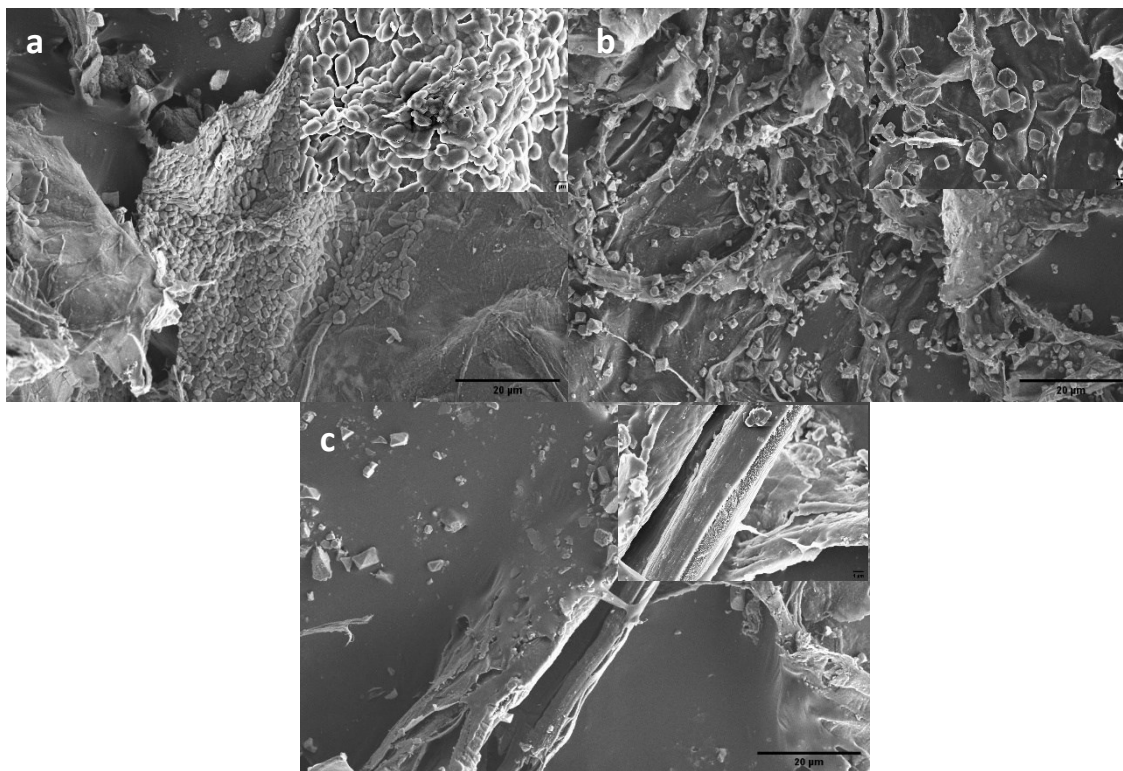


*Figure 19: SEM images of CNF-Lime (a) CNF 1.7-Lime (b) CNF1.35-Lime (c) CNF 1.23-Lime at a scale of 20 µm and the inset images are of 1 µm in scale*

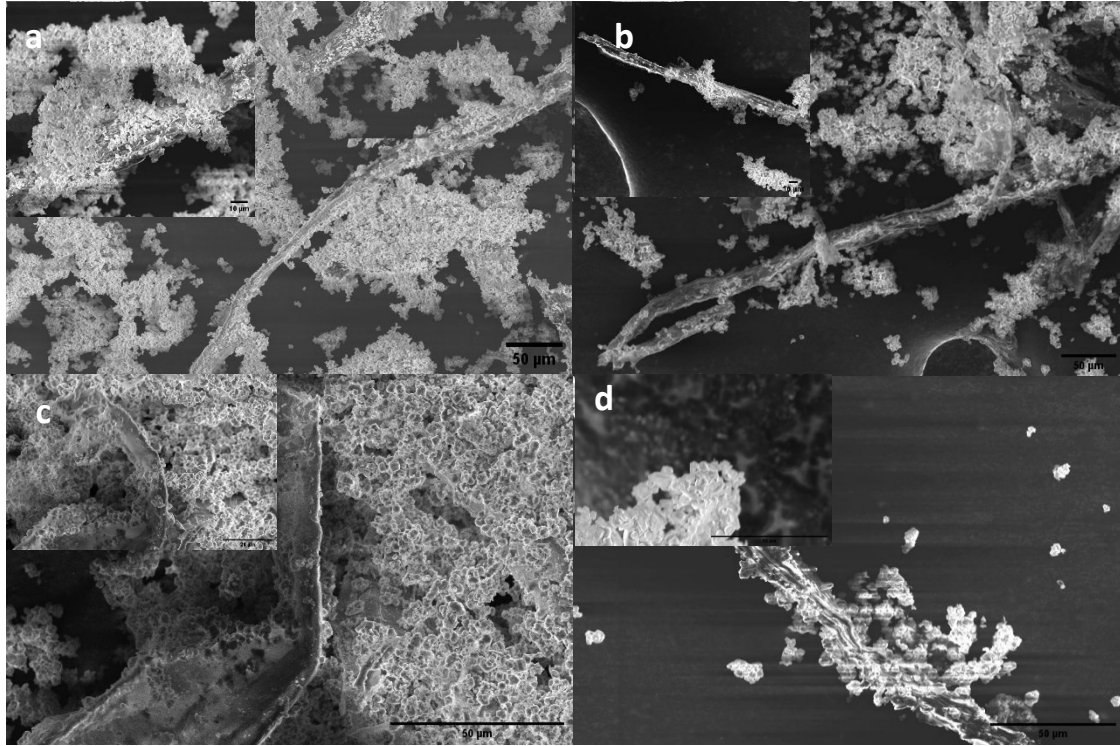


*Figure 20: SEM images of CNF-Lime (a) CNF 1.6-Lime (b) CNF1.35-Lime (c) CNF 1.23-Lime and (d) CNF 1-Lime at a scale of 50 µm and the inset images are of 10 µm in scale*

## 4.2.2. Thermal Decomposition

Thermogravimetric analysis and the corresponding derivative (DTG) curves of the CNF/Lime made from mechanically dispersed Kraft pulp and supermass collider BCTMP are shown in Figures 21. The first decomposition occurs at 40 °C as a result of the residual water in the sample. This peak plateaus at around 100 °C. Thermal degradation of CNF starts at 220 °C. The decomposition stopped at 96%. Unlike cellulose nanofibres, decomposition is unimodal at 220 °C. This indicates that some of the CNF did not decompose completely. The mode occurs at 300 °C for all the MC CNF/lime samples, BCTMP CNF/lime also follows the same unimodal decomposition except CNF 1.7/lime, which shows bimodal decomposition.

The decomposition at 400 °C is because of water loss from the decomposition of  $\text{Ca}(\text{OH})_2$  to  $\text{CaO}$ . For BCTMP, the decomposition was at 420 °C. The third decomposition appears at 580 °C for MC and at 600 °C for BCTMP. CNF 1.7/lime has a larger decomposition because of the decomposition of  $\text{CaCO}_3$  present as an impurity (carbonated during washing). The final residue at 1,000 °C was around 67% for both the cellulose sources.

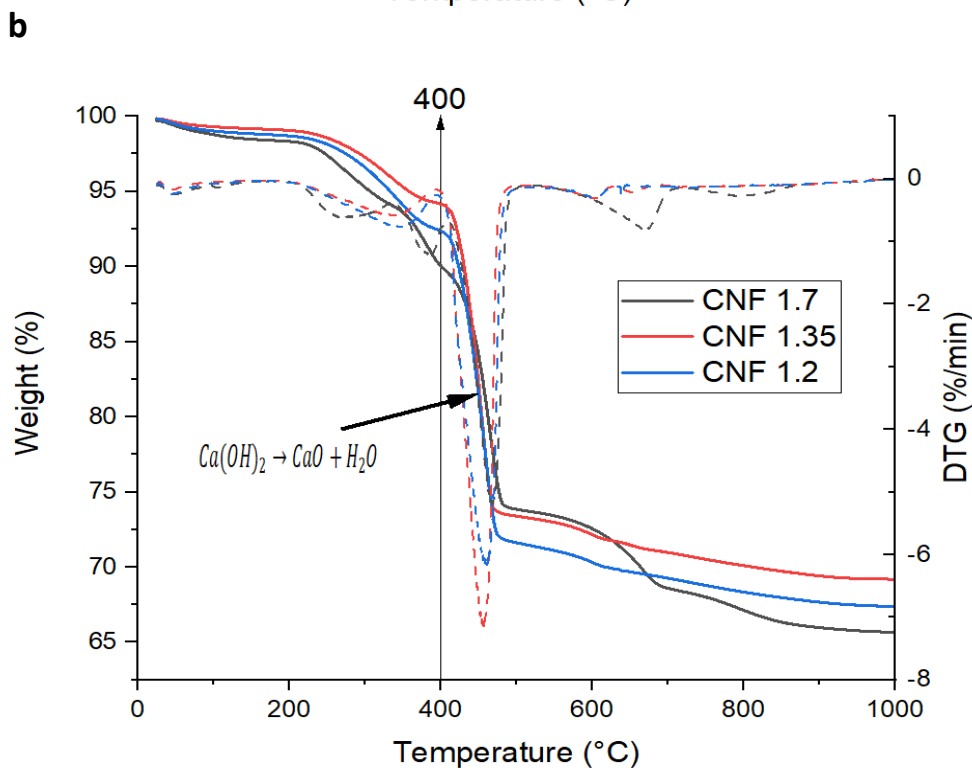
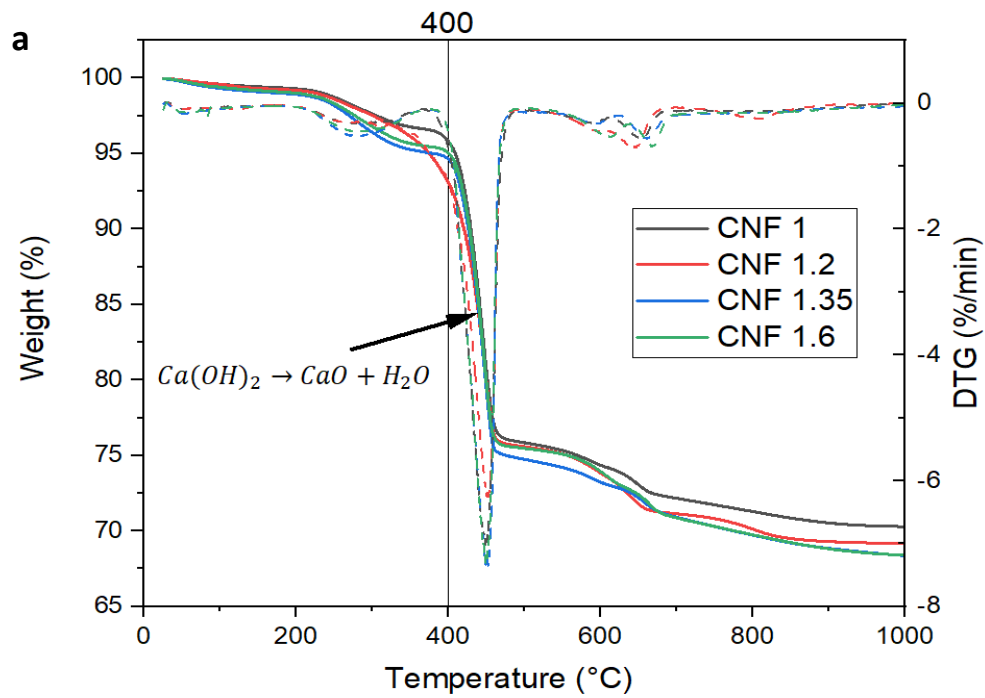


Figure 21: TG and DTG curves of (a) CNF-lime produced from mechanically dispersed Kraft pulp (b) CNF-lime from supermasscollider BCTMP, of different carboxylate content.

### 4.2.3. Analysis of Crystallography Using X-Ray Crystallography

The X-ray diffraction pattern of CNF 1.35/lime is shown in Figure 22. Small peaks at 10, 15 and 22° show the characteristic peaks of cellulose nanofibres [67] [68]. The high intensities of calcium hydroxide hide the lower intensities of cellulose nanofibres. The sample contains hexagonal calcium hydroxide [Ca(OH)<sub>2</sub>] phases having space group p-3m1 (space group no: 164, PDF card no. PDF#98-000-0359) as major phase was Portlandite Ca(OH)<sub>2</sub>. Peaks at 18.04, 28.69, 34.11 47.12, 50.84 and 54.38 ° indicate hexagonal crystal system.

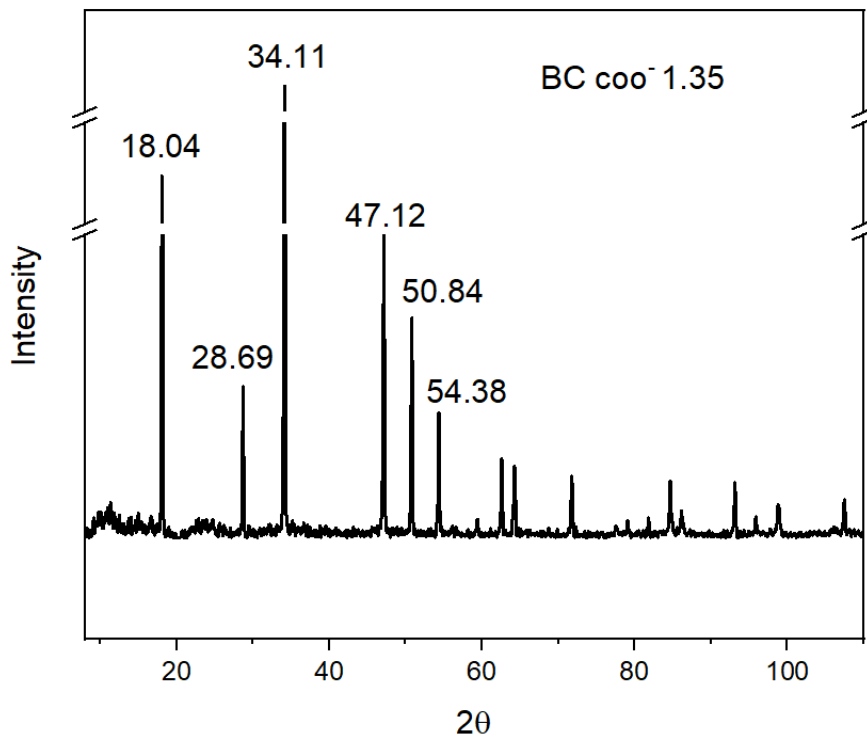
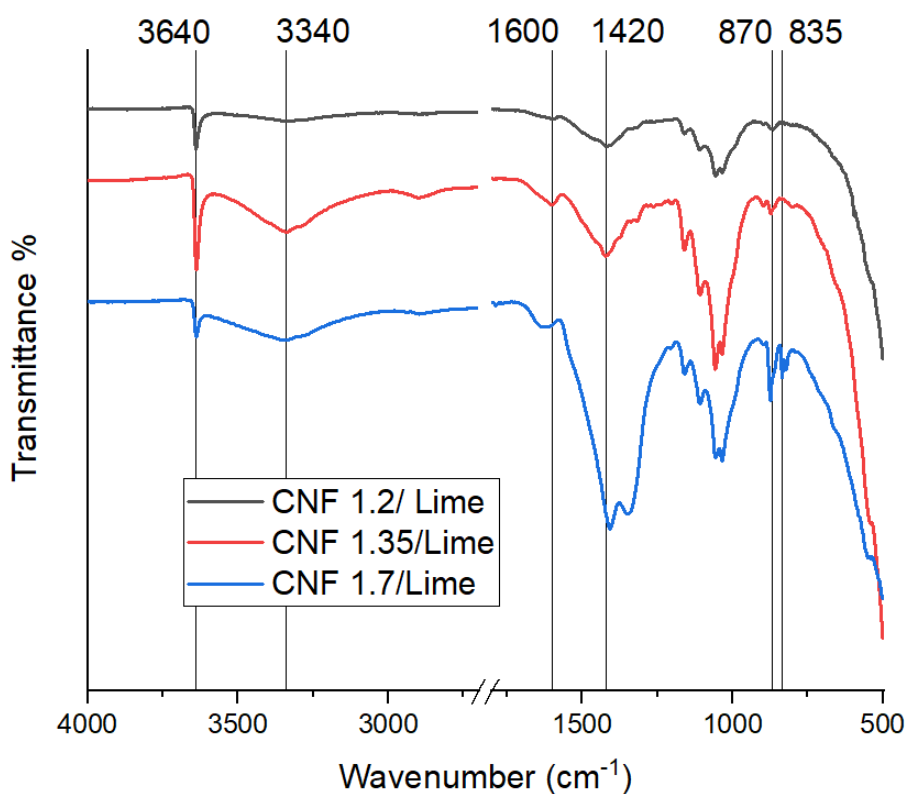


Figure 22: XRD pattern of fresh CNF 1.35-lime indicating the portlandite peaks

## 4.3. Aging of CNF-Nanolime Composite

### 4.3.1. Conformation of Formation of Calcium Carbonate Particles

Increase in the intensities at 1,420, 870, 835 shows the C=O asymmetric stretching because of the calcite [69]. The cellulose lime with the highest carboxylate content (1.6 mmol) shows a clear calcite characteristic transmittance. The peaks at 3,640  $\text{cm}^{-1}$  shows the presence of calcium



*Figure 23: FTIR curves of carbonated CNF-lime of different carboxylate contents*

hydroxide because of the OH stretching, the broad peak at 3,340  $\text{cm}^{-1}$  also confirms this. The transmittance at 870 is stronger for CNF 1.7/lime indicating that the carbonation was faster, whereas in CNF 1.2/lime only a small peak can be observed.

### 4.3.2. Thermal Degradation of Carbonated Particles

Thermal decomposition of the carbonated CNF/lime is shown in the following figures. The decomposition of the material at 400 °C is the same as that of fresh CNF/lime. The decomposition at 400 °C reduced slightly because of the carbonation as some of the portlandite converted to calcite. This can be noted by decrease in the length of the decomposition curve at 400 °C. This is more pronounced in CNF 1.7/Lime as shown in Figure 26. The residue at 1,000 °C was slightly reduced to about 67-65%.

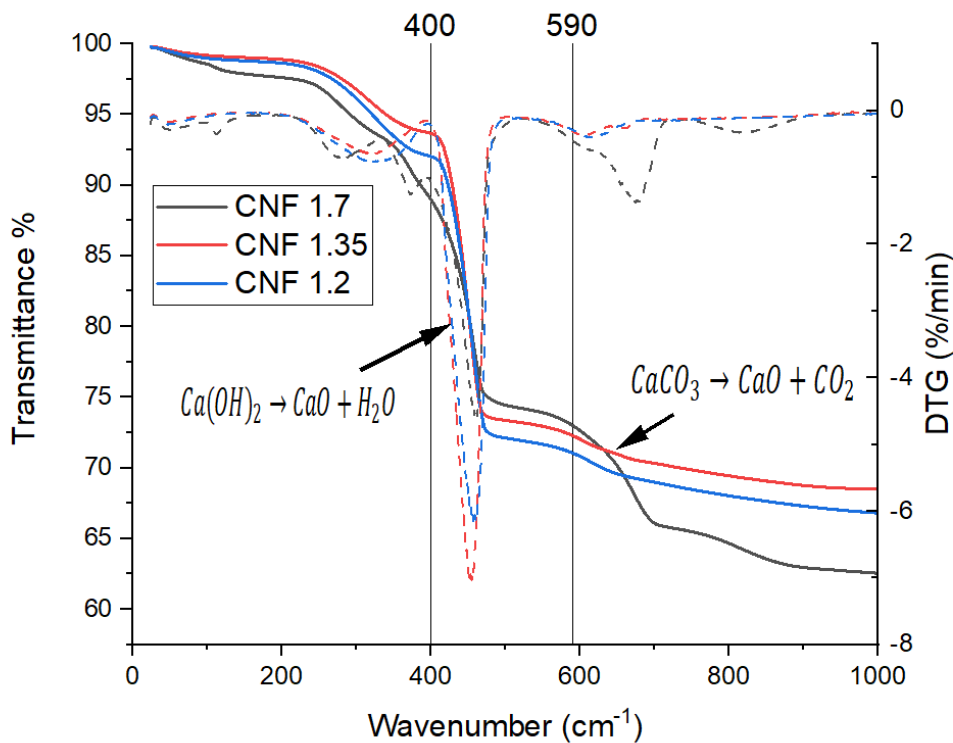


Figure 24: Carbonated TG and DTG curves of different CNF-limes of different carboxylate content

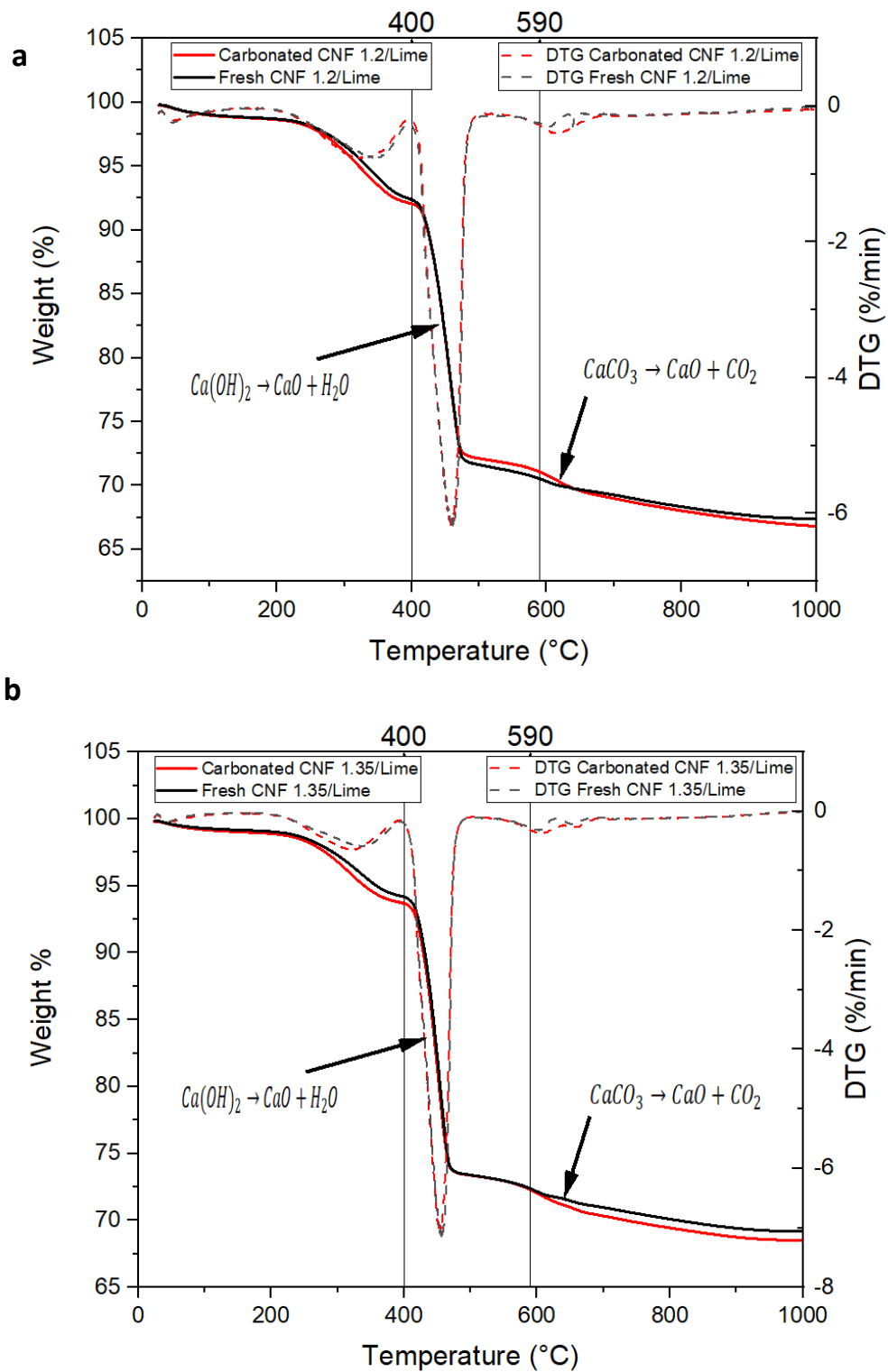


Figure 25: Carbonated vs fresh TGA curves and DTG curves of (a) CNF 1.23-Lime and (b) CNF 1.35-lime

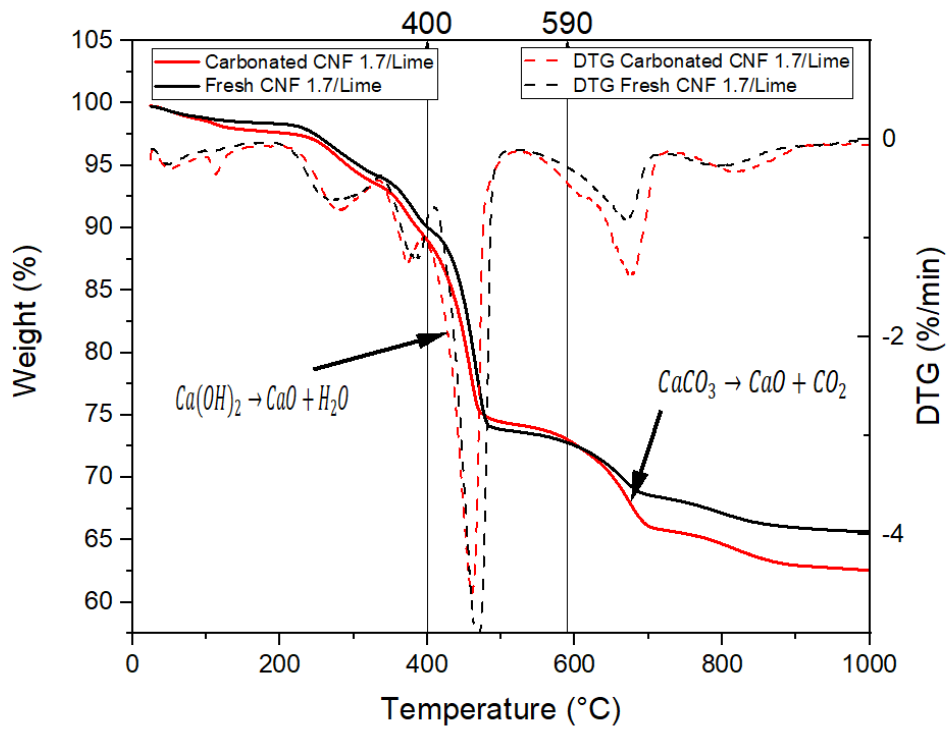


Figure 26: Carbonated vs fresh CNF 1.7-lime shows the TG curve and DTG curve, indicating the increase in calcium carbonate and reduction in calcium hydroxide

### 4.3.3. Analysis of Crystallography of Calcium Carbonate Particles

The sample contains hexagonal calcium hydroxide [Ca(OH)<sub>2</sub>], hexagonal [CaCO<sub>3</sub>], orthorhombic [CaCO<sub>3</sub>], and trace amounts of monoclinic [CaCO<sub>3</sub>] phases having space group p-3m1, r-3c, pmcn, p21/c (space group no: 164, PDF#98-000-0359; 167, PDF#98-000-0141; 62, PDF#98-000-0098; 14, PDF#98-000-0458) as major phase was portlandite, calcite, aragonite and whewellite. The aragonite phase generally appears at  $2\theta=28.79^\circ$ , calcite phase generally occurs at  $2\theta=47.19^\circ$  and whewellite phase occurs at  $16^\circ$ . The FTIR peak at  $1,350\text{ cm}^{-1}$  indicate the presence of CaC<sub>2</sub>O<sub>4</sub>.H<sub>2</sub>O (whewellite). The distinction between lime and mixture of lime, calcite and other crystals are very subtle. The calcite peak has a shift of  $0.1^\circ$  from the portlandite peak. The high intensity at  $28.79^\circ$  in the carbonated CNF/ lime indicate the formation of calcium carbonate.

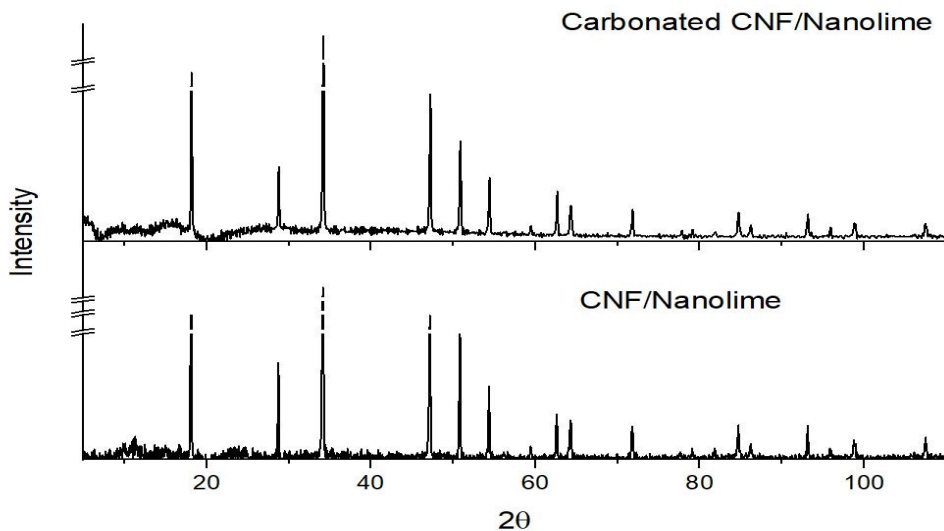


Figure 27: XRD patterns of fresh CNF 1.35-lime and carbonated CNF 1.35-lime

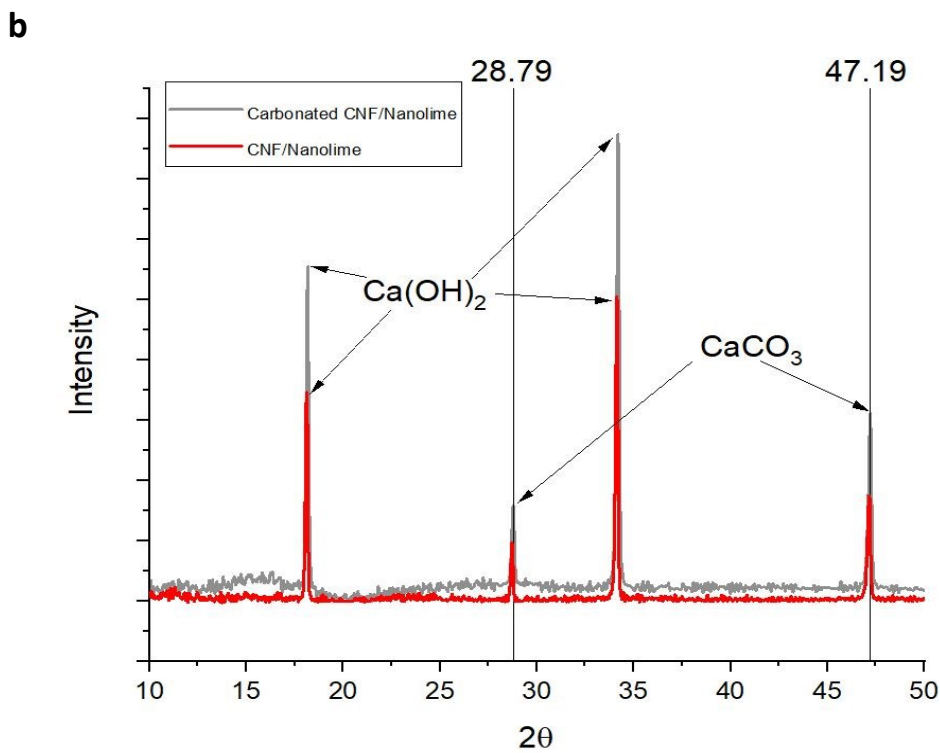
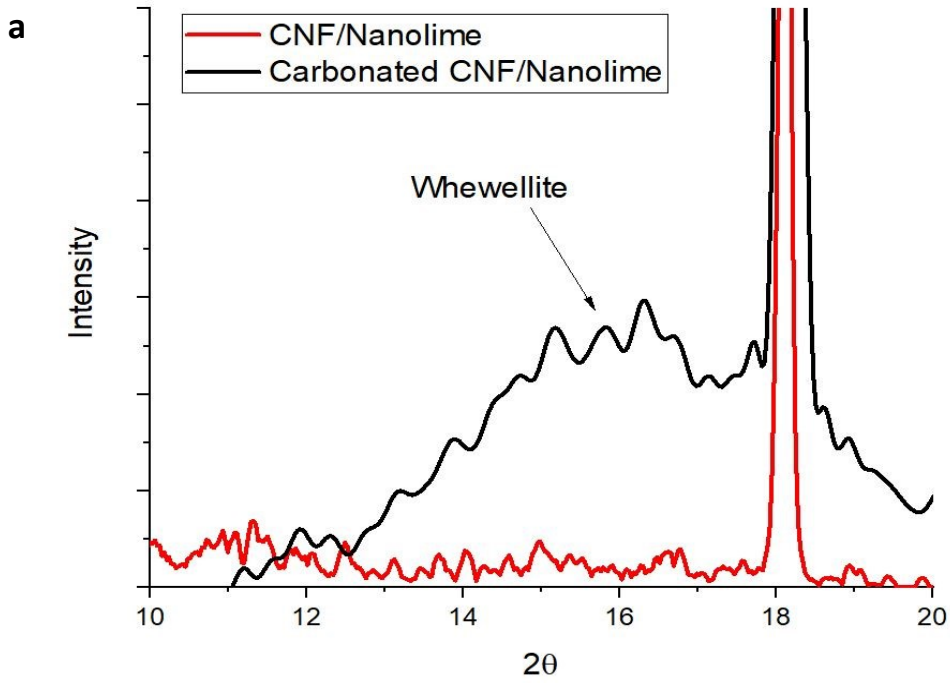


Figure 28: XRD patterns of fresh CNF-Lime and carbonated CNF-Lime, (a) shows appearance of Whewellite; (b) shows the carbonate and hydroxide peaks.

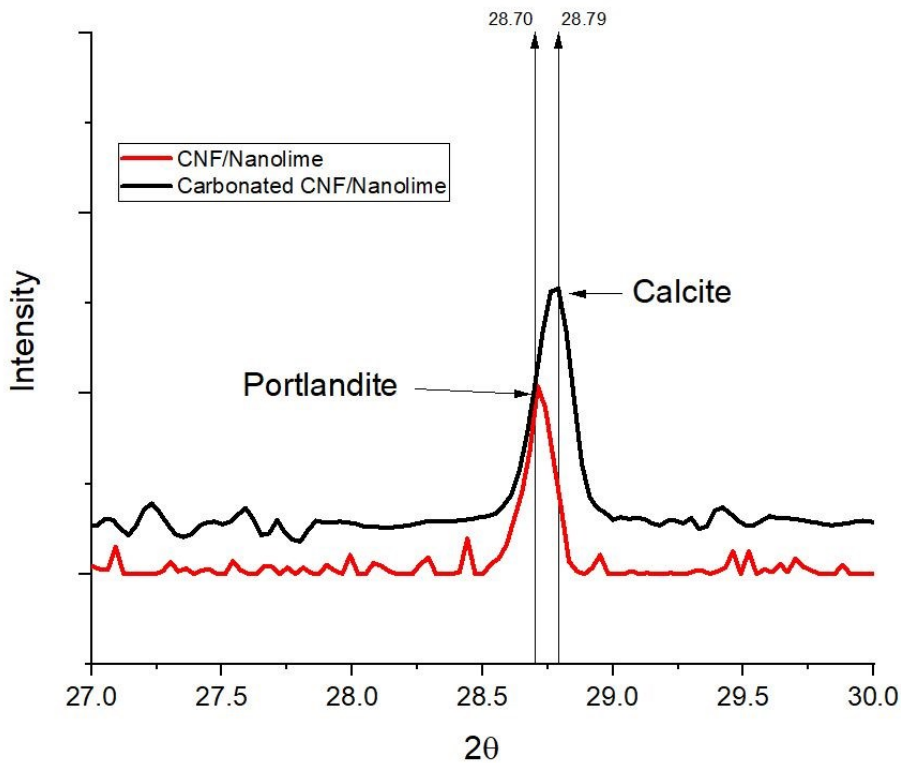


Figure 29: XRD of fresh CNF-lime and carbonated CNF-lime, indicating the peak shift

## 4.4. Flow and Film Properties of CNF-Lime Composite

### 4.4.1. Rheology

Suspensions with various carboxylate concentrations and solid concentrations of cellulose nanofibres were subjected to frequency sweep studies. To illustrate the impact of concentration of cellulose nanofibre on the suspension viscoelastic properties, Figures 30, 31, 32 show the variation in the linear complex shear modulus  $G^*$  which can be written as  $G^*(\omega) = G'(\omega) + jG''(\omega)$ , where  $G'$  and  $G''$  are the shear storage and shear loss modulus.

The viscosity reduces as the shear increases, indicating a shear thinning behaviour. At high oscillatory shear the second region on the curve shows that the viscosity increased as the shear rate

after a critical state. And this was enhanced as the concentration increased. In the initial stage, the fibres were arranged into linear structures thus showing shear thinning behaviour, but after a threshold, the fibres physically entangled leading to increasing in viscosity.

The storage modulus shows positive correlation with the concentration for most of the samples and most of the samples indicated viscoelastic behaviour. The storage modulus shows two distinctive patterns in the curve. The low frequency region the storage modulus is lower than the loss modulus indicating viscous behaviour or liquid like behaviour; at high frequency region after the critical point the modulus increases sharply, which is higher than the loss modulus indicating elastic behaviour or solid behaviour. The sharp increase in storage modulus occurred after the critical point, showing that the sudden increase could be because of the physical entanglement of the fibres. This was not observed in cellulose nanofibres with a carboxylate content of 1.35. The storage modulus is on the order of  $10^2$  Pa. [70]. Figures 30 and 31 (d,e,f,) show the characteristic crossover point indicating reorganization of fibres [71].

The viscous behaviour of the CNF 1.35 could be due to the settling of the fibers. This can be observed from the storage modulus and complex viscosity curves. The complex viscosity contains no critical point where the viscosity increases with frequency. The storage modulus is much higher than the loss modulus and shows no cross over, indicating that the fibres settled during the measurements. The fibres could have moved outward during the measurement.

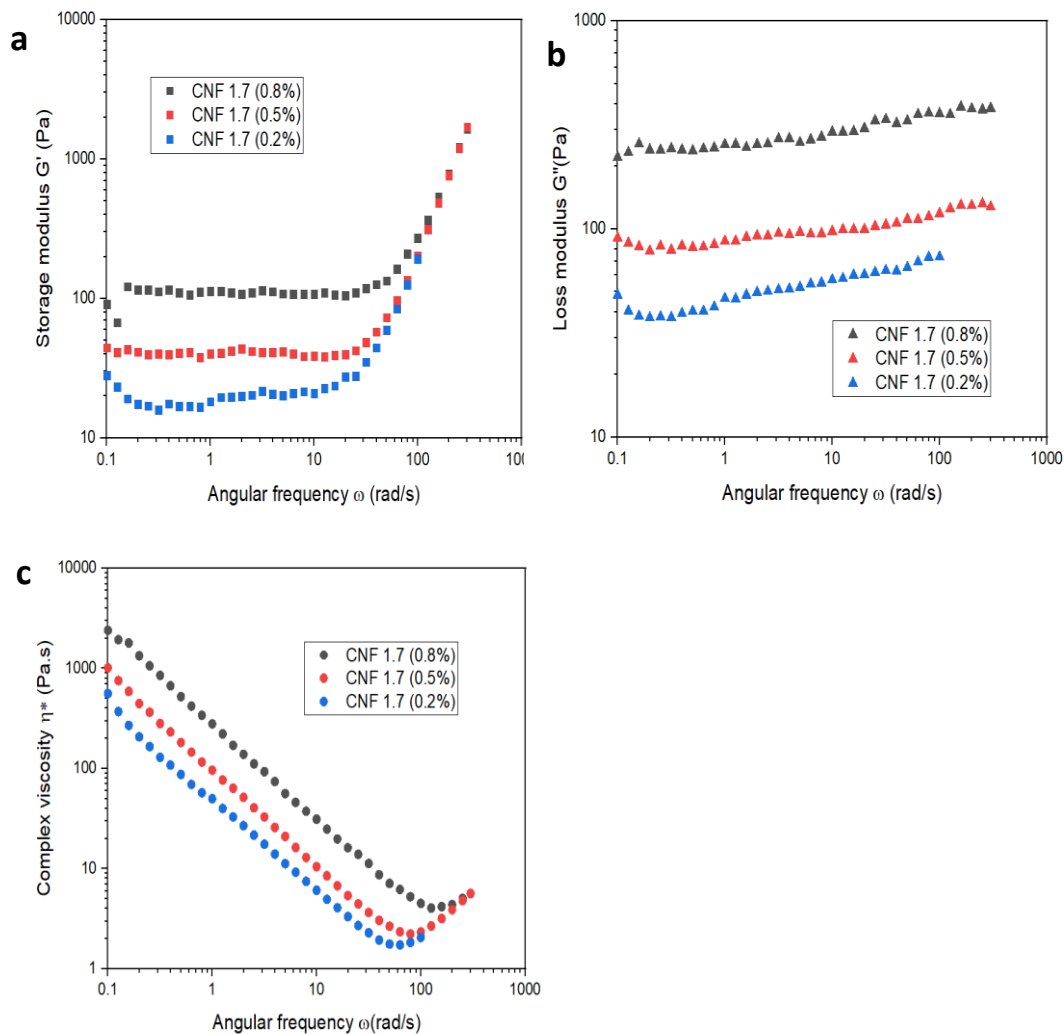


Figure 30: (a) shows storage modulus, (b) loss modulus and (c) shows the complex viscosity of CNF 1.7 at different concentrations

The low amplitude frequency sweep of the CNF and CNF lime blends have very large modulus values. The storage modulus is higher than the loss modulus, indicating that the suspension had particles settling due to shear. In HEC -CNF/Lime blends, the modulus behaviour is visco-elastic. Initially,  $G' < G''$  and this indicates viscous behaviour and after the crossover point the  $G' > G''$ , the behaviour is more elastic. Unlike in CNF, HEC-CNF/Lime blends the storage modulus does not correlate with the concentration, as the smallest and the largest concentration of the blends have similar behaviour.

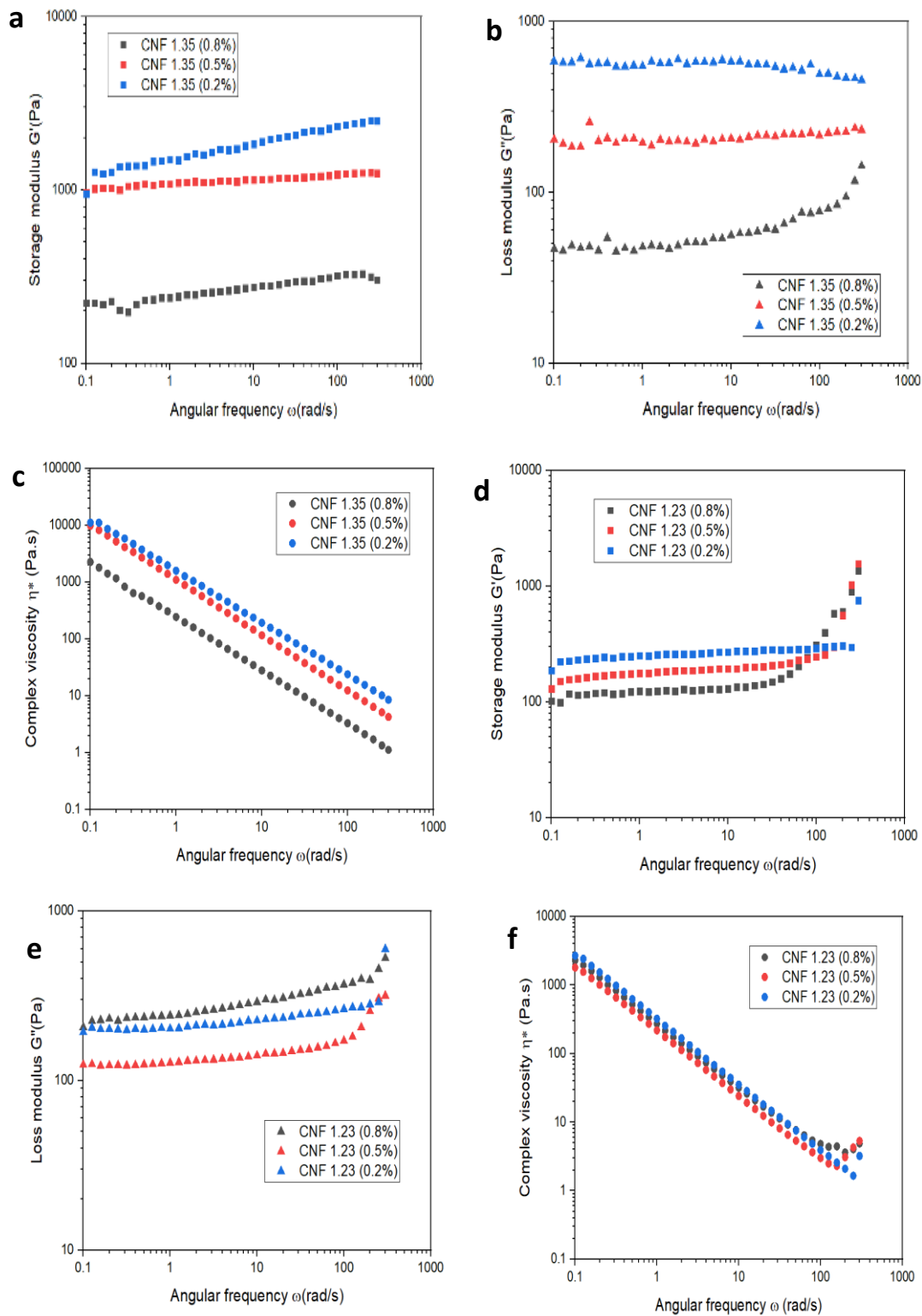


Figure 31: (a)(b)(c) shows the storage modulus, loss modulus and complex viscosity of CNF 1.35 at different concentrations; (d)(e)(f) shows the storage modulus, loss modulus and complex viscosity of CNF 1.23 at different concentrations.

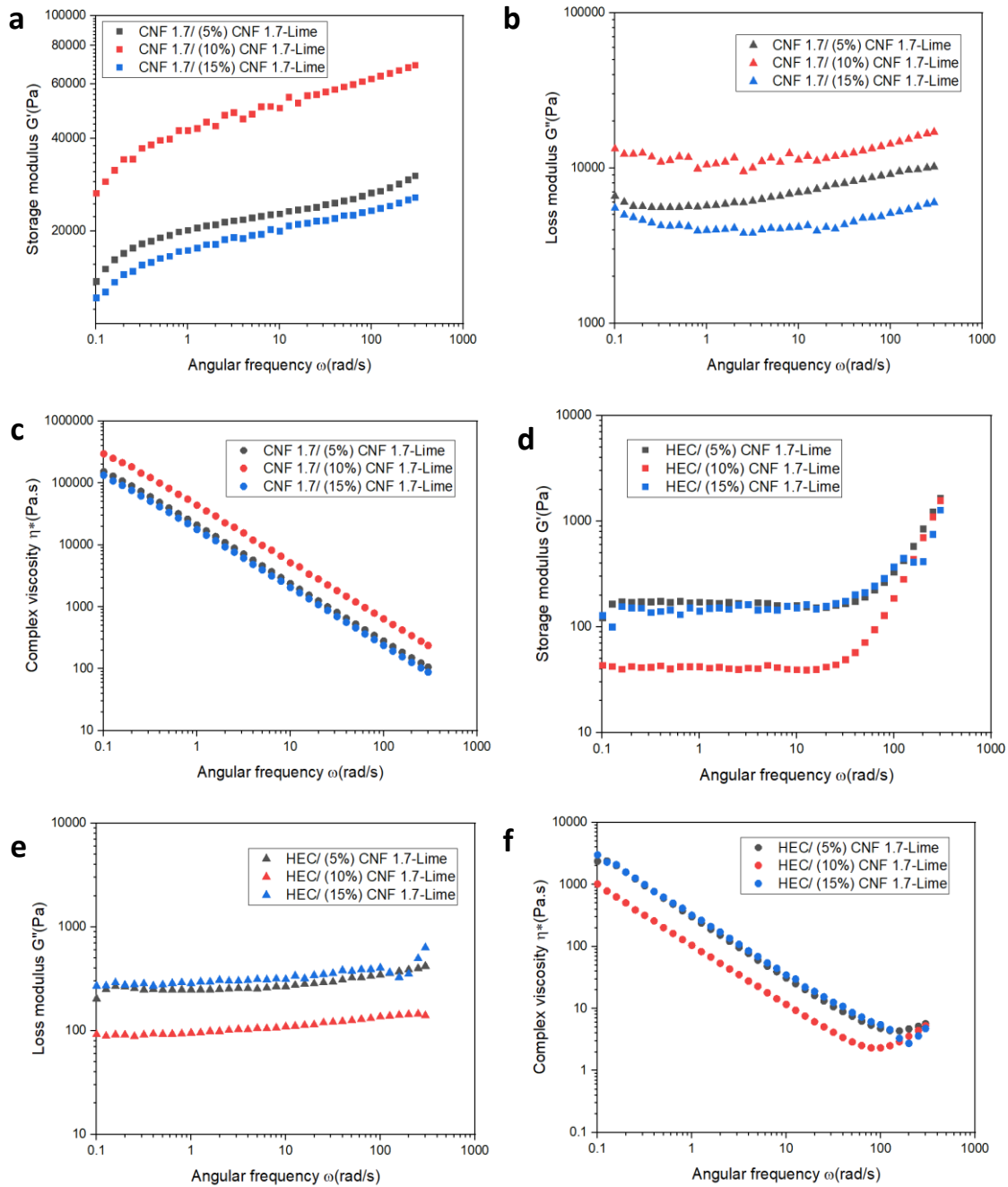


Figure 32: (a)(b)(c) shows the storage modulus, loss modulus and complex viscosity of CNF 1.7 blended with CNF 1.7-Lime; (d)(e)(f) shows the storage modulus, loss modulus and complex viscosity of HEC blended with CNF 1.7-lime.

Addition of CNF-lime to CNF 1.7 disrupted the viscoelastic behaviour of CNF 1.7, thus no critical viscosity point was present, and the fibrous matrix did not interlock at higher frequency ranges.

The storage modulus of the sample was much higher than the loss modulus indicating that the

suspension had a lot of coarse particles. HEC-CNF-lime suspension exhibits viscoelastic behaviour, the increase in the storage modulus after the critical viscosity point is similar to CNF gel rheological behaviour. The blend behavior of CNF and HEC is similar in one aspect; the 10% blend behaviour is different from the 5% and 15% blends. The addition of the particles reduced the storage modulus and viscosity values but when the concentration reached a threshold, the fibres likely formed entanglements with blended CNf-lime, which has particles attached to high aspect ratio cellulose nanofibres, thus increasing the storage modulus. This is an interesting rheological behaviour indicating that even larger weight percent of blends can be used without losing the viscoelastic property, which is a required property for the roll to roll coating. The rheological behaviour of HEC blends shows an ideal rolling behaviour, as even in higher concentration of blend the fibrous sheets can respond elastically at high shear. This will in turn take the shape of the rolling surface and also not flows outwards after rolling.

## 4.4.2. Mechanical Properties

Tensile testing of the films was carried out. The films were about 10-40 microns in thickness. The tensile strengths of the materials prepared using air drying of the solutions at different dilutions

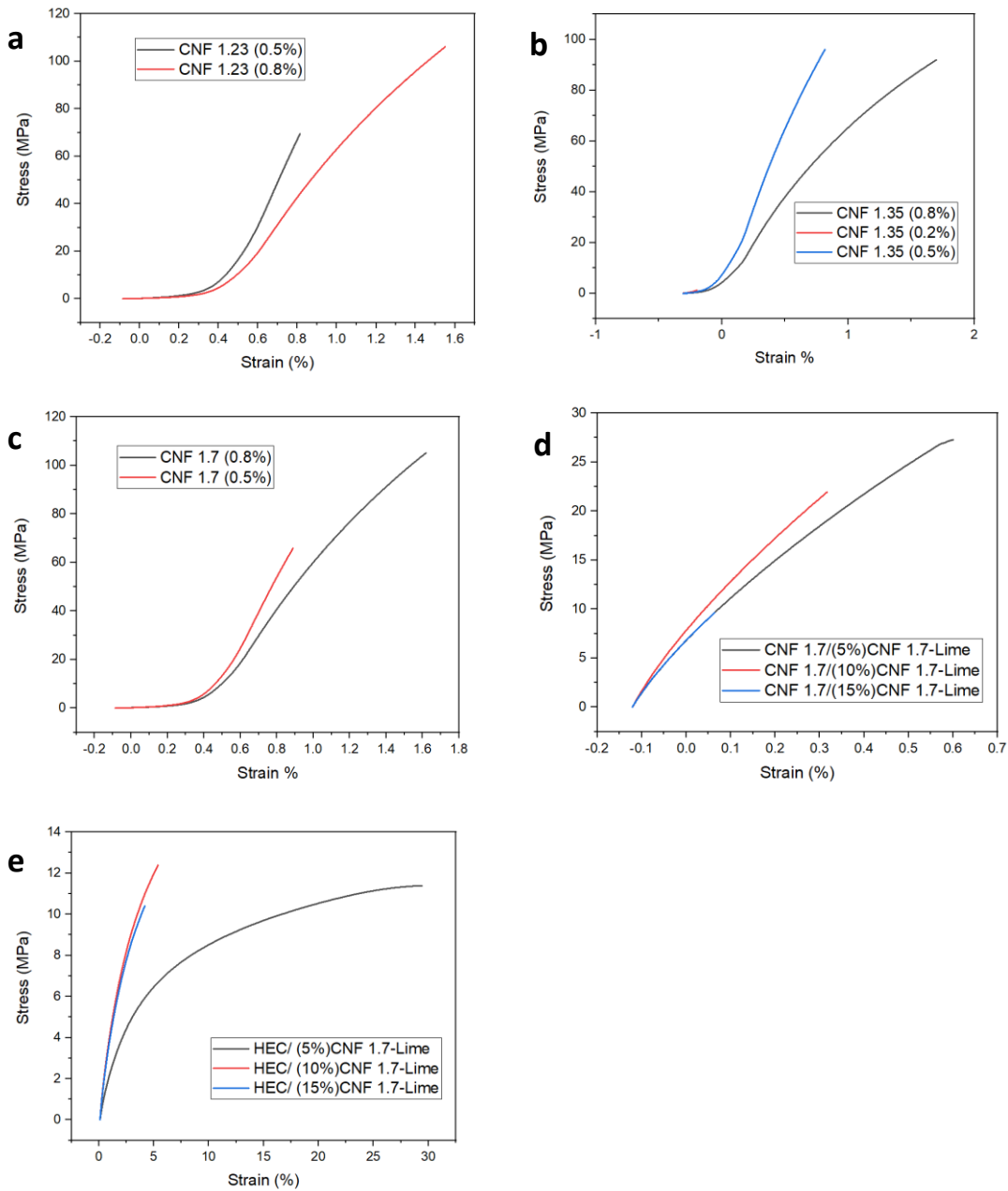


Figure 33: Stress-Strain diagram of different films measured by dynamic mechanical analysis; (a) CNF 1.23; (b) CNF 1.35; (c) CNF 1.7; (d) CNF 1.7 blended with CNF 1.7-Lime; (e) HEC blended with CNF 1.7-Lime; at different concentrations

increased with increasing concentration. The tensile strength of sample with concentration (0.2%) was substantially lower. Some of the films were very weak to make any measurements. In the CNF

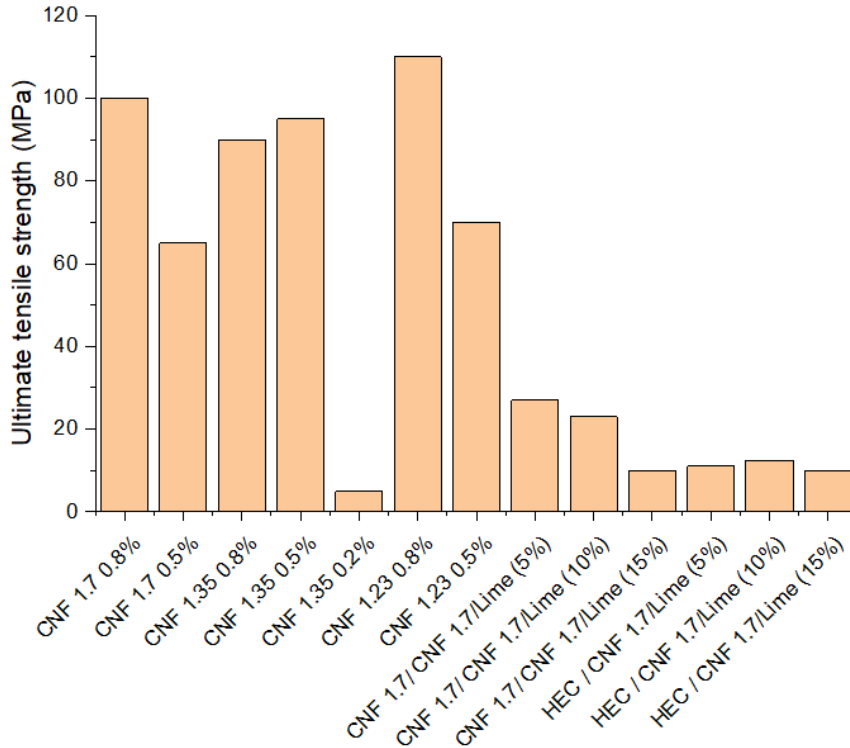


Figure 34: Ultimate tensile strength of different films measured by dynamic mechanical analysis measurements, artifacts can be observed. This is because of the wrinkles present in the CNF film when it was clamped in between the stationary and mobile shafts of the tensile test tool.

CNF's are very stiff, as their storage modulus is around the magnitude of  $10^3$  GPa. As the sample concentration reduces, the stiffness increases. CNF/lime blends behaved more elastic, increasing the CNF-lime concentrations in the blend increased the stiffness. Addition of CNF-lime to CNF 1.7 reduced the strain indicating even higher stiffness than itself, as the failure appears to have occurred well below 1% strain. HEC CNF/Lime blends showed perfect elastic behaviour, especially 5% blend sample. From the characteristic elastic curve, the tensile strength is found to

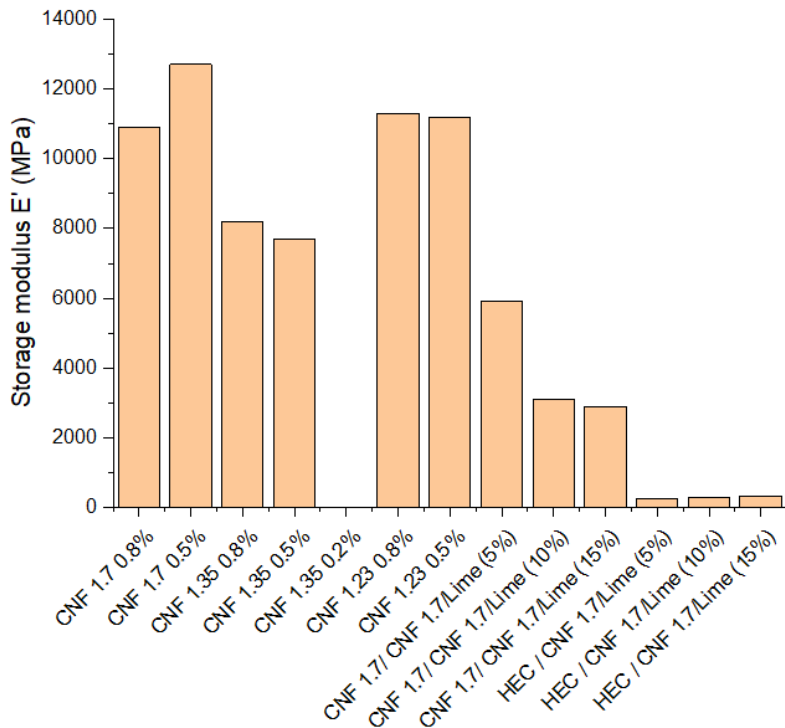


Figure 35: Storage modulus of the films measured by dynamic mechanical analysis

be 7 MPa, and the ultimate tensile strength or failure occurs at 11 MPa. As the blend concentration increases similar to CNF the material becomes stiffer.

Similar to the rheological behaviour of the blends, the CNF blend showed that the increase in the blend concentration showed similar behaviour, but in HEC blends, the increase in concentration of the blend increased the stiffness of the film. In 5% blend, the failure occurred after 30% strain, whereas in higher concentrations, the failure occurred below 5% strain.

## 4.5. Shelf Life Test

Two randomly chosen fuji apples were used for the study. The apples were nearly the same size, one third of the apples were yellow. Although studies have shown that color does not indicate the ripeness. The only ripeness indicating factor are the hardness and the amount of ripening agents. The apples were fuji type bought on the same day, indicating that the hardness of the apples would

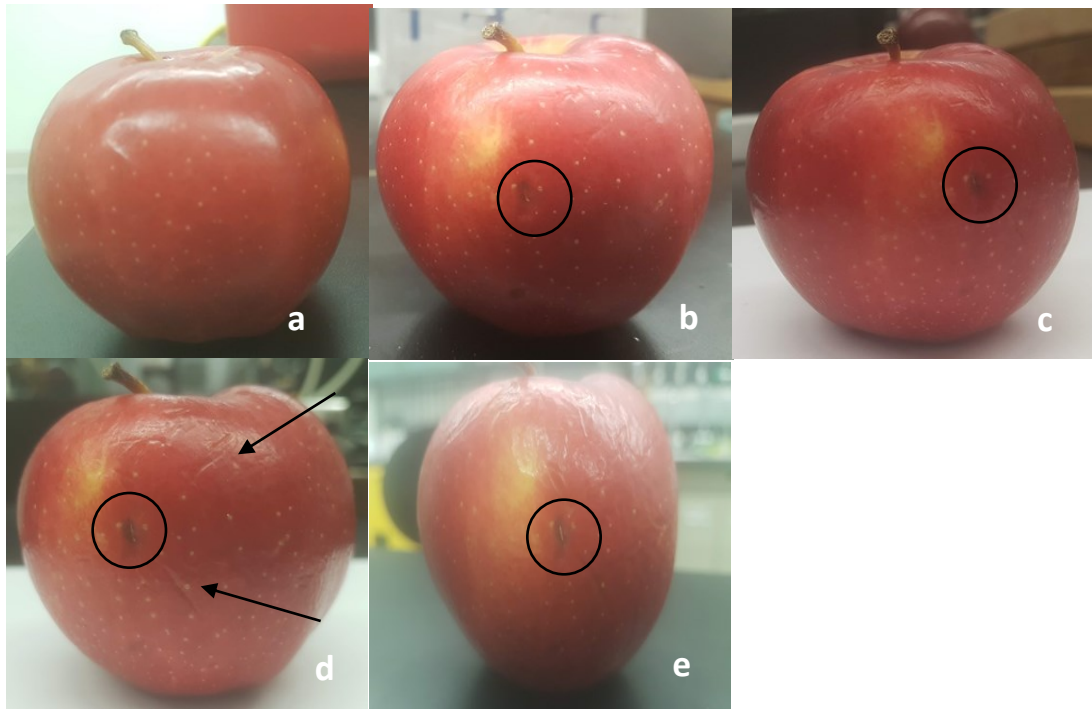


*Figure 36: Apples stored in box 1, images taken before storing (day 0) (a), day 7 (b), day 14 (c), day 21 (d), day 28 (e)*

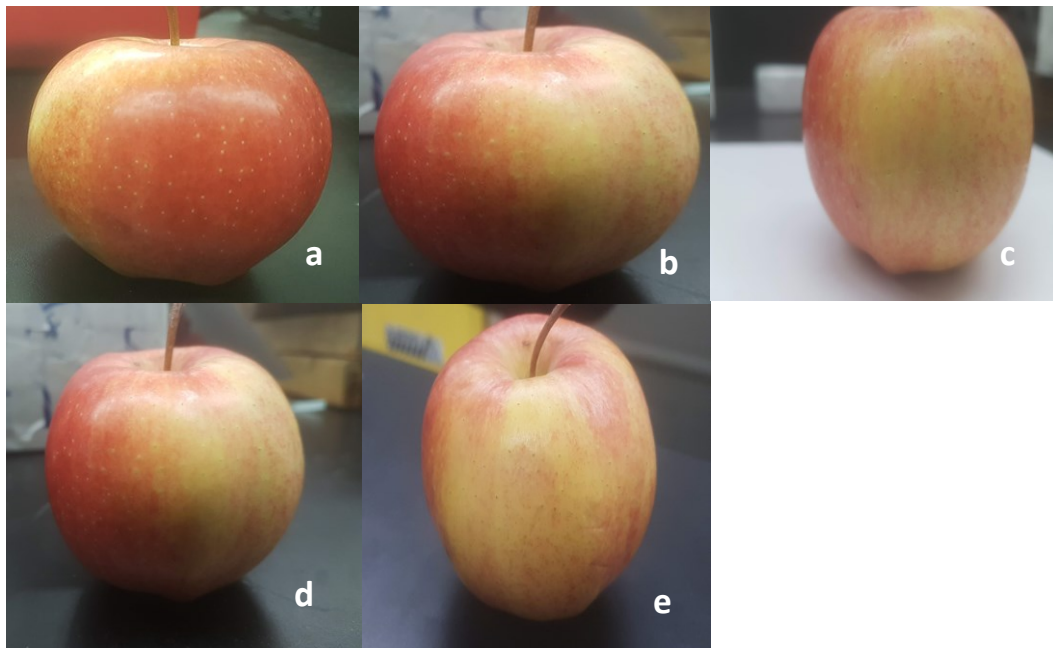


*Figure 37: Apples stored in box 2, images taken after day 0 (before storing in the box) (a), day 7 (b), day 14 (c), day 21 (d), day 28 (e)*

be the same as each batch of the apple was previously stored in the modified atmosphere by the farm [16]. The only factor that could affect the conclusion of this test would be if the apples were

already damaged by carbon dioxide.

Box 1, was coated with only HEC and one of the randomly chosen apple was stored in it. Box 2, was coated with HEC with 10% CNF-lime. The box was opened every 7 days to check the appearance of the apples.

Table 2: Results of shelf life test

Days	Box 1	Box 2
0	No abnormalities, no wrinkles	No abnormalities, no wrinkles
7	One small shallow blemish	No abnormalities, no wrinkles
14	One small shallow blemish, few wrinkles	No abnormalities, no wrinkles
21	Second shallow blemish appears, the first blemish is deeper, the hardness reduced	No abnormalities, no wrinkles
28	The first blemish was deeper, the entire apple is covered with wrinkles and the harness reduced	Few wrinkles were present and the hardness reduced
40	Bletting	the entire apple was covered with wrinkles

The addition of CNF-lime to HEC had improved the shelf life of apple based on this test. Figure 38 shows the apple in Box 1 after 40 days, which started bletting due to carbon dioxide damage.

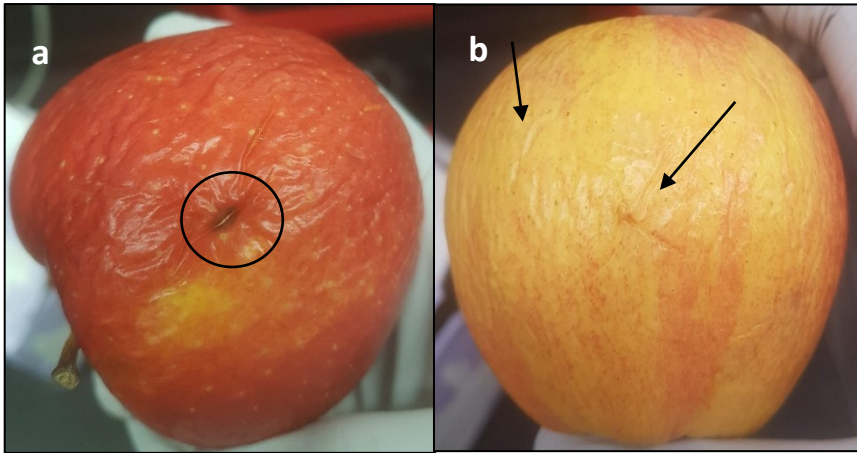


*Figure 38: apple stored in Box 1 (a); apple stored in Box 2 (b) after 40th day*

Figure 37 shows the apple in the Box 2 after 40 days which showed no signs of bletting but the hardness was reduced and many wrinkles can be seen on the surface.

## SUMMARY AND CONCLUSION

### 5.1. Summary

Cellulose from different sources were used for the TEMPO oxidation process to produce cellulose nanofibres. It was found that beaten Kraft pulp was the easiest cellulose source to make cellulose nanofibres. The carboxylate contents of the nanofibres made in this work were lower than those nanofibres produced by the same TEMPO oxidization process but with never dried Kraft pulps as the starting materials that was reported in the literature [1]. The carboxylate content measured by the potentiometric titration was used to confirm the extent of the TEMPO oxidation reaction. The progression of the TEMPO oxidation reaction can also be monitored by the addition of NaOH during the reaction. However, in the case of the starting material being microcrystalline cellulose, no change in pH was observed. This indicates that when the crystallinity of cellulose is high, the TEMPO oxidation reaction does not occur. The TGA and DTG curves show that the thermal degradation of the nanofibres starts at a temperature below the degradation temperature of cellulose (i.e., the starting material) and this is another indicating factor that the nanofibres were oxidized. Freeze-drying of the nanofibres yielded thin films as shown by the corresponding SEM images.

Calcium hydroxide was chemically precipitated on the nanofibre template. It was done by adding sodium hydroxide solution into solution containing the nanofibres and calcium nitrate. The reaction between sodium hydroxide and calcium nitrate led to the formation of calcium hydroxide crystals on the surfaces of the nanofibers. The crystallization process was heterogeneous and no

crystals were formed in the solution. It is believed that at a given temperature, the two main variables that control heterogeneous crystallization are the diameter of the nanofibres and their concentration. However, SEM results do not support the above speculation. The results only showed that the calcium hydroxide particles with different shapes are attached to the nanofibres. And the shapes of such particles were in either ellipsoidal or hexagonal form. It was found that the ellipsoidal particles exhibited distinctive FTIR spectra. The presence of the calcium hydroxide particles on the nanofiber surfaces did not affect the self-assembly behaviour of the nanofibres. The presence of calcium hydroxide significantly improved the thermal stability of the nanofibres. In particular, only small amounts of nanofibres degraded at their degradation temperature of 220 °C. The calcium hydroxide decomposition was observed at 400 °C and the calcium carbonate decomposition was observed at 590 °C, as expected. It is worth pointing out that calcium carbonate was formed by the reaction between calcium hydroxide and carbon dioxide in the present experiments. The sharp peaks of DTG appeared at 450 °C and 700 °C, respectively. The rate of the carbonation of the films performed on a test bench for a week showed that lime formed on nanofibres with a carboxylate content of 1.7 mmol/g of cellulose was the highest. This was observed from the TGA and FTIR spectrum.

The flow properties of cellulose nanofibres at different dilutions prepared at constant mixing and ultrasonication aided redispersion times were measured. It was found that some samples formed gels while others did not. The gels showed viscoelastic behaviour whereas settling of nanofibres in some suspensions took place during the flow measurements. However, blend of HEC and CNF-lime showed viscoelastic behaviour. In addition, the film properties of the HEC/CNF-lime blend were considerably better than those of the CNF films.

## 5.2. Conclusion

Cellulose nanofibres from various sources were prepared. The average diameter of the resultant nanofibres from the beaten cellulose Kraft pulp was found to be around 4 nm based upon TEM measurements. The gelation of the nanofibres was found to be strongest when they were prepared from the mechanically dispersed cellulose. The carboxylate content of the TEMPO oxidized nanofibres is linearly related to the amount of primary oxidant added but the linearity varies based on the cellulose source. It was observed that high crystallinity and high lignin content of cellulose decreased the degree of TEMPO oxidation. All the cast films made from different cellulose nanofibres were transparent, but CNF produced from the bleached thermomechanical pulp showed a yellowish tint. The TGA and DTG curves show that the decomposition of all the CNF took place at temperatures under 250 °C. CNF made from both BCTMP and Kraft pulp showed self-assembly from freeze drying as confirmed by SEM. This shows a unique cellulose property to reassemble the cellulose nanofibres into thin sheets. The BCTMP sample showed that nanofibres were tightly packed as sheets with some fibrils protruding from the ends of the sheets whereas Kraft pulp was much loosely packed and the sheets had holes with fibrils connects from one side to the other. The chemical precipitation of the calcium hydroxide formed on the surface of the fibrils was demonstrated by the SEM image. The FTIR and TGA analyses indicate that all calcium hydroxide particles formed on the nanofibres and they decomposed at 400 °C. The aging studies have shown that nanolime on cellulose nanofibres with a carboxylate content of 1.7 mmol/g cellulose exhibiting the highest rate of conversion into carbonates. The FTIR, XRD patterns and TGA confirmed the formation of calcium carbonate. The blend studies showed that CNF blends were too stiff to be used as a packaging material. Nevertheless, it could be used as excellent coating material over other polymers. The HEC blends were elastic and suitable for the use as a packaging

material. Finally the preliminary shelf life studies showed that the blend of HEC and CNF-lime increased the shelf life of apples.

### 5.3. Future prospects

Although cellulose nanofibres are well studied materials, the coatings of cellulose nanofibres over biopolymers have not yet been studied. PLA is the only material which was studied and had been proven that CNF improves the permeability property and mechanical property. Adding CNF improved the elastic modulus of PLA and lowered the oxygen permeability by a factor of 100. Similarly, properties of other biomaterials can be improved similarly. CNF can be blended with natural and synthetic polymers to improve other properties of films. The dry properties of CNF can be studied in detail.

Adding different particles to cellulose nanofibres should also be studied. Currently, particles studied are silver, titanium, calcium, ferrous, and gold. Also controlling the amount of nanoparticles deposited on CNF can be studied by controlling the saturation of the salt in the chemical precipitation process. This could help study the amount of particles that can be added to CNF before it loses its characteristic property. Likewise, the higher concentration of CNF can be used in the chemical precipitation process, and the effect of particle size can be studied.

The reassembly of cellulose nanofibres from all the desiccation methods can affect the application of these materials. Freeze drying and air drying has demonstrated that fibers interconnect back into sheets realigning the particles thus affecting other properties.

# Bibliography

- [1] T. Saito and A. Isogai, "Cellulose nanofibers prepared by TEMPO-Mediated oxidation of Native Cellulose," *Biomacromolecules*, vol. 8, pp. 2485-2491, 2007.
- [2] M. Guimaraes and V. R. Botaro, "Preparation of Cellulose Nanofibrils from Bamboo Pulp by Mechanical Defibrillation for their Applications in Biodegradable composites," *Journal of Nanoscience and Nanotechnology*, vol. 15, pp. 1-18, 2015.
- [3] W. K. Son and J. H. Youk, "Antimicrobial cellulose acetate nanofibers containing silver nanoparticles," *Carbohydrate Polymers*, vol. 65, pp. 430-434, 2006.
- [4] M. Faust, "Disorders of carbohydrate metabolism of apples (Watercore, internal breakdown, low temperature and carbon dioxide injuries)," *The Botanical Review*, vol. 35, no. 2, pp. 169-194, 1969.
- [5] A. Samanta and D. K. Chanda, "Synthesis of Nano Calcium Hydroxide in Aqueous Medium," *Journal of American Ceramic Society*, vol. 99, no. 3, pp. 787-795, 2016.
- [6] M. Kurek and D. Klepac, "Gas barrier and morphological characteristics of linear low-density polyethylene and two different polypropylene films," *Polym. Bull.*, vol. 67, pp. 1293-1309, 2011.
- [7] D. Zagory, "Modified atmosphere packaging of Fresh Produce," *Food Technology*, vol. 42(9), pp. 70-74, 1988.
- [8] I. J. Church, "Modified Atmosphere Packaging Technology: A Review," *J Sci Food Agric*, vol. 67, pp. 143-152, 1995.
- [9] M. Mcdaniel, "Effect of different packaging treatments on microbiological and sensory evaluation of precooked beef roasts," *Journal of Food Protection*, vol. 47, pp. 23-26, 1984.
- [10] J. An, "Changes in some quality indexes in fresh cut green asparagus pretreated with aqueous ozone and subsequent modified atmosphere packaging," *Journal of Food Engineering*, vol. 78, pp. 340-344, 2007.
- [11] M. Ozdemir and J. D. Floros, "Active Food Packaging Technologies," *Critical Reviews in Food Science and Nutrition*, vol. 44:3, pp. 185-193, 2004.
- [12] P. N. Skandamis, "Preservation of fresh meat with active and modified atmosphere packaging conditions," *International Journal of Food Microbiology*, vol. 79, pp. 35-45, 2002.

- [13] D. S. Lee, "Carbon dioxide absorbers for food packaging," *Trends in Food Science and Technology*, vol. 57, pp. 146-155, 2016.
- [14] M. Rooney, *Active Food Packaging*, Springer Science+Business Media Dordrecht , 1995.
- [15] M. R. Shipway and W. J. Bramlage, "Effects of Carbon Dioxide on Activity of Apple Mitochondria," *Plant Physiol.* , vol. 51, pp. 1095-1098, 1973.
- [16] M. Lopez, "Changes in aroma quality of 'Golden Delicious' apples after storage at different oxygen and carbon dioxide concentrations," *J. Sci. Food Agric.* , vol. 80, pp. 311-324, 2000.
- [17] A. Rudin and P. Choi, *The Elements of Polymer Science and Engineering*, Elsevier Inc., 2013.
- [18] P. R. Nanou Peelman, "Application of biopolymers for food packaging," *Trends in Food Science & Technology*, pp. 32 128-141, 2013.
- [19] R. Grujic, *Advances in applications of Industrial Biomaterials*, Springer International Publishing, 2017.
- [20] L. C. Duchesne and D. W. Larson, "Cellulose and the Evolution of Plant Life," *BioScience*, vol. 39, pp. 238-241, 1989.
- [21] J. Sugiyama, "Electron Diffraction study on the two crystalline phases occurring in Native Cellulose from an Algal Cell Wall," *Macromolecules*, vol. 24, pp. 4168-4175, 1991.
- [22] H. Yamamoto, "CP/MAS C13 NMR Analysis of the Crystal Transformation Induced for Valonia Cellulose by Annealing at High Temperatures," *Macromolecules*, vol. 26, pp. 1313-1317, 1993.
- [23] S. Y. Lin and C. W. Dence, *Methods in Lignin Chemistry*, Springer-Verlag, 1992.
- [24] P. Ma and H. Zhai, "Influence of TEMPO-mediated oxidation on the lignin of thermomechanical pulp," *Bioresource Technology*, vol. 118, pp. 607-610, 2012.
- [25] I. Usov and G. Nystrom, "Understanding nanocellulose chirality and structure-properties relationship at the single fibril level," *nature communications* , vol. 6, p. 7564, 2015.
- [26] H. Kargarzadeh and I. Ahmad, "Effects of hydrolysis conditions on the morphology crystallinity and thermal stability of cellulose nanocrystals extracted from kenaf bast fibers," *Cellulose* , vol. 19, pp. 855-866, 2012.
- [27] Y. Boluk, "Analysis of cellulose nanocrystal rod lengths by dynamic light scattering and electron microscopy," *J Nanopart Res*, vol. 16, p. 2174, 2014.

- [28] Y. Cao and P. Zavatteri, "The influence of cellulose nanocrystal additions on the performance of cement paste," *Cement & Concrete Composites*, vol. 56, pp. 73-83, 2015.
- [29] H. Fukuzumi and A. Isogai, "Transparent and High Gas Barrier Films of Cellulose Nanofibers prepared by TEMPO-Mediated Oxidation," *Biomacromolecules*, vol. 10, pp. 162-165, 2009.
- [30] M. E. Bakkari and Y. Boluk, "Preparation of cellulose nanofibers by TEMPO-oxidation of bleached chemi-thermomechanical pulp for cement applications," *Carboxylate Polymers*, vol. 203, pp. 238-245, 2019.
- [31] S. Fujisawa, T. Saito and A. Isogai, "Surface Engineering of ultrafine Cellulose Nanofibrils toward Polymer Nanocomposite Materials," *Biomacromolecules*, vol. 14, no. 5, pp. 1541-1546, 2013.
- [32] O. Olatunji and R. T. Olsson, "Microneedles from Fishscale-Nanocellulose Blends Using Low Temperature Mechanical Press Method," *Pharmaceutics*, vol. 7, pp. 363-378, 2015.
- [33] S. Sultan and G. Siqueira, "3D printing of nano-cellulosic biomaterials for medical applications," *Biomedical Engineering*, vol. 2, pp. 29-34, 2017.
- [34] S. P. Mishra, "variables, Ultrasound-Catalyzed TEMPO-Mediated oxidation of Native cellulose for the production of Nanocellulose: Effect of process," *BioResources*, vol. 6(1), pp. 121-143, 2011.
- [35] M.-C. Hsieh and H. Koga, "Hazy Transparent Cellulose Nanopaper," *Scientific Reports*, vol. 7:41590, 2017.
- [36] C. Tahiri and M. R. Vignon, "TEMPO-oxidation of cellulose: Synthesis and characterisation of polyglucuronans," *Cellulose*, vol. 7, pp. 177-188, 2000.
- [37] M. Hirota and A. Isogai, "Oxidation of regenerated cellulose with NaClO<sub>2</sub> catalyzed by TEMPO and NaClO under acid-neutral conditions," *Carbohydrate Polymers*, vol. 78, pp. 330-335, 2009.
- [38] X. Cao and S. Al-Deyab, "Cellulose nanowhiskers extracted from TEMPO-oxidized jute fibers," *Carbohydrate Polymers*, vol. 90, pp. 1075-1080, 2012.
- [39] P. Lahtinen, "A comparative study of fibrillated fibers from different mechanical and chemical pulps," *BioResources*, vol. 9(2), pp. 2115-2127, 2014.
- [40] L. Dai and B. Wang, "Properties of hydroxypropyl guar/TEMPO-oxidized cellulose nanofibers composite films," *Cellulose*, vol. 22, pp. 3117-3126, 2015.

- [41] S. Fujisawa and A. Isogai, "Preparation and characterization of TEMPO-oxidized cellulose nanofibril films with free carboxyl groups," *Carbohydrate Polymers*, vol. 84, pp. 579-583, 2011.
- [42] H. Fukuzumi and A. Isogai, "Influence of TEMPO-oxidized cellulose nanofibril length on film properties," *Carbohydrate polymers*, vol. 93, pp. 172-177, 2013.
- [43] E.-L. Hult, "Enhancing the barrier properties of paper board by a novel lignin coating," *Industrial Crops and Products*, no. 50, pp. 694-700, 2013.
- [44] T. Hirvikorpi and M. Vaha-Nissi, "Comparison some coating techniques to fabricate barrier layers on packing materials," *Thin Solid Films*, no. 518, pp. 5463-5466, 2010.
- [45] T. Hirvikorpi and M. Vaha-Nissi, "Thin Al<sub>2</sub>O<sub>3</sub> barrier coatings onto temperature-sensitive packaging materials by atomic layer deposition," *Surface and Coatings Technology*, vol. 205, no. 21-22, pp. 5088-5092, 2011.
- [46] M. Arrieta and E. Fortunati, "Bionanocomposite films based on plasticized PLA-PHB/cellulose nanocrystal blends," *Carbohydrate Polymers*, vol. 121, pp. 265-275, 2015.
- [47] M. P. Arrieta, "Ternary PLA-PHB-Limonene blends intended for biodegradable food packaging applications," *European Polymer Journal*, vol. 50, pp. 255-270, 2014.
- [48] H. angellier, "Surface Chemical Modification of Waxy Maize Starch Nanocrystals," *Langmuir*, vol. 21, pp. 2425-2433, 2005.
- [49] H. Namazi, "Surface Modification of Starch Nanocrystals through Ring-Opening polymerization of caprolactone and investigation of their microstructures," *Journal of Applied Polymer Science*, vol. 110, pp. 2405-2412, 2008.
- [50] Y. Boluk, "Suspension viscosities and shape parameter of cellulose nanocrystals (CNC)," *Colloids and Surfaces A: Physicochem. Eng. Aspects*, vol. 377, pp. 297-303, 2011.
- [51] T. Saito and A. Isogai, "Homogeneous Suspension of Individualized Microfibrils TEMPO-Catalyzed Oxidation of Native Cellulose," *Biomacromolecules*, vol. 7, no. 6, 2006.
- [52] S. H. Osong and S. Norgren, "Processing of wood-based microfibrillated cellulose and nanofibrillated cellulose and application relating to papermaking: a review," *Cellulose*, vol. 23, pp. 93-123, 2016.
- [53] T. Taniguchi and k. Okamura, "New Films Produced from Microfibrillated Natural Fibres," *Polymer International*, vol. 47, pp. 291-294, 1998.
- [54] T. Saito and A. Isogai, "TEMPO-Mediated Oxidation of Native Cellulose. The Effect of Oxidation Conditions on Chemical and Crystal Structures of Water-Insoluble Fractions," *Biomacromolecules*, vol. 5, pp. 1983-1989, 2004.

- [55] M. E. Bakkari and Y. Boluk, "Preparation of cellulose nanofibers by TEMPO-oxidation of bleached chemi-thermomechanical pulp for cement applications," *Carbohydrate Polymers*, vol. 203, pp. 238-245, 2019.
- [56] J. Araki and M. wada, "Steric Stabilization of a Cellulose Microcrystal Suspension by Poly(ethylene glycol) Grafting," *Langmuir*, vol. 17, pp. 21-27, 2001.
- [57] A. Samanta and D. K. Chandra, "Sythesis of Nano Calcium Hydroxide in Aqueous Medium," *J. Am. Ceram. Soc.*, vol. 99[3], pp. 787-795, 2016.
- [58] Y. Okita and A. Isogai, "TEMPO-mediated oxidation of softwood thermomechanical pulp," *Holzforschung*, vol. 63, pp. 529-535, 2009.
- [59] W. Chen and H. Yu, "Isolation and characterization of cellulose nanofibers from four plant cellulose fibers using a chemical-ultrasonic process," *Cellulose*, vol. 18, pp. 433-442, 2011.
- [60] H. Fukuzumi and A. Isogai, "Thermal stabilization of TEMPO-oxidation cellulose," *Polymer Degradation and Stability*, vol. 95, pp. 1502-1508, 2010.
- [61] H. Yang, "Characteristics of hemicellulose, cellulose and lignin pyrolysis," *Fuel*, vol. 86, no. 12-13, pp. 1781-1788, 2007.
- [62] F. Jiang and Y.-L. Hsieh, "Super water absorbing and shape memory nanocellulose aerogels from TEMPO-oxidized cellulose nanofibrils via cyclic freezing-thawing," *Journal of Materials Chemistry A*, vol. 2, pp. 350-359, 2014.
- [63] J. Han and Q. Wu, "Self-Assembling behavior of cellulose nanoparticles during freeze-drying: Effect of suspension concentration, particle size, crystal structure and surface charge," *Biomacromolecules*, vol. 14, pp. 1529-1540, 2013.
- [64] F. Jiang and Y.-L. Hsieh, "Assembling and redispersibility of Rice straw Nanocellulose: Effect of tert-Butanol," *ACS Applied matter interfaces*, vol. 6, pp. 20075-20084, 2014.
- [65] T. liu and X. li, "Synthesis and characterization of calcium hydroxide nanoparticles by hydrogen plasma-metal reaction method," *Material letters*, vol. 64, pp. 2575-2577, 2010.
- [66] A. Bodin, "Surface-engineered bacterial cellulose as template for crystallization of calcium phosphate," *Journal of Biomaterials Science, Polymer Edition*, vol. 14, no. 4, pp. 435-447, 2012.
- [67] W. Chen and H. Yu, "Isolation and characterization of cellulose nanofibers from four plant cellulose fibers using a chemical-ultrasonic process," *Cellulose*, vol. 18, pp. 433-442, 2011.

- [68] B. Soni and E. B. Hassan, "Transparent bionanocomposite films based on chitosan and TEMPO-oxidized cellulose nanofibers with enhanced mechanical and barrier properties," *Carboxylate Polymers* , vol. 151, pp. 779-789, 2016.
- [69] M. Galvan-Ruiz, "Characterization of Calcium carbonate, Calcium oxide and Calcium Hydroxide as Starting Point to the Improvement of Lime for Their use in Construction," *Journal of Materials in Civil Engineering* , vol. 21, no. 11, pp. 694-698, 2009.
- [70] P. Chen and H. Yu, "Concentration effects on the isolation and dynamic rheological behavior of cellulose nanofibers via ultrasonic processing," *Cellulose* , vol. 20, pp. 149-157, 2013.
- [71] K. Benhamou and H. Kaddami, "Control of size and viscoelastic properties of nanofibrillated cellulose from palm tree by varying the TEMPO-mediated oxidation time," *Carbohydrate Polymers* , vol. 99, pp. 74-83, 2014.